

CHAOTIC DYNAMICAL SYSTEM AND GRAVITATIONAL WAVES

Kenta Kiuchi

A Doctoral Dissertation Submitted to
Department of Physics, Waseda University

September, 2007



Department of Physics, Waseda University

CONTENTS

1	Introduction	5
2	Einstein Equations as Initial Value Problem and Gravitational Waves	11
2.1	Newtonian dynamics	11
2.2	(3+1)-formalism of Einstein's equation	12
2.3	Linear perturbation theory and Quadrupole formula	16
2.3.1	Perturbed Einstein's equation	16
2.3.2	Conservation Law and Conserved variables	20
2.3.3	Energy, Momentum and Angular Momentum of Gravitational Wave . . .	22
2.3.4	Quadrupole Wave	25
2.3.5	Angular Dependence of Quadrupole Wave	27
2.3.6	Quadrupole Formula	28
2.4	Multipole Expansion of Gravitational Field	31
3	Basic Equation of Test Particle	33
3.1	Test Particle in General Relativistic Spacetime	33
3.1.1	Single-pole particle	33
3.1.2	Pole-Dipole Particle	35
3.2	Constant Of Motion	42
3.3	Equation of motion in Tetrad frame	44
4	Chaos in Relativistic Two Body Problem	47
4.1	Chaos in Schwarzschild Space Time	47
4.2	Can relativistic binary really behave chaotically ?	52
4.2.1	Post-Newtonian Approximation	52
4.2.2	Chaos in binary merger	53
4.3	Associated Topics	57
4.3.1	Radiation reaction effect	57
4.3.2	Extreme mass ratio black hole binary	57
5	Gravitational Wave from particle orbiting around Black Hole spacetime	61
5.1	Basic Equations for Test Particle	61
5.1.1	Background Spacetime	61
5.1.2	Spinless Test Particle	62
5.1.3	Spinning Test Particle	64
5.2	Orbital parameters and initial condition	65
5.2.1	spinless particle	65
5.2.2	spinning particle	65

5.3	Numerical Analysis	68
5.3.1	Particle Motion	68
5.3.2	Gravitational Wave	70
5.4	Summary	76
6	Gravitational Wave Signals from Chaotic System: A point mass with disk	79
6.1	Basic equations	80
6.2	Numerical Analysis	81
6.2.1	Two phases of chaos in particle motion	81
6.2.2	Indication of chaos in gravitational waves	85
6.3	Summary and Discussion	86
7	Conclusion	91
7.1	Spinning particles in the Kerr spacetime	91
7.2	Test particle in point mass and disk system	92
7.3	Future works	92
A	Ricci rotation, Riemann tensor, Christoffel symbol	95
B	Local Lyapunov Exponent	97

CHAPTER 1

INTRODUCTION

Researches on chaos have stared from the famous Poincaré 3-body problem [81]. So far, various researches on chaos not only in physics but also in several fields, such as mathematics, biology, and sociology, have been done and revealed that chaos could be one of the universal features of the nature. We are observing chaos in daily life, e.g., weather forecast. Is chaos also “daily” in the universe as well ? If one answers “Yes”, he/she might think that because the universe is a part of the nature, it can be expected that chaos also appears in the universe. If one answers “No”, he/she might invoke that phenomena in the universe would happen in a high energy state and a strong gravitational field, which are never realized in our daily life. Study of chaos in the universe might answer this question.

What has been done in a field of chaos in the universe, in particular in the theory of general relativity ? Researches in this field have just started recently and its history is shorter than that of the research on chaos in the Newtonian mechanics [46]. Research subjects of chaos in general relativity are classified into two types. One is a chaotic behaviour of the spacetime itself. It is of course a solution of Einstein’s equation and therefore can be chaotic due to the high nonlinearity of Einstein’s equation. Researches dealing with this subject have started from a work by Misner [75]. He has investigated a behavior of the Bianchi IX type universe and following this work, some remarkable works have been done [3, 9, 23, 100]. The other subject is a motion of the object in a relativistic spacetime. The pioneering work on this subject is Contopoulos’s work [18, 19]. He has studied a behavior of test body in the Majumdar-Papapetou solution, which is multiple extreme Reissner-Nordström black hole (BH) system. Many works studying a chaotic motion of test body in relativistic frameworks have been done [13, 54, 67, 76, 82, 83, 96, 108, 111, 97, 98, 99]. Our works in this thesis belong to the latter type and we will refer to a motivation and purpose.

The main subject of this thesis is to analyze a feature of chaos, which is missed in the previous works. We know that there is a wide variety of chaos. In particular, recent notable progress in the Hamiltonian system¹ is finding a statistical law in the chaotic system. This statistical law is related to a long time correlation of the object motion as well as to a structure of the phase space. More detailed explanation is as follows: if a system is integrable, tori exit in a phase space. The motion of the object in this system is along the tori and as a result, it becomes a periodic motion. On the contrary, the tori are broken down if the system is non-integrable. Only the remnant of the tori exists. Then, the motion of the object will lose its predictability, which indicates the chaos. This feature can be cleanly seen if you draw the Poincaré map, which is an intersection of the phase space. What about an “intermediate” state ? “Intermediate” means although a part of tori is broken down, the main structure still remains. In this state, the structure of the phase space consists of main tori surrounded by small tori, which is parts of the broken tori (see Figure 1.1). In the phase space, the motion will move around these small tori. This is a so-called stagnant motion and such a motion has a long-time correlation. This feature appears in a power spectrum of the motion as a power-law; so-called 1/f fluctuation. This is the statistical law as mentioned above. Therefore, measuring the power-law spectrum means that you can pick up information of the phase space structure even if the system is chaotic. The power-spectrum analysis is important when you investigate a chaotic system. However, this

¹Most famous example is Hénon-Heiles system [44]

analysis was missed in the previous works, in particular the chaos in general relativity.

A view point for searching a way to extract information from a chaotic system is also missed. Conventional ways to analyze a chaotic system are the Poincaré map analysis, as explained above, and the Lyapunov exponent analysis, which measures a growth rate of initial small deviation in two nearby trajectories. If the Lyapunov exponent has a positive value, it represents that the system is chaotic. Both methods measure the motion of the object directly. In general, phenomena in universe occurs far from us and ambient matter often contaminates the environment. So, it may be difficult to observe a chaotic motion directly. In this thesis, we propose gravitational waves as a tool to extract information from a chaotic system. Why do we choose gravitational waves ? From here, we refer to the reason.

At first, we should explain gravitational waves. General relativity proposed by Einstein in 1915 is the theory that describes the gravity as a spacetime distortion. As Maxwell's equation in electrodynamics represents electromagnetic waves as the non trivial vacuum solution, Einstein's equation describes that the gravity propagates; gravitational waves. The fact that the gravity propagates in a finite time is essential difference from the Newton gravity, in which the gravity is expressed as a potential. So, gravitational waves are one of the essential part of general relativity and whether it exists or not is concerned with the root of general relativity. In 1974, Hulse and Taylor have observed the binary pulsar PSR1913+16 and found the decrease of its orbital period. After the observation of this phenomena, they have shown that the decreasing rate of the orbital period agrees with that predicted by a gravitational radiation within 0.3 percents [48]. A series of their works are widely accepted as the indirect evidence of the existence of gravitational waves today. Hulse and Taylor have been awarded the Nobel prize in 1993. Although, following Hulse and Taylor's works, many attempts for the direct observation of gravitational waves have been done and are now being done, a report for the direct observation has not been done yet.

But, the ground based laser interferometers such as First LIGO / Advanced LIGO (USA) [1], VIRGO (France, Italy) [37], GEO600 (UK, Germany) [45], and TAMA300 (Japan) [106] are now operating and the spacecraft type laser interferometer such as LISA(USA) [105] will launch in 2015. So, the direct observation of gravitational waves will come true in the near future. What is expectation for gravitational waves ? Up to today, the astronomy with various observational methods, e.g., radio, infrared, optical, ultraviolet, X-ray, gamma-ray, and neutrino, have developed and succeeded in each categories. On the other hand, gravitational waves are more transparent than these signals because the gravity interacts weakly with the matter. This implies that gravitational waves could not only play a supplementary role to the existing observational methods but also play a leading role in the astrophysics. We might be able to observe regions, e.g., a central region of collapsing stellar, or the merger of binary composed of a BH and/or a neutron star (NS). It is impossible to observe these events with the existing methods.

Then, what should we do theoretically for gravitational wave astrophysics ? For gravitational wave astronomy, we have to make theoretical templates of gravitational waves. There are two meanings in making templates. The first is closely related to a method to identify gravitational waves from the observation data, in particular the laser interferometers. It is demanded to make a high accurate theoretical template to extract gravitational wave signals from observed data, i.e., the matched filtering method. The linear perturbation theory and the Post Newton expansion are appropriate to make such a kind of templates. On the other hand, numerical relativity is a supplementary method to the two methods. Numerical relativity is a powerful method to estimate gravitational waves in a situation that the nonlinearity of gravity is strong, e.g., the merger of a closed binary, the final phase of a stellar collapse, and so on. Although, recently, the progress in this field is remarkable, the high accurate templates are not made yet because numerical relativity is a large-scale numerical simulation. Then, how do you utilize such templates ? The answer is following: If gravitational waves are observed without

the matched filtering mentioned above and compared to a theoretical template, we can extract various information of wave sources, e.g., their distance, mass, spin, and so on. This is the second meaning.

Next, we shall briefly explain the three kind of method, the BH perturbation theory, the Post Newton expansion, and numerical relativity.

1. The BH perturbation theory : A basic assumption is that you can separate a spacetime into a background and a perturbation part. The perturbation is too small to affect on the background. Therefore, the basic equation is a linearly perturbed Einstein's equation. The equation is semi-analytically formulated by using the symmetry of the background. Because Einstein's equation is classified into a hyperbolic type, the perturbation equation can be recast into the wave equation; gravitational waves. Remarkable point of this method is that you can expect a high accurate template because you can estimate the gravitational waves alone. Various formulations have been done in the BH spacetime [5, 15, 16, 17, 31, 36, 51, 56, 58, 61, 72, 43, 78, 79, 86, 89, 90, 102, 112].

2. The post Newtonian expansion : If typical velocity, v , in a system is sufficiently smaller than the speed of light, c , it is possible to expand an equation of motion (EOM) in the system in terms of the parameter v/c [10]. A schematic form of the post Newtonian EOM is

$$\ddot{\mathbf{r}} = \mathbf{a}_N + \mathbf{a}_{PN} + \mathbf{a}_{2PN} + \mathbf{a}_{SO} + \mathbf{a}_{RR} + \mathbf{a}_{3PN} + \mathbf{a}_{SS},$$

where \mathbf{a} is acceleration and N, PN, 2PN, SO, RR, 3PN, SS denote the Newtonian term, the Post Newtonian term, the second order Post Newtonian term, the spin-orbit coupling term, radiation reaction term due to gravitational radiation, the third order Post Newtonian term, the spin-spin coupling term, respectively. Benefit of post-Newton approximation to the BH perturbation theory is to be able to calculate an accurate motion of two bodies with comparable masses. Moreover, the radiation reaction force can be took into account. Therefore, this method is powerful to produce theoretical templates of gravitational wave from coalescing binaries.

3. Numerical Relativity : Einstein's equation is directly and numerically solved in this method. For a long time, it has been non-trivial to formulate for stable numerical simulations. However, Shibata and Nakamura have developed a robust method based on the conformal transverse decomposition method in 1995 [94]. Baumgarte and Shapiro have independently formulated in 1999 [7]. Their formulation is essentially same as that by Shibata and Nakamura. This method is called the BSSN formulation from their initial and being used in several research groups in the world. Numerical relativity covers a broad range of topics and we do not explain more in this thesis (see a review [8] in details).

Our next task is to review concrete targets, gravitational wave sources, for the current ground based detectors or future designed detectors. Up to now, promising candidates of gravitational wave source are distinguished into a high frequency source with $1 - 10^3$ Hz and a low frequency source with $10^{-4} - 1$ Hz. The ground based detectors such as LIGO, TAMA, and so on are designed to be sensitive to the former type sources and LISA is for the later type sources. Concrete candidates of the high frequency source are as follows:

- Inspiral of compact binaries composed of a stellar size BH and/or a NS
- Tidal disruption of a NS due to a BH in NS-BH binaries
- The merger and the quasi-normal mode ringing of binary BHs
- Low mass X-ray binaries
- Known pulsars (Spinning NS with pulse frequency above 100 Hz)
- Unknown pulsars
- The high/low $T/|W|$ instability of NS in accretion induced collapse of white dwarf binaries
- Proto NS convection in supernovae
- Long and short gamma-ray bursts

- Stochastic background

Fig. 1.2 is the sensitivity curves of LIGO and Advanced LIGO.

Concrete candidates of the low frequency source are as follows:

- Short period binaries
- The mergers of a supermassive BH binaries
- Inspiral of compact objects with $\sim 1\text{-}1000M_{\odot}$ into massive BHs
- Gravitational collapse of supermassive stars

Fig. 1.3 is the LISA's sensitivity curve.

A number of works for these various sources have been done. Note that proposal for a new kind of gravitational wave source is also important. This thesis plays such a kind of role in the field of gravitational wave physics. In this thesis, we adopt two kinds of chaotic systems in the Newtonian dynamics and general relativity.

1. A spinning particle around a BH spacetime

As a first concrete chaotic system, we adopt this general relativistic model. It invokes compact objects orbiting around a supermassive BH. Recent observations support the existence of such massive BHs at the galactic nuclei. As for a background spacetime, we assume the Kerr metric since such a supermassive BH is usually rotating. We evaluate the gravitational waves emitted from this system by using the multipole expansion of a gravitational field [65]-[103].

Carter showed [14] that the equations of motion for a non-spinning particle are integrable. After his work, Johnston discovered that, for some tuned initial parameters, the particle motion can be very complicated as if chaos occurred, although the system is integrable [52]. Then we also analyze such a non-chaotic but complicated orbital motion to clarify whether the chaos is essential for the gravitational wave emission or not.

We compare the gravitational wave forms, the energy fluxes and the gravitational wave energy spectrum, for a chaotic and non-chaotic systems. We analyze the effects of the chaos on gravitational waves. We study some observational features of the chaos in the general relativistic dynamical system.

2. A point mass and thick disk system

This model mimics a system of a BH with a massive accretion disk. Saa analyzed this system and showed that particle motions can be chaotic [87]. This model can describe both an almost regular motion and a highly chaotic one by changing the ratio of a disk mass to a BH mass. Hence, a mechanism of the chaos is different from that of the model 1. In Ref. [87], however, the analysis based on the Poincaré map has been done and the characters of the chaos have not been studied. Therefore, our strategy is the following: First, we analyze the particle motion and investigate the characters of the chaos emerging in this system. Secondly, we evaluate the gravitational waves from this system. We utilize the quadrupole formula to estimate the gravitational waves. Finally, to study some observational features of the chaos in the gravitational waves, we investigate correlation between types of the chaotic motions and the gravitational waves, and then discuss a possibility to extract information of this chaotic system by the gravitational waves.

The organization of this thesis is as follows. In Chapter 2 we review the Arnowitt-Deser-Misner formalism and how Einstein's equation contains gravitational waves. Subsequently, we derive the quadrupole wave and the quadrupole formula by using the linear perturbation theory. In Chapter 3 we review the derivation of the basic equations of both a non-spinning particle and a spinning particle in general relativity. First, we derive the equations of motion. Second, we review a supplementary condition. Finally, we derive the constants of motion. Chapter 4 devotes to review the chaos in general relativity. We show our results in Chapter 5 and Chapter 6. Summary and some remarks are given in Chapter 7. Throughout this thesis, the units $c = G = 1$ are used. We utilize the notation according to Misner Thorne and Wheeler (MTW) [75].

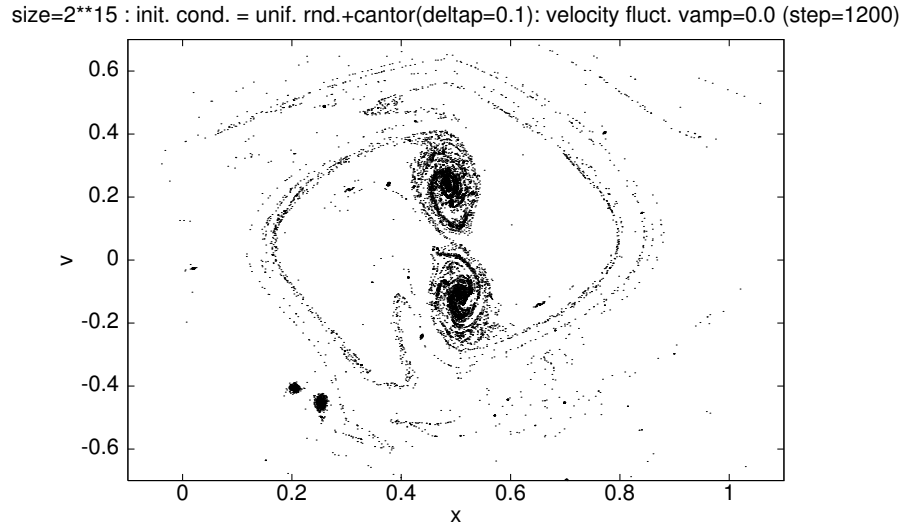


Figure 1.1: Schematic figure of the phase space which produces 1/f fluctuation. This figure is cited from [63].

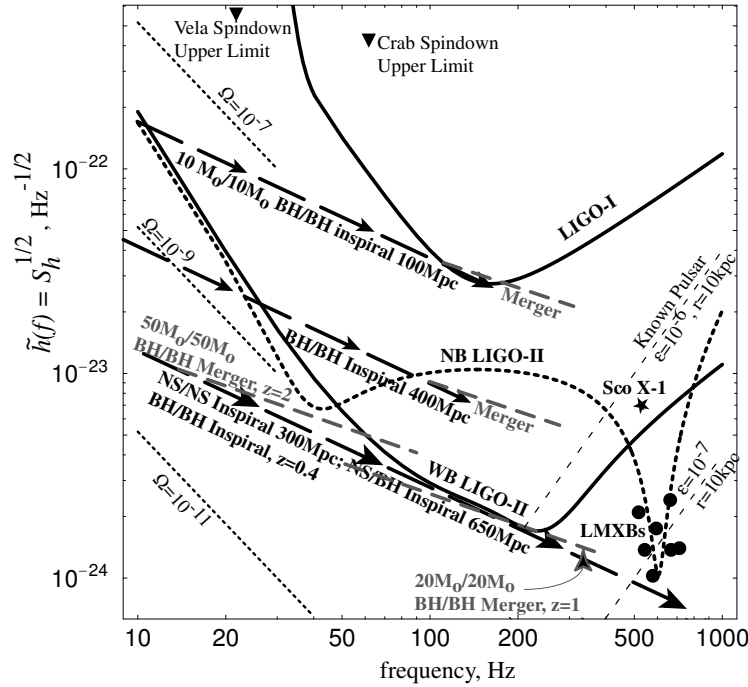


Figure 1.2: The strain $\tilde{h}(f)$ as a function of gravitational wave frequency f . In this figure, the design sensitivity curve for the initial LIGO, as LIGO-I, and that for several planned advanced LIGO, as NB LIGO-II and WB LIGO-II, are plotted. We also plot the several candidates such as BH-BH binary coalescence, NS-NS binary coalescence, and the spin down of the known pulsars. This figure is cited from [29].

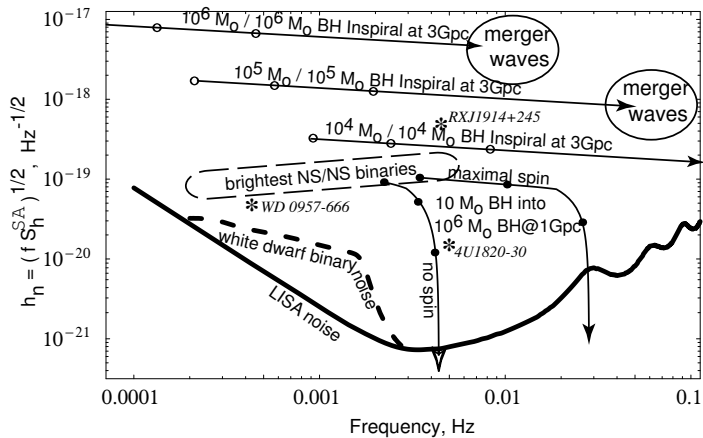


Figure 1.3: The strain $h_n(f)$ as a function of gravitational wave frequency. The design sensitivity curve for the LISA as well as expected strain for the various candidates such as a supermassive BH binary coalescence and white dwarf binary coalescence are plotted. This figure is cited from [29].

CHAPTER 2

EINSTEIN EQUATIONS AS INITIAL VALUE PROBLEM AND GRAVITATIONAL WAVES

As mentioned in Introduction, Einstein's equation represents that the gravity propagates as waves with the speed of light; gravitational waves. Gravitational waves correspond to a new degree of freedom (d.o.f) of the gravitational field. Einstein's equation is a set of the highly non-linear partial differential equations. At a glance of this equation, it is hard to understand how Einstein's equation describes the gravitational waves. The Arnowitt-Deser-Misner (ADM) formalism, sometimes called the (3+1)-formalism, is one of the method to solve Einstein's equation as an initial value problem and it helps us to understand d.o.f of general relativistic gravity [4, 77, 110].

This chapter is devoted to a review of the ADM formalism and the gravitational waves. In the latter part of this chapter, a basic formalism to estimate gravitational waves propagating in flat space, the quadrupole formula, is reviewed [65].

2.1 Newtonian dynamics

A set of equations governing the Newtonian dynamics are as follows:

(1) The mass conservation equation

$$\partial_t \rho + \partial_i (\rho v_i) = 0, \quad (2.1)$$

(2) The Euler equation

$$\partial_t (\rho v_i) + \partial_j (\rho v_i v_j) = -\partial_i p - \rho \partial_i \phi, \quad (2.2)$$

(3) The Energy conservation equation

$$\partial_t \left(\rho \left(\frac{1}{2} v^2 + \epsilon \right) \right) + \partial_j \left(\left(\rho \left(\frac{1}{2} v^2 + \epsilon \right) + P \right) v_j \right) = -\rho \partial_i \phi v_i, \quad (2.3)$$

(4) An equation of state

$$p = p(\rho, \epsilon), \quad (2.4)$$

(5) Poisson equation

$$\Delta \phi = 4\pi G \rho, \quad (2.5)$$

where ρ, p, ϵ, v^i , and ϕ are the rest mass density, pressure, specific internal energy, velocity, and gravitational potential, respectively. We show the energy equation in a conservative form. Sometimes, the energy equation is expressed with respect to the internal energy $\rho\epsilon$. A procedure to solve the set of the equation governing the Newtonian dynamics as an initial value problem is as follows:

Step 0

Given distributions of ρ, v_i , and ϵ , we will solve Eq. (2.5) to determine ϕ at $t = 0$.

Step 1

Update ρ, v_i , and ϵ to $t = t + \Delta t$ with Eqs. (2.1)-(2.3)
and subsequently determine ϕ with Eq. (2.5) at $t = t + \Delta t$.

Step 2

Update t to $t + \Delta t$
Return to Step 1

2.2 (3+1)-formalism of Einstein's equation

Let us consider a space-like hypersurface $\Sigma(t)$ with $t = \text{const.}$ in four dimensional spacetimes. We define γ_{ij} to be a metric tensor of 3-space $\Sigma(t)$ as

$$dl^2 = \gamma_{ij}dx^i dx^j. \quad (2.6)$$

We assume a certain point P on $\Sigma(t)$. At P , let us consider a time-like unit vector n^μ normal to $\Sigma(t)$. The normalization of the vector is $n^\mu n_\mu = -1$. We consider another space-like hypersurface $\Sigma(t + \Delta t)$. A certain point P' on $\Sigma(t + \Delta t)$ is connected to P and the vector $\overrightarrow{PP'}$ is normal to $\Sigma(t)$. In the limit of $\Delta t \rightarrow 0$, the proper length of $\overrightarrow{PP'}$ is proportional to Δt ;

$$|\overrightarrow{PP'}| = \alpha \Delta t, \quad (2.7)$$

where α is a proportionality constant and we call it a lapse function. We consider a line which passes through the point P and along which a spatial coordinate is constant. This path intersects the hypersurface $\Sigma(t + \Delta t)$ at a point P'' . In general, P'' does not always coincide with P' because the coordinate line does not do with the normal vector. Therefore, P'' is not P' . A spatial vector $\overrightarrow{P'P''}$ defined on $\Sigma(t + \Delta t)$ is proportional to Δt in the limit of $\Delta t \rightarrow 0$;

$$(\overrightarrow{P'P''})^i = \beta^i \Delta t, \quad (2.8)$$

where β^i is a proportionality constant and we call it a shift vector. α and β^i express four d.o.f of coordinate transformation.

The proper distance between a point $P(t, x^i)$ on $\Sigma(t)$ and a point $Q(t + \Delta t, x^i + \Delta x^i)$ on $\Sigma(t + \Delta t)$ is calculated by the Pythagoras theorem (see Fig. 2.1);

$$\begin{aligned} ds^2 &= -(\overrightarrow{PP'})^2 + (\overrightarrow{P'Q})^2 \\ &= -\alpha^2 dt^2 + \gamma_{ij}(dx^i + \beta^i dt)(dx^j + \beta^j dt) \\ &= g_{\mu\nu} dx^\mu dx^\nu. \end{aligned} \quad (2.9)$$

The covariant metric tensor $g_{\mu\nu}$ is given by

$$g_{\mu\nu} = \begin{pmatrix} -\alpha^2 + \beta_i \beta^i & \beta_j \\ \beta_i & \gamma_{ij} \end{pmatrix} \quad (2.10)$$

and the contravariant tensor $g^{\mu\nu}$ is by

$$g^{\mu\nu} = \begin{pmatrix} -1/\alpha^2 & \beta^j/\alpha^2 \\ \beta^i/\alpha^2 & \gamma^{ij} - \beta^i \beta^j / \alpha^2 \end{pmatrix}, \quad (2.11)$$

where

$$\beta_i = \gamma_{ij}\beta^j.$$

Let us define a projection tensor $h_{\mu\nu}$;

$$h_{\mu\nu} = g_{\mu\nu} + n_\mu n_\nu \quad (2.12)$$

where

$$\begin{aligned} n_\mu &= (-\alpha, 0, 0, 0), \\ n^\mu &= \left(\frac{1}{\alpha}, -\frac{\beta^i}{\alpha} \right). \end{aligned} \quad (2.13)$$

is the unit normal vector. With this, any vector field V^μ can be projected on $\Sigma(t)$ as $h_{\mu\nu}V^\nu$ and this projected vector is normal to n^μ ;

$$n^\mu h_{\mu\nu} V^\nu = 0. \quad (2.14)$$

Given a four dimensional tensor $T_{\mu\nu\rho\sigma\dots}$, a projected tensor $h^{\mu\alpha}h^{\nu\beta}h^{\rho\gamma}h^{\sigma\delta}T_{\alpha\beta\gamma\delta\dots}$ is a tensor on $\Sigma(t)$.

We define the extrinsic curvature K_{ij} as

$$K_{ij} \equiv -h_i^\mu h_j^\nu n_{\mu;\nu}. \quad (2.15)$$

Using Eq. (2.13), K_{ij} is expressed as

$$\begin{aligned} K_{ij} &= -n_{i;j} \\ &= \Gamma_{ij}^\alpha n_\alpha \\ &= \frac{1}{2\alpha} \left(-\frac{\partial \gamma_{ij}}{\partial t} + \beta_{ilj} + \beta_{jli} \right), \end{aligned} \quad (2.16)$$

where $|$ means the covariant derivative in terms of the spatial metric γ_{ij} . The definition is a projection of the covariant derivatives with respect to the four dimensional metric;

$$T^{ij\dots}|_k = T^{\mu\nu\dots}_{;\alpha} h_\mu^i h_\nu^j \dots h_k^\alpha. \quad (2.17)$$

Let us consider the projection of Einstein's equation. Einstein's equation is written as

$$R_{\mu\nu} - \frac{1}{2}g_{\mu\nu}R = 8\pi T_{\mu\nu}. \quad (2.18)$$

The projection should be done along the time coordinate and on $\Sigma(t)$. Therefore, Einstein's equation in the (3+1) formalism is expressed as

- 1) $G_{\mu\nu}n^\mu n^\nu = 8\pi\rho_H \equiv 8\pi T_{\mu\nu}n^\mu n^\nu,$
- 2) $G_{\mu\nu}n^\mu h_i^\nu = -8\pi J_i \equiv 8\pi T_{\mu\nu}n^\mu h_i^\nu$
- 3) $G_{\mu\nu}h_i^\mu h_j^\nu = 8\pi S_{ij} \equiv 8\pi T_{\mu\nu}h_i^\mu h_j^\nu,$

where ρ_H and J_i correspond to the energy and the momentum density observed by the normal observer, respectively. Consequently, we have

1) the Hamiltonian constraint equation;

$${}^{(3)}R + K^2 - K_{ij}K^{ij} = 16\pi\rho_H, \quad (2.19)$$

2) the momentum constraint equation;

$$K_i^j|_j - K_{lj} = 8\pi J_i, \quad (2.20)$$

3) the evolution of the metric tensor;

$$\begin{aligned} \frac{\partial}{\partial t} K_{ij} &= \alpha({}^{(3)}R_{ij} + KK_{ij}) - 2\alpha K_{il}K^l_j \\ &\quad - 8\pi\alpha(S_{ij} + \frac{1}{2}\gamma_{ij}(\rho_H - S^l_l)) - \alpha_{lj} + \beta^m_{lj}K_{mi} + \beta^m_{li}K_{mj} + \beta^m_{lj|m}, \end{aligned} \quad (2.21)$$

where K is the trace of K_{ij} and ${}^{(3)}R_{ij}$ is the Ricci tensor with respect to γ_{ij} . Einstein's equation has originally ten components and they are decomposed into the four constraint equations (2.19-2.20) and six evolution equations (2.21).

Equations of motion of the relativistic fluid is derived by the Bianchi identities;

$$T_{\mu}^{\nu}_{;\nu} = \frac{1}{8\pi} \left(R_{\mu}^{\nu} - \frac{1}{2} \delta_{\mu}^{\nu} R \right)_{;\nu} = 0, \quad (2.22)$$

If we assume a matter as the perfect fluid, $T_{\mu\nu}$ is

$$T_{\mu\nu} = (\rho + \rho\epsilon + P)u_{\mu}u_{\nu} + Pg_{\mu\nu}, \quad (2.23)$$

where ρ , ϵ , P and u_{μ} are the rest mass density, the specific internal energy, the pressure, and the four velocity, respectively.

Let us rewrite the dynamical equation of matter with the analogy of the Newtonian dynamics (2.1)-(2.3). Before writing down the concrete form of the equation, we define the basic variables as

$$\rho_* \equiv \rho\alpha u^t \sqrt{\gamma}, \quad (2.24)$$

$$v^i \equiv \frac{u^i}{u^t}, \quad (2.25)$$

$$\hat{u}^i \equiv hu_i, \quad (2.26)$$

$$\hat{e} \equiv \frac{\sqrt{\gamma}}{\rho_*} T_{\mu\nu} n^{\mu} n^{\nu} = hau^t - \frac{P}{\rho\alpha u^t}, \quad (2.27)$$

$$\omega \equiv \alpha u^t, \quad (2.28)$$

where $h = 1 + e + P/\rho$ is relativistic enthalpy and w is relativistic Lorenz factor and $\gamma = \det(\gamma_{ij})$.

(1) Mass conservation equation ($(\rho u^{\mu})_{;\mu} = 0$)

$$\partial_t \rho_* + \partial_i (\rho_* v^i) = 0, \quad (2.29)$$

(2) Euler equations ($h_m^{\mu} T_{\mu}^{\nu}_{;\nu} = 0$)

$$\partial_t (\rho_* \hat{u}_j) + \partial_i (\rho_* v^i \hat{u}_j) = -\alpha \sqrt{\gamma} \partial_j P - \rho_* \sqrt{\gamma} \left[wh \partial_j \alpha - u^i \partial_j \beta^i + \frac{\hat{u}_k \hat{u}_l}{2u^t h} \partial_j \gamma^{kl} \right], \quad (2.30)$$

(3) Energy equation ($n^{\mu} T_{\mu}^{\nu}_{;\nu} = 0$)

$$\partial_t (\rho_* \hat{e}) + \partial_i \left[\rho_* v^i \hat{e} + P \sqrt{\gamma} (v^i + \beta^i) \right] = \alpha \sqrt{\gamma} PK + \frac{\rho_*}{u^t h} \hat{u}_k \hat{u}_l K^{kl} - \rho_* \hat{u}_i \gamma^{ij} \partial_i \alpha, \quad (2.31)$$

(4) Equation of state

$$P = P(\epsilon, \rho). \quad (2.32)$$

The advantage of (2.29) to (2.31) is that by regarding α as a gravitational potential their form strongly resembles that of the Newtonian mechanics. This is due to the fact that the acceleration of normal line observer is proportional to the gradient of α .

Equations (2.30-2.31) have a nontrivial relation with Eqs. (2.19-2.21). Let us define a tensor $A_{\mu\nu}$ by

$$A_{\mu\nu} \equiv R_{\mu\nu} - \frac{1}{2}g_{\mu\nu}R - 8\pi T_{\mu\nu}. \quad (2.33)$$

Einstein's equation correspond to $A_{\mu\nu} = 0$. The Hamiltonian constraint (2.19), the momentum constraint (2.20), and the evolution equation (2.21) are

$$H_0 \equiv n^\mu n^\nu A_{\mu\nu} = 0, \quad (2.34)$$

$$H_\alpha \equiv -n^\mu h_\alpha^\nu A_{\mu\nu} = 0, \quad (2.35)$$

and

$$H_{\alpha\beta} \equiv h_\alpha^\mu h_\beta^\nu A_{\mu\nu} = 0. \quad (2.36)$$

Let us assume that the the evolution equations (2.21), $H_{\alpha\beta} = 0$, and the equation of motion of the fluid, $T^{\mu\nu}_{;\nu} = 0$, hold. H_0 and H_α would not be equal to zero in general. $A_{\mu\nu}$ is expressed as

$$A_{\mu\nu} = H_{\mu\nu} + n_\mu H_\nu + n_\nu H_\mu + n_\mu n_\nu H_0. \quad (2.37)$$

With $H_{\alpha\beta} = 0$, it can be reduced to

$$A_{\mu\nu} = n_\mu H_\nu + n_\nu H_\mu + n_\mu n_\nu H_0. \quad (2.38)$$

The Bianchi identities guarantee

$$A^{\mu\nu}_{;\nu} = 0. \quad (2.39)$$

If we multiply Eq. (2.39) by n^μ and h^μ_i and substitute Eq. (2.38), we obtain

$$\left(\frac{\partial}{\partial t} - \beta^l \frac{\partial}{\partial x^l}\right)H_0 = -\frac{1}{\sqrt{\gamma}} \frac{\partial}{\partial x^l}(\sqrt{\gamma}H^l) + \alpha KH_0 - 2H^l \frac{\partial \alpha}{\partial x^l} \quad (2.40)$$

and

$$\frac{\partial H_i}{\partial t} - \beta^l H_{il} = \alpha KH_i + \beta_{il} H^l - \frac{\partial \alpha}{\partial x^i} H_0. \quad (2.41)$$

Equations (2.40) and (2.41) implies that H_0 and H_i remain to be zero for $t > 0$ once $H_0 = 0$ and $H_i = 0$ are satisfied on $t = 0$ plane. This leads a important consequence: Given an initial data which satisfies the constraint equation (2.19) and (2.20), the evolution according to the Eqs. (2.16, 2.21, 2.29, 2.32) guarantees that we obtain a solution of Einstein's equation on any time slice. Finally, let us consider d.o.f of the system. γ_{ij} and K_{ij} have the twelve d.o.f. Using the four constraint equations, d.o.f is reduced to eight. Furthermore, if we determine the lapse function α and the shift vector β^i , the four d.o.f are vanished. As a result, the true freedom of the system is four. These residual freedoms represent gravitational wave.

Procedure to solve Einstein's equation as initial value problem is as follows:

Step 0

Give distributions of ρ , u^μ , and e .

Solve Eqs. (2.19)-(2.20) to determine the metric γ_{ij} and K_{ij} at $t = 0$.

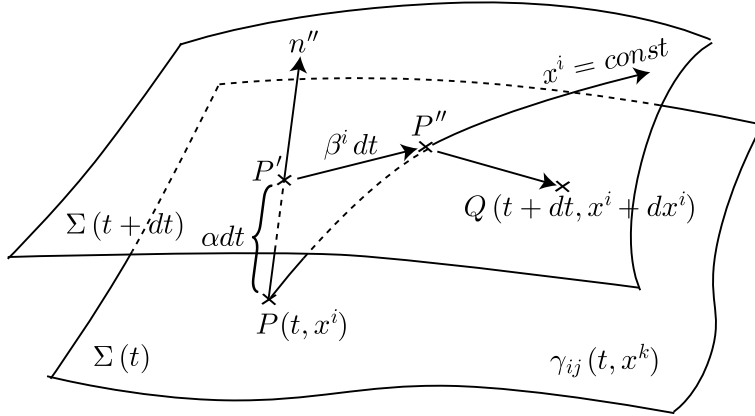


Figure 2.1: The 3+1 decomposition

Step 1Determine α, β^i to fix gauge conditionStep 2Update hydrodynamical variables to $t = t + \Delta t$ with Eqs. (2.29)-(2.32)
Update geometrical variables to $t = t + \Delta t$ with Eqs. (2.16) and (2.21)Step 3Update t to $t + \Delta t$
Return to Step 1

2.3 Linear perturbation theory and Quadrupole formula

In Sec. 2.2, we review Einstein's equation has a non-trivial solution, gravitational waves, and show a procedure to solve these equations. However, in general, it is difficult to solve Einstein's equation directly, which is called numerical relativity. Alternative approach is a perturbation theory and this method greatly simplifies the field equations. Quadrupole formula is one of most famous formula in the linear perturbation theory to estimate gravitational wave and is widely used in numerical simulations. This section is devoted to review this approach and associated topics.

2.3.1 Perturbed Einstein's equation

First, let us consider the case $T = 0$ in Einstein's equation

$$R_{\mu\nu} - \frac{1}{2}g_{\mu\nu}R = 0. \quad (2.42)$$

We also assume that the metric $g_{\mu\nu}$ slightly deviates from the Minkowski metric $\eta_{\mu\nu}$

$$g_{\mu\nu} = \eta_{\mu\nu} + h_{\mu\nu}, \quad (2.43)$$

where $h_{\mu\nu}$ is a tensor representing perturbation and $|h_{\mu\nu}| \ll 1$. A perturbed Riemann tensor of the first order smallness is given with respect to the metric perturbation $h_{\mu\nu}$:

$$\delta R_{\mu\nu\alpha\beta} = \frac{1}{2}(h_{\mu\beta,\nu\alpha} + h_{\nu\alpha,\mu\beta} - h_{\nu\beta,\mu\alpha} - h_{\mu\alpha,\nu\beta}). \quad (2.44)$$

An inverse of matrix $g^{\mu\nu}$ is defined by $g_{\mu\nu}$ and the form of the first order smallness is

$$g^{\mu\nu} = \eta^{\mu\nu} - h^{\mu\nu}. \quad (2.45)$$

We can raise or lower tensor indices using the background tensor $\eta_{\mu\nu}$. A perturbed Ricci tensor is

$$\delta R_{\nu\beta} = \frac{1}{2}(h^\mu{}_{\beta,\mu\nu} + h^\mu{}_{\nu,\mu\beta} - h_{\nu\beta,\mu}{}^\mu - h^\mu{}_{\mu,\nu\beta}), \quad (2.46)$$

where $\delta R_{\nu\beta}$ is a first order of smallness. Subsequently, a scalar curvature is obtained by

$$\delta R = (h^{\mu\beta}{}_{,\beta\mu} - h^\mu{}_\mu{}^{\beta}{}_{,\beta}). \quad (2.47)$$

Therefore we can obtain the linearized Einstein's equation as follow:

$$h^\rho{}_{\mu,\rho\nu} + h^\rho{}_{\nu,\rho\mu} - h_{\mu\nu}{}^\rho{}_{,\rho} - h^\rho{}_{\rho,\mu\nu} - \eta_{\mu\nu}(h^{\rho\sigma}{}_{,\sigma\rho} - h^\rho{}_\rho{}^{\sigma}{}_{,\sigma}) = 0. \quad (2.48)$$

To simplify Eq. (2.48), we introduce new functions defined by

$$\begin{aligned} \bar{h}_{\mu\nu} &\equiv h_{\mu\nu} - \frac{1}{2}\eta_{\mu\nu}h, \\ h &\equiv h^\rho{}_\rho. \end{aligned} \quad (2.49)$$

Using these functions, Eq. (2.48) is rewritten

$$\bar{h}^\rho{}_{\mu,\rho\nu} + \bar{h}^\rho{}_{\nu,\rho\mu} - \bar{h}_{\mu\nu}{}^\rho{}_{,\rho} - \eta_{\mu\nu}\bar{h}^\rho{}_{\sigma,\rho} = 0. \quad (2.50)$$

To simplify linearized Einstein's equation (2.50) more, we make use of d.o.f of gauge condition, α, β^i in Sec. 2.2. The harmonic condition is one of useful gauge to achieve this purpose,

$$\bar{h}^{\mu\alpha}{}_{,\alpha} = 0. \quad (2.51)$$

Imposing this condition, Eq. (2.50) is reduced to

$$\bar{h}_{\mu\nu,\alpha}{}^\alpha = 0. \quad (2.52)$$

However, the condition Eq. (2.51) does not fix the gauge uniquely. Consider the infinitesimal coordinate transformation

$$x'^\mu = x^\mu + \xi^\mu \quad (2.53)$$

with

$$\xi_{\mu,\alpha}{}^\alpha = 0. \quad (2.54)$$

This transformation changes $\bar{h}_{\mu\nu}$ into

$$\bar{h}'_{\mu\nu} = \bar{h}_{\mu\nu} - \xi_{\mu,\nu} - \xi_{\nu,\mu} + \eta_{\mu\nu}\xi^\alpha{}_{,\alpha} \quad (2.55)$$

and Eqs. (2.51) and (2.52) are kept unchanged. Therefore, the gauge freedom, which satisfies the condition Eq. (2.54), still remains. To extract a physical d.o.f in $h_{\mu\nu}$, we show a simple example as follows.

Now we consider a monochromatic plane wave with the wave number k . Thus the metric perturbations are written

$$h_{\mu\nu} = e_{\mu\nu}e^{ik_\alpha x^\alpha}, \quad (2.56)$$

where $e_{\mu\nu}$ is a symmetric tensor representing polarization. Equation (2.56) must be satisfied the condition (2.51). Therefore we obtain

$$k_\nu e^\nu_\mu - \frac{1}{2} k_\mu e^\rho_\rho = 0. \quad (2.57)$$

Because Eq. (2.56) is the solution of Eq. (2.52), we obtain

$$(e_{\mu\nu} - \frac{1}{2} \eta_{\mu\nu} e^\rho_\rho) k^\alpha k_\alpha = 0. \quad (2.58)$$

This equation is satisfied if $k^\alpha k_\alpha = 0$.

At first, using the freedom of ξ^μ , we make the form of $e_{\mu\nu}$ simple. Assume that ξ^μ is also expanded by a monochromatic plane wave,

$$\xi^\mu = i c^\mu e^{ik_\alpha x^\alpha}, \quad (2.59)$$

where c^μ is a constant vector. Equation (2.54) is automatically satisfied if $k^\alpha k_\alpha = 0$. Substituting (2.59) to (2.55), we obtain

$$e'_{\mu\nu} = e_{\mu\nu} + k_\mu c_\nu + k_\nu c_\mu. \quad (2.60)$$

For simplicity, we choose a spacial direction of k^μ as z axis

$$k^1 = k^2 = 0, \quad k^0 = k^3 \equiv k > 0. \quad (2.61)$$

It is obvious that $e_{0\mu}$ corresponds to a gauge freedom in 3+1 formalism, α, β^i (see Sec. 2.2). So, using Eq. (2.61), we choose c_μ as $e'_{00} = e'_{0i} = 0$ is satisfied, that is

$$e'_{00} = e_{00} + 2k_0 c_0 = 0, \quad (2.62)$$

$$e'_{0i} = e_{0i} + k_0 c_i + k_i c_0 = 0. \quad (2.63)$$

Therefore, c_μ is fixed as

$$c_0 = \frac{e_{00}}{2k}, \quad c_1 = \frac{e_{01}}{k}, \quad c_2 = \frac{e_{02}}{k}, \quad c_3 = \frac{e_{03} + kc_0}{k}. \quad (2.64)$$

From now on, we drop subscript ' because Eq. (2.57) is invariant under the gauge transformation (2.53). Next task is to search the components of $h_{\mu\nu}$ which can be eliminated by virtue of the harmonic condition (2.57). Eq. (2.57) can be written by using Eqs. (2.62) and (2.63) as

$$ke_{3\mu} - \frac{1}{2} k_\mu (e_{11} + e_{22} + e_{33}) = 0. \quad (2.65)$$

If we choose $\mu = 0$, we obtain $e_{30} = e_{03} = 0$ and consequently obtain

$$e_{11} + e_{22} + e_{33} = 0. \quad (2.66)$$

Using Eq. (2.66), Eq. (2.65) means

$$e_{3l} = 0. \quad (2.67)$$

Choosing $l = 3$, we obtain $e_{33} = 0$ and therefore Eq. (2.66) becomes $e_{11} + e_{22} = 0$. Thus we can express a explicit form of $e_{\mu\nu}$ as

$$e_{\mu\nu} = \begin{pmatrix} 0 & 0 & 0 & 0 \\ 0 & e_{11} & e_{12} & 0 \\ 0 & e_{12} & -e_{11} & 0 \\ 0 & 0 & 0 & 0 \end{pmatrix}. \quad (2.68)$$

Therefore we can set tensor as

$$\begin{aligned} h_{xx} &= -h_{yy} \equiv h_+, \\ h_{xy} &= h_{yx} \equiv h_x. \end{aligned} \quad (2.69)$$

In the consequence, the metric can be written as

$$ds^2 = -dt^2 + (1 + h_+)dx^2 + (1 - h_+)dy^2 + 2h_x dxdy + dz^2, \quad (2.70)$$

where h_+ and h_x are the functions of $t \pm z$. The waves of + sign and - sign propagate inward and outward, respectively. As a result, only e_{11} and e_{22} remain as the components which can not be eliminated by the coordinate transformation. This is gravitational wave propagating in flat spacetime and wave has two independent polarization, h_+ and h_x .

Although, in this discussion, d.o.f of gravitational waves is two, $e_{\mu\nu}$ should be defined as complex number and $h_{\mu\nu}$ is expressed with respect to $e_{\mu\nu}$ as

$$\begin{aligned} h_{\mu\nu} &= \text{Re}(e_{\mu\nu} e^{ik_a x^\alpha}), \\ \dot{h}_{\mu\nu} &= -k_0 \text{Im}(e_{\mu\nu} e^{ik_a x^\alpha}). \end{aligned}$$

This result is consistent with one shown in Sec. 2.2.

Although in this discussion we choose a spatial direction of k^μ as z axis, in general Eq. (2.69) means

$$\begin{aligned} h &= 0, \quad (\text{traceless}) \\ h_i^j, j &= 0. \quad (\text{transverse}) \end{aligned} \quad (2.71)$$

The coordinate satisfying the condition (2.71) is called Transverse-Traceless (TT) gauge. TT gauge is essential to estimate gravitational wave. Why? The answer is as follow: gravitational waves are not the unique solution of Eq. (2.48), the basic equation in this section. From the Newton limit of Einstein equations, the stationary solution, which describes a gravitational field around the point mass M , is

$$\begin{aligned} g_{00} &= -\left(1 - \frac{2GM}{c^2 r}\right), \\ g_{0i} &= 0, \\ g_{ij} &= \delta_{ij}. \end{aligned} \quad (2.72)$$

Considering a distance r_0 which is sufficiently far from the point mass, we can set

$$\epsilon \equiv \frac{2GM}{c^2 r_0} \ll 1, \quad (2.73)$$

$$g_{00} = -1 + \epsilon \frac{r_0}{r}. \quad (2.74)$$

This equation shows that Eq. (2.72) is written as

$$g_{\mu\nu} = \eta_{\mu\nu} + \epsilon h_{\mu\nu}, \quad (2.75)$$

and that Eq. (2.48) can contain the static solution. Moreover, if an arbitrary solution $h_{\mu\nu}$ is given in an arbitrary coordinate condition, the freedom of coordinate transformation is also mixed in the solution. So, to extract gravitational waves from the solution, we have to find TT components in the solution. How do we extract TT component? In general, it is difficult to

separate TT component from solution. However, assuming that we can expand solution with plane wave solution, we can easily extract TT component.

Define a direction vector of gravitational waves with a wave vector k_i as

$$n_i = \frac{k_i}{k}, \quad (2.76)$$

where k is a wave number. A projection tensor P_{ij} which makes an arbitrary vector transverse is

$$P_{ij} = \delta_{ij} - n_i n_j. \quad (2.77)$$

Thus for a given $h_{\mu\nu}$,

$$h_{ij}^T = P_i^l P_j^m h_{lm} \quad (2.78)$$

is transverse. As the same manner, we can extract the TT components of $h_{\mu\nu}$ as

$$h_{ij}^{TT} = (P_i^l P_j^m - \frac{1}{2} P_{ij} P^{lm}) h_{lm}. \quad (2.79)$$

In reality, the plane wave approximation (2.56) is reasonable, because observer, e.g., on the earth, is far from gravitational wave source.

2.3.2 Conservation Law and Conserved variables

In this subsection, we consider the energy conservation law in general relativity. From the presence of Bianchi identities, we can obtain the energy momentum conservation law of matter (especially of perfect fluid). The conservation law is

$$T^{\mu\nu}_{;\nu} = 0. \quad (2.80)$$

If we expand a covariant derivative, Eq. (2.80) is expressed as

$$\frac{1}{\sqrt{-g}} \frac{\partial}{\partial x^\nu} \sqrt{-g} T_\mu^\nu - \frac{1}{2} \frac{\partial g_{\alpha\beta}}{\partial x^\mu} T^{\alpha\beta} = 0. \quad (2.81)$$

Integrating Eq. (2.81), we obtain

$$0 = \int \frac{\partial}{\partial x^\nu} (\sqrt{-g} T_\mu^\nu) d^4x - \int \frac{1}{2} \frac{\partial g_{\alpha\beta}}{\partial x^\mu} T^{\alpha\beta} \sqrt{-g} d^4x. \quad (2.82)$$

If $g_{\alpha\beta} = const.$, the second term of Eq. (2.82) vanishes and using the Gauss's theorem we can obtain the result that $\int T_\mu^0 \sqrt{-g} d^3x$ is conserved. In general, the second term of Eq. (2.82) is not zero, we are unable to derive a conservation law from Eq. (2.82). Although there is no local conservation law in general relativity, we can derive a global conservation law. From Eq. (2.50), the perturbed Einstein tensor of the first order smallness is

$$2\delta G_{\mu\nu} = \bar{h}_{\mu,\rho\nu}^\rho + \bar{h}_{\nu,\rho\mu}^\rho - \bar{h}_{\mu\nu}^{\rho,\rho} - \eta_{\mu\nu} \bar{h}_{\sigma,\rho}^{\rho,\sigma}. \quad (2.83)$$

Let us define a four-rank tensor $H_{MTW}^{\mu\alpha\nu\beta}$

$$H_{MTW}^{\mu\alpha\nu\beta} \equiv -(\bar{h}^{\mu\nu} \eta^{\alpha\beta} + \eta^{\mu\nu} \bar{h}^{\alpha\beta} - \bar{h}^{\alpha\nu} \eta^{\mu\beta} - \bar{h}^{\mu\beta} \eta^{\alpha\nu}), \quad (2.84)$$

where the index MTW means Misner, Thorne and Wheeler. $H^{\mu\alpha\nu\beta}$ has the same symmetry of Riemann tensor, that is

$$\begin{aligned} H_{\text{MTW}}^{\alpha\mu\nu\beta} &= -H_{\text{MTW}}^{\mu\alpha\nu\beta}, \quad H_{\text{MTW}}^{\mu\alpha\beta\nu} = -H_{\text{MTW}}^{\mu\alpha\nu\beta} \\ H_{\text{MTW}}^{\mu\alpha\nu\beta} + H_{\text{MTW}}^{\mu\nu\beta\alpha} + H_{\text{MTW}}^{\mu\beta\alpha\nu} &= 0. \end{aligned} \quad (2.85)$$

Using this tensor, the perturbed Einstein tensor is expressed as

$$2\delta G^{\mu\nu} = H_{\text{MTW},\alpha\beta}^{\mu\alpha\nu\beta}. \quad (2.86)$$

Taking the partial derivative with respect to x^ν in Eq. (2.86) and using the antisymmetry of $H_{\text{MTW}}^{\mu\alpha\nu\beta}$, we obtain

$$\delta G^{\mu\nu}_{,\nu} = 0. \quad (2.87)$$

This is the Bianchi identities in the linear perturbation theory. Thus, starting from Eq. (2.86) and using Einstein's equation, we obtain

$$\begin{aligned} H_{\text{MTW},\alpha\beta}^{\mu\alpha\nu\beta} &= 2\delta G^{\mu\nu} \\ &= 2G^{\mu\nu} + 2(\delta G^{\mu\nu} - G^{\mu\nu}) \\ &= 16\pi(T^{\mu\nu} + t^{\mu\nu}), \end{aligned} \quad (2.88)$$

where $t^{\mu\nu}$ is defined as

$$\begin{aligned} 16\pi t^{\mu\nu} &\equiv 2(\delta G^{\mu\nu} - G^{\mu\nu}) \\ &= H_{\text{MTW},\alpha\beta}^{\mu\alpha\nu\beta} - 2G^{\mu\nu}. \end{aligned} \quad (2.89)$$

Note that $t^{\mu\nu}$ is of the second order smallness. From Eq. (2.88), a conservation law is derived as

$$(T^{\mu\nu} + t^{\mu\nu})_{,\nu} = 0. \quad (2.90)$$

Therefore total energy P^0 and total momentum P^i

$$P^\mu \equiv \int (T^{0\mu} + t^{0\mu}) d^3x \quad (2.91)$$

are conserved quantities. The volume integration in Eq. (2.91) is carried out as

$$\begin{aligned} P^\mu &= \frac{1}{16\pi} \int H_{\text{MTW},\alpha\beta}^{\mu\alpha 0\beta} d^3x \\ &= \frac{1}{16\pi} \int H_{\text{MTW},\alpha j}^{\mu\alpha 0j} d^3x \\ &= \frac{1}{16\pi} \oint H_{\text{MTW},\alpha}^{\mu\alpha 0j} d^2S_j, \end{aligned} \quad (2.92)$$

where the second equality and the third one hold by virtue of Eq. (2.85) and the Gauss's law, respectively.

The choice of $H^{\mu\alpha\nu\beta}$ is not unique. The tensor $H^{\mu\alpha\nu\beta}$ defined by Landau and Lifshitz in [65] is

$$H_{\text{LL}}^{\mu\alpha\nu\beta} \equiv (-g)(g^{\mu\nu}g^{\alpha\beta} - g^{\mu\alpha}g^{\nu\beta}). \quad (2.93)$$

Assuming that $g_{\mu\nu} = \eta_{\mu\nu} + h_{\mu\nu}$ in Eq. (2.93) and taking the first order smallness quantities, we can easily prove

$$H_{\text{LL}}^{\mu\alpha\nu\beta} = H_{\text{MTW}}^{\mu\alpha\nu\beta}. \quad (2.94)$$

Using the same manner in Eq. (2.86), the perturbed Einstein equation can be rewritten with respect to the $H_{\text{LL}}^{\mu\alpha\nu\beta}$ as

$$H_{\text{LL},\alpha\beta}^{\mu\alpha\nu\beta} = 16\pi(-g)(T^{\mu\nu} + t_{\text{LL}}^{\mu\nu}). \quad (2.95)$$

A local conservation law and conserved quantity are

$$((-g)(T^{\mu\nu} + t_{\text{LL}}^{\mu\nu}))_{,\nu} = 0, \quad (2.96)$$

$$P^\mu = \int (-g)(T^{\mu 0} + t_{\text{LL}}^{\mu 0}) d^3x, \quad (2.97)$$

where $t_{\text{LL}}^{\mu\nu}$ is the Landau-Lifshitz's pseudo energy-momentum tensor and its concrete form is

$$\begin{aligned} (-g)t_{\text{LL}}^{\alpha\beta} &= \frac{1}{16\pi} [\tilde{g}_{,\lambda}^{\alpha\beta}\tilde{g}_{,\mu}^{\lambda\mu} - \tilde{g}_{,\lambda}^{\alpha\lambda}\tilde{g}_{,\mu}^{\beta\mu} + \frac{1}{2}g^{\alpha\beta}g_{\lambda\mu}\tilde{g}_{,\nu}^{\lambda\nu}\tilde{g}_{,\rho}^{\rho\mu} - (g^{\alpha\lambda}g_{\mu\nu}\tilde{g}_{,\rho}^{\beta\nu}\tilde{g}_{,\lambda}^{\mu\rho} + g^{\beta\lambda}g_{\mu\nu}\tilde{g}_{,\rho}^{\alpha\nu}\tilde{g}_{,\lambda}^{\mu\rho}) \\ &\quad + g_{\lambda\mu}g^{\nu\rho}\tilde{g}_{,\nu}^{\alpha\lambda}\tilde{g}_{,\rho}^{\beta\mu} + \frac{1}{8}(2g^{\alpha\lambda}g^{\beta\mu} - g^{\alpha\beta}g^{\lambda\mu})(2g_{\nu\rho}g_{\sigma\tau} - g_{\rho\sigma}g_{\nu\tau})\tilde{g}_{,\lambda}^{\nu\tau}\tilde{g}_{,\mu}^{\rho\sigma}], \end{aligned} \quad (2.98)$$

The meaning of pseudo is both $t_{\text{LL}}^{\mu\nu}$ and $t_{\text{MTW}}^{\mu\nu}$ are not tensor because its definition contains the derivative of $g_{\mu\nu}$, which can be reduced to zero by equivalent principle. Thus, we cannot prove P^μ , which is expressed as the surface integral of $H^{\mu\alpha\nu\beta}$ at spacial infinity, is invariant for general coordinate transformation. However, if a spacetime is asymptotically flat, P^μ is proved to be invariant (see [65] in details).

Angular momentum tensor $J^{\mu\nu}$ is also defined as

$$\begin{aligned} J^{\mu\nu} &\equiv \int \sqrt{-g} \{x^\mu(T^{\nu 0} + t_{\text{LL}}^{\nu 0}) - x^\nu(T^{\mu 0} + t_{\text{LL}}^{\mu 0})\} d^3x \\ &= \frac{1}{16\pi} \int (x^\mu H_{\text{LL}}^{\mu\alpha 0\beta}_{,\alpha\beta} - x^\nu H_{\text{LL}}^{\nu\alpha 0\beta}_{,\alpha\beta}) d^3x \\ &= \frac{1}{16\pi} \oint (x^\mu H_{\text{LL}}^{\nu\alpha 0j}_{,\alpha} - x^\nu H_{\text{LL}}^{\mu\alpha 0j}_{,\alpha} + H_{\text{LL}}^{\mu j 0\nu} - H_{\text{LL}}^{\nu j 0\mu}) d^2S_j, \end{aligned} \quad (2.99)$$

where the second equality and the third one hold by virtue of Eq. (2.89) and the Gauss's law, respectively.

2.3.3 Energy, Momentum and Angular Momentum of Gravitational Wave

In the previous subsection, we derive the conservation law in the general relativity, especially the *local* conservation law. How about gravitational waves? How can we define stress-energy tensor of gravitational wave? Landau-Lifshitz pseudo tensor (2.98) can not be used for this purpose because it can always be set as zero with the equivalence principal. The answer for this question is nonlinear effect of Einstein's equation. This subsection is devoted how stress energy tensor of gravitational waves can be defined by use of the nonlinear effect.

At first, let us set the order of magnitude of background Riemann tensor as $O(L^{-2})$, where L is the order of magnitude of curvature radius. We also define wave length of gravitational

waves as λ . In a region $\lambda/L \ll 1, \epsilon \ll 1^1$, gravitational waves are expressed as

$$\bar{h}_{\mu\nu\rho}^{|\rho} = 0, \quad (2.100)$$

where $|$ denotes the covariant derivative with respect to the background metric $g_{\mu\nu}^{(B)}$. Although orders of magnitude of g^B and h are unity, its gradient is estimated as

$$\partial g^{(B)} \sim \frac{1}{L}, \quad \partial h \sim \frac{1}{\lambda}. \quad (2.101)$$

Furthermore, a second order of magnitude of $G^{\mu\nu}$ in terms of ϵ is $\epsilon^2 \lambda^{-2}$. Taking this tensor as the energy-momentum tensor of gravitational wave, $T_{\mu\nu}^{\text{GW}} = O(\epsilon^2 \lambda^{-2})$ is obtained. Because $G_{\mu\nu}^{(0)}$ is $O(L^{-2})$, a condition that gravitational waves do not affect on the background is given as

$$L^{-2} \gg 8\pi T_{\mu\nu}^{\text{GW}} \sim \left(\frac{\epsilon}{\lambda}\right)^2. \quad (2.102)$$

This condition can be read as

$$\epsilon \ll \frac{\lambda}{L} \ll 1. \quad (2.103)$$

Conversely if $\epsilon \simeq \lambda L^{-1}$, the nonlinear effects will influence the background. Subsequently, we expand the Ricci tensor as follow:

$$R_{\mu\nu}(g_{\alpha\beta}^{(B)} + \epsilon h_{\alpha\beta}) = R_{\mu\nu}^{(0)} + \epsilon R_{\mu\nu}^{(1)} + \epsilon^2 R_{\mu\nu}^{(2)} + O(\epsilon^3), \quad (2.104)$$

where

$$R_{\mu\nu}^{(0)} = R_{\mu\nu}(g_{\alpha\beta}^{(B)}), \quad (2.105)$$

$$R_{\mu\nu}^{(1)} = \frac{1}{2}(-h_{\mu\nu\rho}^{|\rho} - h_{\mu\nu|\rho}^{|\rho} + h_{\mu\rho}^{|\rho}{}_{|\nu} + h_{\nu\rho}^{|\rho}{}_{|\mu}), \quad (2.106)$$

$$\begin{aligned} R_{\mu\nu}^{(2)} = & \frac{1}{2}\{\frac{1}{2}h^{\rho\tau}{}_{|\nu}h_{\rho\tau|\mu} \\ & + h^{\rho\tau}(h_{\tau\rho|\mu\nu} + h_{\mu\nu|\tau\rho} - h_{\tau\mu|\nu\rho} - h_{\tau\nu|\mu\rho}) \\ & + h_{\nu}{}^{\tau|\rho}(h_{\tau\mu|\rho} - h_{\rho\mu|\tau}) \\ & - (h^{\tau\rho}{}_{|\rho} - \frac{1}{2}h^{|\tau})(h_{\tau\mu|\nu} + h_{\tau\nu|\mu} - h_{\mu\nu|\tau})\}. \end{aligned} \quad (2.107)$$

Now we assume vacuum, $R_{\mu\nu} = 0$. Note that the covariant derivative of $h_{\mu\nu}$ is communicative because the non-communicative part is proportional to the background Riemann tensor and therefore such parts is higher order term.

Orders of the expansion terms in Eq. (2.104) are

$$R_{\mu\nu}^{(0)} = O(L^{-2}), \quad \epsilon R_{\mu\nu}^{(1)} = O\left(\frac{\epsilon}{\lambda^2}\right), \quad \epsilon^2 R_{\mu\nu}^{(2)} = O\left(\frac{\epsilon^2}{\lambda^2}\right). \quad (2.108)$$

If $\epsilon \sim \lambda L^{-1}$, the orders are

$$R_{\mu\nu}^{(0)} = O(L^{-2}), \quad \epsilon R_{\mu\nu}^{(1)} = O\left(\frac{1}{L\lambda}\right), \quad \epsilon^2 R_{\mu\nu}^{(2)} = O\left(L^{-2}\right). \quad (2.109)$$

¹We set the metric perturbation as $g_{\mu\nu} = \bar{g}_{\mu\nu}^{(B)} + \epsilon h_{\mu\nu}$ in this subsection.

Because the short wave length limit, $\lambda/L \ll 1$, is read as $O(L^{-2}) \ll O(1/L\lambda)$, the second term in Eq. (2.104) must be zero firstly,

$$R_{\mu\nu}^{(1)} = 0. \quad (2.110)$$

Eq. (2.110) is written as

$$\bar{h}_{\mu\nu\rho}^{\rho} - \bar{h}_{\mu\rho\nu}^{\rho} - \bar{h}_{\nu\rho\mu}^{\rho} + g_{\mu\nu}^{(B)} \bar{h}_{\sigma}^{\rho} \bar{h}_{\rho}^{\sigma} = 0, \quad (2.111)$$

where

$$\bar{h}_{\mu\nu} = h_{\mu\nu} - \frac{1}{2} g_{\mu\nu}^{(B)} h. \quad (2.112)$$

Secondly $R_{\mu\nu}^{(0)}$ and $\epsilon^2 R_{\mu\nu}^{(2)}$ become to the same order. Therefore we require

$$R_{\mu\nu}^{(0)} + \epsilon^2 R_{\mu\nu}^{(2)} = 0. \quad (2.113)$$

We rewrite this equation as

$$\begin{aligned} G_{\mu\nu}^{(0)} &= R_{\mu\nu}^{(0)} - g_{\mu\nu}^{(B)} \frac{1}{2} R^{(0)} \\ &= -\epsilon^2 (R_{\mu\nu}^{(2)} - \frac{1}{2} g_{\mu\nu}^{(B)} R_{\alpha\beta}^{(2)} g_{(B)}^{\alpha\beta}) \\ &\equiv 8\pi T_{\mu\nu}^{\text{GW}}, \end{aligned} \quad (2.114)$$

where

$$T_{\mu\nu}^{\text{GW}} \equiv -\frac{\epsilon^2}{8\pi} (R_{\mu\nu}^{(2)} - \frac{1}{2} g_{\mu\nu}^{(B)} R_{\alpha\beta}^{(2)} g_{(B)}^{\alpha\beta}). \quad (2.115)$$

Eq. (2.114) directly represents that the nonlinear effect of the gravitational waves influences the background spacetime. Furthermore we have to take an average, the Brill-Hartle average. The reason is as follow. The right-hand side of Eq. (2.115) contains the term such as $\partial h \cdot \partial h$. Therefore it contains components changing in short wave length. On the other hand, the left-hand side of Eq. (2.114) only contains the quantity changing in the length $L (\gg \lambda)$. Hence, $T_{\mu\nu}^{\text{GW}}$ must be averaged with a length d . The length d satisfies a condition, longer than λ and shorter than L . Concretely, the several wave length is appropriate for d . Symbol $\langle \rangle$ means such the kind of average. Hence we obtain

$$\langle T_{\mu\nu}^{\text{GW}} \rangle \equiv -\frac{\epsilon^2}{8\pi} \left(\langle R_{\mu\nu}^{(2)} \rangle - \frac{1}{2} g_{\mu\nu}^{(B)} \langle g_{(B)}^{\alpha\beta} R_{\alpha\beta}^{(2)} \rangle \right). \quad (2.116)$$

Finally, we show the concrete form of $T_{\mu\nu}^{\text{GW}}$.

$$T_{\mu\nu}^{\text{GW}} = \frac{\epsilon^2}{32\pi} \langle \bar{h}_{\alpha\beta|\mu} \bar{h}_{\nu}^{\alpha\beta} - \bar{h}_{\alpha\beta}^{\rho\alpha} (\bar{h}_{\mu|\nu}^{\beta} + \bar{h}_{\nu|\mu}^{\beta}) - \frac{1}{2} \bar{h}_{|\mu} \bar{h}_{|\nu} \rangle. \quad (2.117)$$

Such a average is called the Brill-Hartle average [49, 50, 32].

Note that $T_{\mu\nu}^{\text{GW}}$ defined in Eq. (2.117) is gauge invariant quantity.

2.3.4 Quadrupole Wave

From Eqs. (2.83) and (2.88), gravitational wave equation is given by

$$\bar{h}^{\mu\nu,\alpha}_{,\alpha} = -16\pi\tau^{\mu\nu}, \quad (2.118)$$

where we impose the harmonic gauge condition $\bar{h}^{\mu\nu}_{,\nu} = 0$. $\tau^{\mu\nu}$ is defined as

$$\tau^{\mu\nu} \equiv T^{\mu\nu} + t_{\text{MTW}}^{\mu\nu} \quad (2.119)$$

From the discussion in Sec. 2.3.2, $\tau^{\mu\nu}$ satisfy the conservation law

$$\tau^{\mu\nu}_{,\nu} = 0. \quad (2.120)$$

A general solution of (2.118) is

$$\bar{h}^{\mu\nu} = 4 \int \frac{\tau^{\mu\nu}(t - |\mathbf{x} - \mathbf{x}'|, \mathbf{x}')}{|\mathbf{x} - \mathbf{x}'|} d^3\mathbf{x}', \quad (2.121)$$

where we use the retarded Green function

$$G(\mathbf{x} - \mathbf{x}', t - t') = \frac{\delta(t - t' - |\mathbf{x} - \mathbf{x}'|)}{4\pi|\mathbf{x} - \mathbf{x}'|}, \quad (2.122)$$

which is a solution of wave equation

$$\square G = -\delta(\mathbf{x} - \mathbf{x}')\delta(t - t'), \quad (2.123)$$

In the local wave zone, r is estimated as

$$r = |\mathbf{x}| \gg |\mathbf{x}'| \sim L, \quad (2.124)$$

where L is typical size of source. Thus, $|\mathbf{x} - \mathbf{x}'|$ can be expanded as

$$\begin{aligned} |\mathbf{x} - \mathbf{x}'| &= r \left(1 - 2\mathbf{n} \cdot \frac{\mathbf{x}'}{r} + \frac{|\mathbf{x}'|^2}{r^2} \right)^{\frac{1}{2}} \\ &\simeq r \left(1 - \mathbf{n} \cdot \frac{\mathbf{x}'}{r} \right) \\ &\simeq r - \mathbf{n} \cdot \mathbf{x}', \end{aligned} \quad (2.125)$$

where $\mathbf{n} \equiv \mathbf{x}/r$.

On the other hand, as mentioned in Sec. 2.3.1, gravitational wave is the TT part of $h_{\mu\nu}$. This part is given by

$$h_{\text{TT}}^{ij} \equiv (P_k^i P_l^j - \frac{1}{2} P^{ij} P_{kl}) \bar{h}^{kl}, \quad (2.126)$$

where P_{ij} is the projection tensor defined in Eq. (2.77). Note that in TT gauge, h^{ij} and \bar{h}^{ij} coincide. Substituting Eqs. (2.125) and (2.126) for (2.121), the gravitational waves are estimated as

$$h_{\text{TT}}^{ij}(t, \mathbf{x}) = \frac{4}{r} \int \tau_{\text{TT}}^{ij}(t - r + \mathbf{n} \cdot \mathbf{x}', \mathbf{x}') d^3\mathbf{x}'. \quad (2.127)$$

If a motion of the source is slow, we can perform retarded expansion as follows [34]:

$$h_{\text{TT}}^{ij}(t, \mathbf{x}) = \frac{4}{r} \int \sum_{m=0}^{\infty} \frac{\partial^m}{\partial t^m} \tau_{\text{TT}}^{ij}(t - r, \mathbf{x}') \frac{(\mathbf{n} \cdot \mathbf{x}')^m}{m!} d^3\mathbf{x}'. \quad (2.128)$$

The slow motion approximation is defined as $v \ll 1$, where v is typical velocity of the source.

Equation (2.128) can be rewritten as following forms:

$$h_{\text{TT}}^{ij}(t, \mathbf{x}) = \frac{2}{r} \sum_{m=0}^{\infty} n_{k_1} n_{k_2} \cdots n_{k_m} \mathcal{T}_{\text{TT}}^{ijk_1 k_2 \cdots k_m}(t - r) \quad (2.129)$$

and

$$\mathcal{T}^{ijk_1 k_2 \cdots k_m} = \frac{2}{m!} \left(\frac{\partial}{\partial t} \right)^m \int \tau^{ij} x^{k_1} x^{k_2} \cdots x^{k_m} d^3 x. \quad (2.130)$$

Let us consider the lowest order case $m = 0$. Eq. (2.130) is

$$\mathcal{T}^{ij} = 2 \int \tau^{ij} d^3 x. \quad (2.131)$$

Using equation (2.120), Eq. (2.131) can be written as another form,

$$\begin{aligned} \tau^{ij} &= \tau^{il} \delta_l^j = \tau^{il} \frac{\partial x^j}{\partial x^l} = \frac{\partial(\tau^{il} x^j)}{\partial x^l} - \frac{\partial \tau^{il}}{\partial x^l} x^j \\ &= \frac{\partial(\tau^{il} x^j)}{\partial x^l} + \frac{\partial \tau^{0i}}{\partial t} x^j. \end{aligned} \quad (2.132)$$

where the last equality holds by Eq. (2.120). Similarly, τ^{0i} is rewritten as

$$\begin{aligned} \tau^{0i} &= \tau^{0l} \delta_l^i = \tau^{0l} \frac{\partial x^i}{\partial x^l} = \frac{\partial(\tau^{0l} x^i)}{\partial x^l} - \frac{\partial \tau^{0l}}{\partial x^l} x^i \\ &= \frac{\partial(\tau^{0l} x^i)}{\partial x^l} + \frac{\partial \tau^{00}}{\partial t} x^i, \end{aligned} \quad (2.133)$$

where the last equality holds by Eq. (2.120) again. Substituting Eq. (2.133) for Eq. (2.132) and using Eq. (2.120) again, we arrive

$$\tau^{ij} = \frac{\partial(\tau^{il} x^j)}{\partial x^l} - x^j \frac{\partial}{\partial x^l} \left(\frac{\partial \tau^{kl}}{\partial x^k} x^i \right) + \frac{\partial^2 \tau^{00}}{\partial t^2} x^i x^j. \quad (2.134)$$

The right-hand side of Eq. (2.134) can be rewritten more as

$$\tau^{ij} = \frac{\partial}{\partial x^l} (\tau^{il} x^j + \tau^{jl} x^i) - \tau^{ij} - \frac{\partial}{\partial x^l} \left(\frac{\partial \tau^{kl}}{\partial x^k} x^i x^j \right) + \frac{\partial^2 \tau^{00}}{\partial t^2} x^i x^j. \quad (2.135)$$

In Eq. (2.135), the divergence term is transformed into the surface integral by virtue of the Gauss's theorem and as a result vanish. Thus, the volume integral of Eq. (2.135) is

$$\int \tau^{ij} d^3 x = \frac{1}{2} \frac{\partial^2}{\partial t^2} \int \tau^{00} x^i x^j d^3 x. \quad (2.136)$$

Combining Eq. (2.136) with Eq. (2.131), \mathcal{T}^{ij} is given by

$$\mathcal{T}^{ij} = \frac{\partial^2}{\partial t^2} \int \tau^{00} x^i x^j d^3 x. \quad (2.137)$$

If we assume that the matter is the perfect fluid and $|v| \ll 1$, T^{00} is roughly estimated as

$$T^{00} \sim \rho \sim \frac{M}{L^3}. \quad (2.138)$$

On the other hand, if $|v| \ll 1$, the Newtonian gravitational potential is

$$\phi \sim \frac{M}{L} \ll 1. \quad (2.139)$$

Finally, t^{00} is estimated as

$$t^{00} \sim -\frac{3}{8\pi} \phi_{,k} \phi_{,k} \sim \frac{M^2}{L^4} \sim \frac{M}{L} T^{00} \ll T^{00}. \quad (2.140)$$

As a result, τ^{00} is estimated as

$$\tau^{00} = T^{00} + t^{00} = \rho(1 + O(\frac{M}{L})). \quad (2.141)$$

Substituting Eq. (2.141) for Eq. (2.137), we arrive

$$\mathcal{T}^{ij} \simeq \frac{\partial^2}{\partial t^2} \int \rho x^i x^j d^3x. \quad (2.142)$$

By the way, quadrupole moment of the mass distribution I_{ij} is given by

$$I_{ij} = \int \rho x^i x^j d^3x. \quad (2.143)$$

Note that \mathcal{T}^{ij} is expressed as the second time derivative of quadrupole moment I_{ij} . Performing TT projection, the gravitational wave is extracted as

$$h_{ij}^{TT}(t, \mathbf{x}) = \frac{2}{r} \frac{\partial^2}{\partial t^2} I_{ij}^{TT}(t-r), \quad (2.144)$$

where I_{ij} is a trace free part of I_{ij} and its definition is

$$I_{ij} = \int \rho(x^i x^j - \frac{1}{3} \delta_{ij} r^2) d^3x. \quad (2.145)$$

2.3.5 Angular Dependence of Quadrupole Wave

As discussed in the previous subsection, quadrupole wave is

$$h_{ij}^{TT} = \frac{2}{r} \ddot{I}_{ij}^{TT} = \frac{2}{r} \left(P^l{}_i P^m{}_j - \frac{1}{2} P_{ij} P^{lm} \right) \ddot{I}_{lm}, \quad (2.146)$$

where the symbol \cdot denotes the derivative with respect to time. Considering the spherical coordinate (r, θ, ϕ) defined as

$$\begin{aligned} x &= r \sin \theta \cos \phi, \\ y &= r \sin \theta \sin \phi, \\ z &= r \cos \theta, \end{aligned}$$

we can write down the components of h_{ij} in the spherical coordinate as

$$\begin{aligned} h_{rr}^{TT} &= h_{ij}^{TT} \frac{\partial x^i}{\partial r} \frac{\partial x^j}{\partial r}, \quad h_{r\theta}^{TT} = h_{ij}^{TT} \frac{\partial x^i}{\partial r} \frac{\partial x^j}{\partial \theta}, \quad h_{r\phi}^{TT} = h_{ij}^{TT} \frac{\partial x^i}{\partial r} \frac{\partial x^j}{\partial \phi}, \\ h_{\theta\theta}^{TT} &= h_{ij}^{TT} \frac{\partial x^i}{\partial \theta} \frac{\partial x^j}{\partial \theta}, \quad h_{\theta\phi}^{TT} = h_{ij}^{TT} \frac{\partial x^i}{\partial \theta} \frac{\partial x^j}{\partial \phi}, \quad h_{\phi\phi}^{TT} = h_{ij}^{TT} \frac{\partial x^i}{\partial \phi} \frac{\partial x^j}{\partial \phi}. \end{aligned} \quad (2.147)$$

Using $\partial x^i / \partial r = n^i$ and $n^i h_{ij}^{\text{TT}} = 0$, it is led that $h_{rr}^{\text{TT}} = 0$, $h_{r\theta}^{\text{TT}} = 0$ and $h_{r\phi}^{\text{TT}} = 0$. Besides using

$$\frac{\partial x^i}{\partial \theta} n_i = 0, \quad \frac{\partial x^i}{\partial \phi} n_i = 0,$$

we obtain

$$\begin{aligned} \frac{h_{\theta\theta}^{\text{TT}}}{r^2} &= \left\{ (h_{xx}^Q - h_{yy}^Q) \frac{(\cos^2 \theta + 1)}{4} \cos 2\phi - \frac{(h_{xx}^Q + h_{yy}^Q - 2h_{zz}^Q)}{4} \sin^2 \theta \right. \\ &\quad + h_{xy}^Q \left(\frac{\cos^2 \theta + 1}{2} \right) \sin 2\phi - h_{xz}^Q \sin \theta \cos \theta \cos \phi \\ &\quad \left. - h_{yz}^Q \sin \theta \cos \theta \sin \phi \right\}, \end{aligned} \quad (2.148)$$

$$\frac{h_{\phi\phi}^{\text{TT}}}{r^2 \sin^2 \theta} = -\frac{h_{\theta\theta}}{r^2} \quad (2.149)$$

and

$$\begin{aligned} \frac{h_{\theta\phi}^{\text{TT}}}{r^2 \sin \theta} &= -\frac{(h_{xx}^Q - h_{yy}^Q)}{2} \cos \theta \sin 2\phi + h_{xy}^Q \cos \theta \cos 2\phi \\ &\quad + h_{xz}^Q \sin \theta \sin \phi - h_{yz}^Q \sin \theta \cos \phi, \end{aligned} \quad (2.150)$$

where

$$h_{ij}^Q \equiv \frac{2}{r} \ddot{\mathbf{I}}_{ij}. \quad (2.151)$$

In general the angular dependence of the gravitational waves is characterized by tensors f_{ij} and d_{ij} . We review in details in Sec. 2.4.

2.3.6 Quadrupole Formula

The energy-momentum tensor of the gravitational waves are given as Eq. (2.117). In TT gauge, this tensor is expressed as

$$T_{\mu\nu}^{\text{GW}} = \frac{1}{32\pi} \langle \bar{h}_{ik,\mu}^{\text{TT}} \bar{h}_{ik,\nu}^{\text{TT}} \rangle, \quad (2.152)$$

where the second term and the third one in Eq. (2.117) vanish via TT condition. Substituting Eq. (2.146) for Eq. (2.152), we obtain

$$T_{00}^{\text{GW}} = \frac{1}{8\pi r^2} \langle \ddot{\mathbf{I}}_{ij}^{\text{TT}}(t-r) \ddot{\mathbf{I}}_{ij}^{\text{TT}}(t-r) \rangle. \quad (2.153)$$

The energy flux in the radial direction is given as

$$T_i{}^0 \text{GW} n^i = -T_{0i}^{\text{GW}} n^i = T_{00}^{\text{GW}} + O\left(\frac{1}{r^3}\right), \quad (2.154)$$

where we use

$$\frac{\partial}{\partial x^i} \ddot{\mathbf{I}}_{jk}(t-r) = -\ddot{\mathbf{I}}_{jk}(t-r) n_i. \quad (2.155)$$

Therefore the energy flux of the gravitational waves L_{GW} is given by

$$\begin{aligned} L_{\text{GW}} &= \int_{r \rightarrow \infty} T_i^{0\text{GW}} n^i r^2 d\Omega \\ &= \frac{1}{8\pi} \int < \ddot{\mathbf{I}}_{jk}^{\text{TT}} \ddot{\mathbf{I}}_{jk}^{\text{TT}} > d\Omega, \\ &= \frac{1}{8\pi} < \int \{ \ddot{\mathbf{I}}_{jk} \ddot{\mathbf{I}}_{jk} - 2n_i \ddot{\mathbf{I}}_{ij} \ddot{\mathbf{I}}_{jk} n_k + \frac{1}{2} (n_i \ddot{\mathbf{I}}_{ij} n_j)^2 \} d\Omega >, \end{aligned} \quad (2.156)$$

where the last equality holds for Eq. (2.146). Finally, by virtue of two formulae

$$\int n_i n_j d\Omega = \frac{4\pi}{3} \delta_{ij} \quad (2.157)$$

and

$$\int n_i n_j n_k n_l d\Omega = \frac{4\pi}{15} (\delta_{ij} \delta_{kl} + \delta_{ik} \delta_{jl} + \delta_{il} \delta_{jk}), \quad (2.158)$$

gravitational wave luminosity is

$$L_{\text{GW}} = \frac{G}{5c^5} < \ddot{\mathbf{I}}_{jk} \ddot{\mathbf{I}}_{jk} >, \quad (2.159)$$

where we explicitly show c and G to make clear the dimension of the energy flux. This equation is called the quadrupole formula [65].

Finally, let us calculate the angular momentum transmitted by the gravitational wave, S_i^{GW} . Time variation of J^{jk} defined in Eq. (2.99) is

$$\frac{dJ^{jk}}{dt} = \int (x^j \partial_t \tau^{k0} - x^k \partial_t \tau^{j0}) d^3x, \quad (2.160)$$

where $\tau \equiv (-g)(T^{\mu\nu} + t_{LL}^{\mu\nu})$. Using the conservation law of $\tau^{\mu\nu}$,

$$\partial_t \tau^{\mu 0} = -\partial_l \tau^{\mu l}, \quad (2.161)$$

and the symmetry, $\tau^{\mu\nu} = \tau^{\nu\mu}$, Eq. (2.160) is written in the form

$$\begin{aligned} \frac{dJ^{jk}}{dt} &= - \int \partial_l (x^j \tau^{kl} - x^k \tau^{jl}) d^3x \\ &= - \int (x^j \tau^{kl} - x^k \tau^{jl}) n_l r^2 d\Omega, \end{aligned} \quad (2.162)$$

where the last equality holds for the Gauss's law. Now, we define the angular momentum gravitational waves contain as

$$S_i \equiv \epsilon_{ijk} J^{jk}, \quad (2.163)$$

where ϵ_{ijk} is the Levi-Civita tensor in flat space. Putting Eq. (2.162) into Eq. (2.163), the time variation of angular momentum in a system is

$$\frac{dS_i}{dt} = - \int \epsilon_{ijk} x^j \tau^{kl} n_l r^2 d\Omega. \quad (2.164)$$

So, the angular momentum transmitted by gravitational waves is

$$\frac{dS_i^{GW}}{dt} = \int \epsilon_{ijk} x^j \tau^{kl} n_l r^2 d\Omega. \quad (2.165)$$

Imposing $T^{\mu\nu} = 0$ in the local wave zone and TT gauge condition, $h = 0$ and $h^{ij,j} = 0$, Eq. (2.165) is

$$\frac{dS_i^{GW}}{dt} = \int \epsilon_{ijk} x^j t_{LL}^{kl} n_l r^2 d\Omega. \quad (2.166)$$

As discussed in the Sec. 2.3.3, we have to average the integrated function in Eq. (2.166) with respect to several wave length (Brill-Hartle average). Therefore, Eq. (2.166) is evaluated as

$$\frac{dS_i^{GW}}{dt} = \int \epsilon_{ijk} x^j \langle t_{LL}^{kl} \rangle n_l r^2 d\Omega. \quad (2.167)$$

From Eq. (2.98), t_{LL}^{kl} in TT gauge is obtained as

$$\begin{aligned} \frac{dS_i^{GW}}{dt} &= \frac{1}{16\pi} \int \epsilon_{ijk} x^j \langle -h^l_{m,p} h^{mp,k} n_l - h^k_{m,p} h^{mp,l} n_l \\ &\quad + h^{kp,m} h^l_{p,m} n_l + \frac{1}{2} h_{mp}^{kp} h^{mp,l} n_l \rangle r^2 d\Omega, \end{aligned} \quad (2.168)$$

where terms proportional to g^{kl} are vanished because $\epsilon_{ijk} x^j x^k = 0$. First term in the bracket $\langle \rangle$ is calculated in TT gauge as

$$\begin{aligned} h^l_{m,p} n_l &= (h^l_m n_l)_p - h^l_m n_{l,p} \\ &= -h^l_m n_{l,p} \\ &= -\frac{h_{mp}}{r}, \end{aligned} \quad (2.169)$$

where we use the TT gauge condition, $h^l_m n_l = 0$, and $n_{l,p} = (\delta_{lp} - n_l n_p)/r$. This term vanishes if we perform the Brill-Hartle average. Second and third term in the bracket $\langle \rangle$ in Eq. (2.168) are estimated in the local wave zone as

$$\begin{aligned} -h^k_{m,p} h^{mp,l} n_l + h^{kp,m} h^l_{p,m} n_l &= h^k_{m,p} (\dot{h}^{mp} + \frac{h^{mp}}{r}) + h^{kp,m} h^l_{p,m} n_l \\ &= h^k_{m,p} (\dot{h}^{mp} + \frac{h^{mp}}{r}) - h^{kp,m} \frac{h_{pm}}{r} \\ &= h^k_{m,p} \dot{h}^{mp}, \end{aligned} \quad (2.170)$$

where first equality holds for

$$h^{mp,l} n_l = -\dot{h}^{mp} - \frac{h^{mp}}{r}, \quad (2.171)$$

, which is derived from (see Eq. (2.129))

$$h_{mp} = \frac{Q_{mp}(t-r, \theta, \phi)}{r}, \quad (2.172)$$

and second equality holds for Eq. (2.169). Forth term in Eq. (2.168) is written in the form

$$\frac{1}{2}h_{mp}^k h^{mp,l} n_l = -\frac{1}{2} \left(h_{mp}^k \dot{h}^{mp} + \frac{h_{mp}^k h^{mp}}{r} \right) \quad (2.173)$$

by virtue of Eq. (2.171). Second term in Eq. (2.173) can be eliminated if we perform the Brill-Hartle average. As a result, the final form of Eq. (2.167) is

$$\frac{dS_i^{GW}}{dt} = \frac{1}{16\pi} \int \epsilon_{ijk} x^j \langle h^k_{m,p} \dot{h}^{mp} - \frac{1}{2} h_{mp}^k \dot{h}^{mp} \rangle r^2 d\Omega. \quad (2.174)$$

Note that this equation holds only in TT gauge condition. Finally, let us calculate angular momentum transmitted by quadrupole wave. Substituting Eq. (2.146) for Eq. (2.174), we arrive

$$\frac{dS_i^{GW}}{dt} = \frac{1}{8\pi} \int \epsilon_{ijk} \langle -6n_j \ddot{\mathbf{I}}_{km} \ddot{\mathbf{I}}_{mp} n_p + 9n_j \ddot{\mathbf{I}}_{km} n_m n_p \ddot{\mathbf{I}}_{pq} n_q \rangle d\Omega. \quad (2.175)$$

Using the formulae Eqs. (2.157) and (2.158), Eq. (2.175) is written in the form,

$$\frac{dS_i^{GW}}{dt} = \frac{2G}{5c^5} \epsilon_{ijk} \langle \ddot{\mathbf{I}}_{km} \ddot{\mathbf{I}}_{mj} \rangle. \quad (2.176)$$

2.4 Multipole Expansion of Gravitational Field

The last section shows what quadrupole gravitational waves are. However, we must remember only lowest order term is considered (2.131) under the slow motion approximation in the last section. Also, the derivation of the angular dependence of the quadrupole wave seems to be arbitrary. In multipole expansion developed by Thorne [103], higher order terms are took account into and its angular dependence becomes more clear. In this section, we review this formalism and show that the quadrupole wave is one example of multipole expansion with $l = 2$, where l is the index of the spherical harmonics function Y_{lm} .

At first, we explain the tensor harmonics expansion. We can construct six tensor basis by using the spherical harmonics functions Y_{lm} as

$$\tilde{a}_{lm} = \begin{pmatrix} Y_{lm} & 0 & 0 \\ * & 0 & 0 \\ * & * & 0 \end{pmatrix}, \quad (2.177)$$

$$\tilde{b}_{lm} = \frac{r}{\sqrt{2l(l+1)}} \begin{pmatrix} 0 & \partial_\theta Y_{lm} & \partial_\phi Y_{lm} \\ * & 0 & 0 \\ * & * & 0 \end{pmatrix}, \quad (2.178)$$

$$\tilde{c}_{lm} = \frac{ir}{\sqrt{2l(l+1)}} \begin{pmatrix} 0 & \frac{1}{\sin\theta} \partial_\phi Y_{lm} & -\sin\theta \partial_\theta Y_{lm} \\ * & 0 & 0 \\ * & * & 0 \end{pmatrix}, \quad (2.179)$$

$$\tilde{g}_{lm} = \frac{r^2}{\sqrt{2}} \begin{pmatrix} 0 & 0 & 0 \\ * & Y_{lm} & 0 \\ * & * & \sin^2\theta Y_{lm} \end{pmatrix}, \quad (2.180)$$

$$\tilde{d}_{lm} = \frac{r^2}{\sqrt{2l(l-1)(l+1)(l+2)}} \begin{pmatrix} 0 & 0 & 0 \\ * & -\frac{1}{\sin\theta} X_{lm} & \sin\theta W_{lm} \\ * & * & \sin\theta X_{lm} \end{pmatrix} \quad (2.181)$$

and

$$\tilde{f}_{lm} = \frac{r^2}{\sqrt{2l(l-1)(l+1)(l+2)}} \begin{pmatrix} 0 & 0 & 0 \\ * & W_{lm} & X_{lm} \\ * & * & -\sin^2 \theta W_{lm} \end{pmatrix}, \quad (2.182)$$

where X_{lm} and W_{lm} are defined as

$$X_{lm} = 2\partial_\phi(\partial_\theta - \cot \theta)Y_{lm}, \quad (2.183)$$

$$W_{lm} = \left(\partial_\theta^2 - \cot \theta \partial_\theta - \frac{1}{\sin^2 \theta} \partial_\phi^2 \right) Y_{lm}. \quad (2.184)$$

The symbol * means components derived from the symmetry of the tensors. In these tensors, \tilde{d}_{lm} and \tilde{f}_{lm} are the transverse-traceless tensor. That is \tilde{d}_{lm} and \tilde{f}_{lm} are the tensors expressing angular dependence of gravitational wave. Therefore gravitational waves more than $l = 2$ is given by

$$h_{ij}^{TT} = \sum_{l=2}^{\infty} \sum_{m=-l}^l \frac{1}{r} \left(\frac{d^l}{dt^l} I^{lm}(t-r) \tilde{f}_{ij}^{lm} + \frac{d^l}{dt^l} S^{lm}(t-r) \tilde{d}_{ij}^{lm} \right), \quad (2.185)$$

where I_{lm} and S_{lm} are source terms. If a source moves slowly, these functions are explicitly expressed as

$$I^{lm} = \frac{16\pi}{(2l+1)!!} \left(\frac{(l+1)(l+2)}{2(l-1)l} \right)^{\frac{1}{2}} \int \tau_{00} Y_{lm}^* r^l d^3x, \quad (2.186)$$

$$S^{lm} = -\frac{32\pi}{(2l+1)!!} \left(\frac{(l+2)(2l+1)}{2(l-1)(l+1)} \right)^{\frac{1}{2}} \times \int \epsilon_{jpq} x_p (-\tau_{0q}) Y_j^{l-1,lm*} r^{l-1} d^3x, \quad (2.187)$$

where $Y_j^{l-1,lm*}$ is called the pure orbital harmonic function defined as

$$Y^{l',lm}(\theta, \phi) = \sum_{m'=-l'}^{l'} \sum_{m''=-1}^1 (1l'm''m'|lm) \xi^{m''} Y^{l'm'},$$

$$\xi^0 \equiv \mathbf{e}_z, \quad \xi^\pm \equiv \mp \frac{1}{\sqrt{2}} (\mathbf{e}_x \pm i\mathbf{e}_y).$$

From Eqs. (2.186) and (2.187), we can interpret I_{lm} and S_{lm} are multipole of mass distribution and angular momentum distribution, respectively.

Finally, energy flux are estimated as

$$L_{GW} = \frac{1}{32\pi} \sum_{l=2}^{\infty} \sum_{m=-l}^{m=l} \left\langle \left| \frac{d^{l+1} I^{lm}}{dt^{l+1}} \right|^2 + \left| \frac{d^{l+1} S^{lm}}{dt^{l+1}} \right|^2 \right\rangle. \quad (2.188)$$

CHAPTER 3

BASIC EQUATION OF TEST PARTICLE

Papapetrou derived equation of motion (EOM) of a spinning test particle in a curved spacetime for the first time [80]. Then, Dixon reformulated it and gave a supplementary condition which specifies the center of the mass of the test particle [33]. We review the derivation of the EOM of the spinning test particle based on a pole-dipole approximation according to the Papapetrou's work.

3.1 Test Particle in General Relativistic Spacetime

Let us consider a trajectory of the center position of a test particle X^μ . We define a world tube with a radius R along trajectory of the center position where R is much smaller than the curvature radius of the background spacetime. A stress energy tensor of the test particle $T^{\mu\nu}$ is not zero within the world tube. The EOM is derived from the Bianchi identity;

$$T^{\mu\nu}_{;\nu} = 0. \quad (3.1)$$

We define a multipole moment of the test particle as

$$\text{(Single pole moment)} \int \mathcal{T}^{\mu\nu} dV, \quad (3.2)$$

$$\text{(Dipole moment)} \int \delta x^\alpha \mathcal{T}^{\mu\nu} dV, \quad (3.3)$$

$$\text{(Quadrupole moment)} \int \delta x^\alpha \delta x^\beta \mathcal{T}^{\mu\nu} dV, \quad (3.4)$$

where we define the tensor $\mathcal{T}_{\mu\nu}$ by

$$\mathcal{T}_{\mu\nu} = \sqrt{-g} T_{\mu\nu}, \quad g = \det|g_{\mu\nu}|, \quad (3.5)$$

and

$$\delta x^\mu = x^\mu - X^\mu. \quad (3.6)$$

V is a volume element of the three dimensional space on $t = \text{const.}$ slice.

The EOM of a non-spinning particle is derived from the lowest moment, i.e., the single pole moment is only non-zero and higher pole moment vanishes. In this case, the EOM is equivalent to a geodesic equation. If we consider the multipole moment up to the second lowest moment, we derive the EOM of a spinning particle.

3.1.1 Single-pole particle

First, let us derive the EOM of a non-spinning particle; a single-pole particle. Equation (3.1) is recast into

$$\mathcal{T}^{\mu\nu}_{;\nu} + \Gamma^\mu_{\rho\sigma} \mathcal{T}^{\rho\sigma} = 0. \quad (3.7)$$

This equation is rewritten as

$$(x^\lambda \mathcal{T}^{\mu\nu})_{,\nu} - \mathcal{T}^{\mu\lambda} + x^\lambda \Gamma_{\rho\sigma}^\mu \mathcal{T}^{\rho\sigma} = 0. \quad (3.8)$$

By integrating Eqs. (3.7) and (3.8) on $t = \text{const.}$ surface, we arrive

$$\frac{d}{dt} \int \mathcal{T}^{0\mu} dV = - \int \Gamma_{\rho\sigma}^\mu \mathcal{T}^{\rho\sigma} dV, \quad (3.9)$$

$$\frac{d}{dt} \int x^\mu \mathcal{T}^{0\nu} dV = \int \mathcal{T}^{\mu\nu} dV - \int x^\mu \Gamma_{\rho\sigma}^\nu \mathcal{T}^{\rho\sigma} dV, \quad (3.10)$$

where we assume that the stress-energy tensor vanishes on the surface of the volume V . $\Gamma_{\rho\sigma}^\mu$ can be expanded around trajectory of the center position:

$$\Gamma_{\rho\sigma}^\mu = {}^{(0)}\Gamma_{\rho\sigma}^\mu + {}^{(0)}\Gamma_{\rho\sigma,\lambda}^\mu \delta x^\lambda + O((\delta x^\lambda)^2), \quad (3.11)$$

where the subscript (0) indicates it is evaluated at X^μ . Putting Eq. (3.11) into Eqs. (3.9) and (3.10), we arrive

$$\frac{d}{dt} \int \mathcal{T}^{0\mu} dV + {}^{(0)}\Gamma_{\rho\sigma}^\mu \int \mathcal{T}^{\rho\sigma} dV = 0, \quad (3.12)$$

$$\int \mathcal{T}^{\mu\nu} dV = \frac{dX^\mu}{dt} \int \mathcal{T}^{\nu 0} dV, \quad (3.13)$$

where the term higher than $\int \mathcal{T}^{\mu\nu} dV$ is neglected and Eq. (3.12) is used to derive Eq. (3.13). Let us introduce $v^\mu = dX^\mu/ds$ and define $M^{\mu\nu}$ by

$$M^{\mu\nu} = v^0 \int \mathcal{T}^{\mu\nu} dV, \quad (3.14)$$

where s is an affine parameter. Equations (3.12) and (3.13) can be rewritten as

$$\frac{d}{ds} \left(\frac{M^{\mu 0}}{v^0} \right) + \Gamma_{\rho\sigma}^\mu M^{\rho\sigma} = 0, \quad (3.15)$$

$$M^{\mu\nu} = \frac{v^\mu}{v^0} M^{\nu 0}. \quad (3.16)$$

We omit the subscript (0) in the Christoffel symbol. The $\nu = 0$ component of Eq. (3.16) is

$$M^{\mu 0} = \frac{v^\mu}{v^0} M^{00}, \quad (3.17)$$

and using Eq. (3.16) again, then we obtain

$$M^{\mu\nu} = \mu v^\mu v^\nu, \quad (3.18)$$

where $\mu \equiv M^{00}/(v^0)^2$. With Eq. (3.18), Eq. (3.15) can be recast into

$$\frac{d}{ds} (\mu v^\mu) + \Gamma_{\rho\sigma}^\mu \mu v^\rho v^\sigma = 0. \quad (3.19)$$

This is the EOM of the single-pole particle. If the affine parameter s is chosen as a proper time τ , v^μ is a four velocity of the particle which satisfies

$$v^\mu v_\mu = -1. \quad (3.20)$$

A four momentum p^μ is defined as

$$p^\mu \equiv \mu v^\mu. \quad (3.21)$$

By making use of these quantities and introducing an absolute derivative, Eqs. (3.19) and (3.20) can be rewritten as

$$\frac{Dp^\mu}{Ds} = 0, \quad (3.22)$$

$$p^\mu p_\mu = -\mu^2. \quad (3.23)$$

In the later section, we prove that μ is a conserved quantity.

3.1.2 Pole-Dipole Particle

The EOM of a pole-dipole particle can be derived by considering the multipole moment up to the dipole moment. In addition to Eqs. (3.7) and (3.8), the equation

$$(x^\alpha x^\beta \mathcal{T}^{\mu\nu})_{,\nu} = x^\beta \mathcal{T}^{\mu\alpha} + x^\alpha \mathcal{T}^{\mu\beta} - x^\alpha x^\beta \Gamma_{\rho\sigma}^\mu \mathcal{T}^{\rho\sigma} \quad (3.24)$$

is used, which can be derived from Eq. (3.7) again. We integrate Eqs. (3.7), (3.8), and (3.24) on the $t = \text{const.}$ surface and expand the Christoffel symbol around the point X^α (see (3.11)). The pole-dipole particle means that we consider the integrals up to $\int \delta x^\rho \mathcal{T}^{\mu\nu} dV$ and neglect the higher order in terms of δx^ρ . Equation (3.7) can be recast into

$$\frac{d}{dt} \int \mathcal{T}^{\alpha 0} dV + \Gamma_{\mu\nu}^\alpha \int \mathcal{T}^{\mu\nu} dV + \Gamma_{\mu\nu\rho}^\alpha \int \delta x^\rho \mathcal{T}^{\mu\nu} dV = 0, \quad (3.25)$$

where we omit the superscript (0) in the Christoffel symbol again. Equation (3.8) is recast into

$$\int \mathcal{T}^{\alpha\beta} dV = \frac{dX^\alpha}{dt} \int \mathcal{T}^{\beta 0} dV + \frac{d}{dt} \int \delta x^\alpha \mathcal{T}^{\beta 0} dV + \Gamma_{\mu\nu}^\beta \int \delta x^\alpha \mathcal{T}^{\mu\nu} dV, \quad (3.26)$$

where we use Eq. (3.25). By making use of Eqs. (3.25) and (3.26) in the integral of Eq. (3.24), we arrive

$$\frac{dX^\alpha}{dt} \int \delta x^\beta \mathcal{T}^{\mu 0} dV + \frac{dX^\beta}{dt} \int \delta x^\alpha \mathcal{T}^{\mu 0} dV = \int \delta x^\alpha \mathcal{T}^{\beta\mu} dV + \int \delta x^\beta \mathcal{T}^{\alpha\mu} dV. \quad (3.27)$$

Equations (3.25)-(3.27) are the basic EOM of the pole-dipole particle. Let us rewrite them in more useful form. First, we define a quantity $M^{\lambda\mu\nu}$ by

$$M^{\lambda\mu\nu} = -v^0 \int \delta x^\lambda \mathcal{T}^{\mu\nu} dV. \quad (3.28)$$

Because all integrals are done on the $t = \text{const.}$ surface, δx^0 should be zero. Therefore,

$$M^{0\mu\nu} = 0. \quad (3.29)$$

Equation (3.27) is rewritten as

$$v^0 (M^{\alpha\beta\mu} + M^{\beta\alpha\mu}) = v^\alpha M^{\beta\mu 0} + v^\beta M^{\alpha\mu 0}. \quad (3.30)$$

We can take a permutation in terms of α, β , and μ in Eq. (3.30). Then, adding the first equation and third equation, and subtracting the second one, we arrive

$$2v^0 M^{\alpha\beta\mu} = v^\alpha (M^{\beta\mu 0} + M^{\mu\beta 0}) + v^\beta (M^{\alpha\mu 0} - M^{\mu\alpha 0}) + v^\mu (M^{\alpha\beta 0} - M^{\beta\alpha 0}). \quad (3.31)$$

Putting $\mu = 0$ into Eq. (3.31), we obtain

$$v^0(M^{\alpha\beta 0} + M^{\beta\alpha 0}) = v^\alpha M^{\beta 00} + v^\beta M^{\alpha 00}. \quad (3.32)$$

Let us define a spin tensor of the test particle as

$$S^{\alpha\beta} = \int \delta x^\alpha T^{\beta 0} dV - \int \delta x^\beta T^{\alpha 0} dV. \quad (3.33)$$

We prove $S^{\mu\nu}$ is a tensor in later. By using Eq. (3.28), $S^{\alpha\beta}$ is related to $M^{\alpha\beta\mu}$;

$$v^0 S^{\alpha\beta} = -(M^{\alpha\beta 0} - M^{\beta\alpha 0}). \quad (3.34)$$

With Eqs. (3.29), (3.32), and (3.34), it is straightforward to show

$$v^0 S^{\alpha 0} = -M^{\alpha 00}, \quad (3.35)$$

$$M^{\alpha\beta 0} + M^{\beta\alpha 0} = v^\alpha S^{0\beta} + v^\beta S^{0\alpha}. \quad (3.36)$$

Putting them into Eq. (3.31), we finally obtain the form;

$$2M^{\alpha\beta\mu} = -(S^{\alpha\beta} v^\mu + S^{\alpha\mu} v^\beta) + \frac{v^\alpha}{v^0} (S^{0\beta} v^\mu + S^{0\mu} v^\beta). \quad (3.37)$$

Next thing we should do is to rewrite Eq. (3.26). Equation (3.26) can be expressed in terms of $M^{\mu\nu}$ and $M^{\mu\nu\lambda}$ (3.14) and (3.28) as

$$M^{\alpha\beta} = \frac{v^\alpha}{v^0} M^{\beta 0} - \frac{d}{ds} \left(\frac{M^{\alpha\beta 0}}{v^0} \right) - \Gamma_{\mu\nu}^\beta M^{\alpha\mu\nu}. \quad (3.38)$$

Putting $\beta = 0$ in this equation, we obtain

$$M^{\alpha 0} = \frac{v^\alpha}{v^0} M^{00} - \frac{d}{ds} \left(\frac{M^{\alpha 00}}{v^0} \right) - \Gamma_{\mu\nu}^0 M^{\alpha\mu\nu}. \quad (3.39)$$

By using this equation, we can get rid of $M^{\beta 0}$ in Eq. (3.38):

$$M^{\alpha\beta} = \frac{v^\alpha}{v^0} \left[\frac{v^\beta}{v^0} M^{00} - \frac{d}{ds} \left(\frac{M^{\beta 00}}{v^0} \right) - \Gamma_{\mu\nu}^0 M^{\beta\mu\nu} \right] - \frac{d}{ds} \left(\frac{M^{\alpha\beta 0}}{v^0} \right) - \Gamma_{\mu\nu}^\beta M^{\alpha\mu\nu}. \quad (3.40)$$

Because $M^{\mu\nu}$ is symmetric with respect to the upper indices, Eq. (3.40) can be recast into

$$\frac{v^\alpha}{v^0} M^{\beta 0} - \frac{v^\beta}{v^0} M^{\alpha 0} + \frac{dS^{\alpha\beta}}{ds} + \Gamma_{\mu\nu}^\alpha M^{\beta\mu\nu} - \Gamma_{\mu\nu}^\beta M^{\alpha\mu\nu} = 0, \quad (3.41)$$

where we use Eqs. (3.34) and (3.39). This equation can be written in a different form with Eqs. (3.35) and (3.39):

$$\frac{dS^{\alpha\beta}}{ds} + \frac{v^\alpha}{v^0} \frac{dS^{\beta 0}}{ds} - \frac{v^\beta}{v^0} \frac{dS^{\alpha 0}}{ds} + \left(\Gamma_{\mu\nu}^\alpha - \frac{v^\alpha}{v^0} \Gamma_{\mu\nu}^0 \right) M^{\beta\mu\nu} - \left(\Gamma_{\mu\nu}^\beta - \frac{v^\beta}{v^0} \Gamma_{\mu\nu}^0 \right) M^{\alpha\mu\nu} = 0. \quad (3.42)$$

We call this equation the EOM of the spin because it expresses an evolution of the spin tensor. Final task is to express Eq. (3.25) in terms of $M^{\alpha\beta}$ and $M^{\alpha\beta\mu}$;

$$\frac{d}{ds} \left(\frac{M^{\alpha 0}}{v^0} \right) + \Gamma_{\mu\nu}^\alpha M^{\mu\nu} - \Gamma_{\mu\nu\rho}^\alpha M^{\rho\mu\nu} = 0. \quad (3.43)$$

Looking at Eq. (3.15), Eq. (3.43) can be recognized as the EOM of the particle.

We have already known $M^{\alpha\beta\mu}$ in Eqs. (3.42) and (3.43) can be expressed in terms of v^α and $S^{\mu\nu}$. Let us count the degree of freedom (d.o.f) in these equations. One d.o.f in M^{00} , three d.o.f. in v^α , and six d.o.f in $S^{\alpha\beta}$. On the other hands, we can easily confirm that $\alpha = 1, 2$, and 3 with $\beta = 0$ in Eq. (3.42) are trivial because of the identity Eq. (3.29). Therefore, the number of the equation for the EOM is insufficient for the ten unknowns. This implies that the complimentary condition is necessary as discussed in later [33].

The EOMs of the spin particle should be expressed in a covariant form. Let us prove $S^{\mu\nu}$ is a tensor. First, we classify two types of the transformation and we can express an arbitrary transformation by a superposition of these two :

$$\begin{aligned} \text{(i)} \quad & x^i = f^i(x'^\mu), \quad x^0 = x'^0 \\ \text{(ii)} \quad & x^i = x'^i, \quad x^0 = f^0(x'^\mu). \end{aligned}$$

In the case (i), it is easy to find a relation between $M^{\lambda\mu\nu}$ and $M'^{\lambda\mu\nu}$ where the former is defined in the coordinate system x^μ and the later is in the coordinate system x'^μ because the hypersurface with $t = \text{const.}$ agrees with that with $t' = \text{const.}$. The relation between the two is

$$M^{\lambda\mu\nu} = \frac{\partial x^\lambda}{\partial x'^\rho} \frac{\partial x^\mu}{\partial x'^\alpha} \frac{\partial x^\nu}{\partial x'^\beta} M'^{\rho\alpha\beta}. \quad (3.44)$$

In the case (ii), the infinitesimal transformation is given as

$$M^{\lambda\mu\nu} = \frac{\partial x^\mu}{\partial x'^\alpha} \frac{\partial x^\nu}{\partial x'^\beta} \left(\frac{\partial x^\lambda}{\partial x'^\rho} - \frac{v^\lambda}{v^0} \frac{\partial x^0}{\partial x'^\rho} \right) M'^{\rho\alpha\beta}. \quad (3.45)$$

Because, in the case (i), the second term of Eq. (3.45) vanishes due to the identity Eq. (3.29), Eq. (3.45) contains the case (i). Furthermore, if Eq. (3.45) holds for the coordinate transformation $x^\mu \rightarrow x'^\mu$ and

$$M'^{\lambda\mu\nu} = \frac{\partial x'^\mu}{\partial x''^\alpha} \frac{\partial x'^\nu}{\partial x''^\beta} \left(\frac{\partial x'^\lambda}{\partial x''^\rho} - \frac{v'^\lambda}{v'^0} \frac{\partial x'^0}{\partial x''^\rho} \right) M''^{\rho\alpha\beta}$$

does for the transformation $x'^\mu \rightarrow x''^\mu$, the following equation holds

$$M^{\lambda\mu\nu} = \frac{\partial x^\mu}{\partial x''^\alpha} \frac{\partial x^\nu}{\partial x''^\beta} \left(\frac{\partial x^\lambda}{\partial x''^\rho} - \frac{v^\lambda}{v^0} \frac{\partial x^0}{\partial x''^\rho} \right) M''^{\rho\alpha\beta}$$

for $x^\mu \rightarrow x''^\mu$. This means that Eq. (3.45) has the group property. Therefore, Eq. (3.45) holds for any infinitesimal transformation. Because any finite transformations can be composed of the series of the infinitesimal transformation, Eq. (3.45) gives the general transformation for $M^{\lambda\mu\nu}$.

For the transformation formula of $M^{\mu\nu}$, the procedure is essentially same as that for $M^{\mu\nu\lambda}$. The final form is given by

$$\begin{aligned} M^{\alpha\beta} = & \frac{\partial x^\alpha}{\partial x'^\mu} \frac{\partial x^\beta}{\partial x'^\nu} M'^{\mu\nu} - \left(\frac{\partial^2 x^\alpha}{\partial x'^\mu \partial x'^\rho} \frac{\partial x^\beta}{\partial x'^\nu} + \frac{\partial x^\alpha}{\partial x'^\mu} \frac{\partial^2 x^\beta}{\partial x'^\nu \partial x'^\rho} \right) M'^{\rho\mu\nu} \\ & + \frac{d}{ds} \left(\frac{\partial x^\alpha}{\partial x'^\mu} \frac{\partial x^\beta}{\partial x'^\nu} \frac{\partial x^0}{\partial x'^\rho} \frac{1}{v^0} M'^{\rho\mu\nu} \right), \end{aligned} \quad (3.46)$$

where this formula holds for both infinitesimal and infinitesimal transformation. Putting $v = 0$ in Eq (3.45), we obtain

$$M^{\lambda\mu 0} = \frac{\partial x^\mu}{\partial x'^\alpha} \frac{\partial x^0}{\partial x'^\beta} \left(\frac{\partial x^\lambda}{\partial x'^\rho} - \frac{v^\lambda}{v^0} \frac{\partial x^0}{\partial x'^\rho} \right) M'^{\rho\alpha\beta}. \quad (3.47)$$

Substituting Eq. (3.37) into this equation, we arrive

$$M^{\lambda\mu 0} = -\frac{1}{2}v^0 \frac{\partial x^\lambda}{\partial x'^\rho} \frac{\partial x^\mu}{\partial x'^\alpha} S'^{\rho\alpha} + \frac{1}{2} \left(v^\lambda \frac{\partial x^\mu}{\partial x'^\alpha} + v^\mu \frac{\partial x^\lambda}{\partial x'^\alpha} \right) \frac{\partial x^0}{\partial x'^\beta} S'^{\beta\alpha}. \quad (3.48)$$

The first term of the right-hand side of the equation is antisymmetric with respect to λ and μ . The second term is symmetric with respect to λ and μ . With this, we obtain

$$M^{\lambda\mu 0} - M^{\mu\lambda 0} = -v^0 \frac{\partial x^\lambda}{\partial x'^\alpha} \frac{\partial x^\mu}{\partial x'^\beta} S'^{\alpha\beta}. \quad (3.49)$$

Putting this equation into Eq. (3.34), we finally prove $S^{\mu\nu}$ is a tensor:

$$S^{\lambda\mu} = \frac{\partial x^\lambda}{\partial x'^\alpha} \frac{\partial x^\mu}{\partial x'^\beta} S'^{\alpha\beta}. \quad (3.50)$$

Equation (3.45) implies that if $M^{\lambda\mu\nu}$ has non-zero components in one frame, they do not vanish in another frame. This indicates that the order of the highest multipole of a test particle is invariant under the coordinate transformation.

Substituting $\beta = 0$ for Eq. (3.46), we obtain

$$\begin{aligned} M^{\alpha 0} &= \frac{\partial x^\alpha}{\partial x'^\mu} \frac{\partial x^0}{\partial x'^\nu} M'^{\mu\nu} - \left(\frac{\partial^2 x^\alpha}{\partial x'^\mu \partial x'^\rho} \frac{\partial x^0}{\partial x'^\nu} + \frac{\partial x^\alpha}{\partial x'^\mu} \frac{\partial^2 x^0}{\partial x'^\nu \partial x'^\rho} \right) M'^{\rho\mu\nu} \\ &\quad + \frac{d}{ds} \left(\frac{\partial x^\alpha}{\partial x'^\mu} \frac{\partial x^0}{\partial x'^\nu} \frac{\partial x^0}{\partial x'^\rho} \frac{1}{v^0} M'^{\rho\mu\nu} \right). \end{aligned} \quad (3.51)$$

The first term of the right-hand side can be rewritten with Eq. (3.38). The second and third terms can be with Eq. (3.37). Furthermore, the transformation formulae for the Christoffel symbol is given as

$$\Gamma'^\mu_{\rho\sigma} = \frac{\partial x'^\mu}{\partial x^\lambda} \frac{\partial x^\nu}{\partial x'^\rho} \frac{\partial x^\gamma}{\partial x'^\sigma} \Gamma^\lambda_{\nu\gamma} + \frac{\partial x'^\mu}{\partial x^\lambda} \frac{\partial^2 x^\lambda}{\partial x'^\rho \partial x'^\sigma}.$$

We derive

$$-\frac{\partial x^\alpha}{\partial x'^\mu} \frac{\partial x^0}{\partial x'^\nu} \Gamma'^\mu_{\rho\sigma} M'^{\nu\sigma\rho} = \Gamma^\alpha_{\mu\nu} v^\mu S^{0\nu} + \frac{\partial^2 x^\alpha}{\partial x'^\rho \partial x'^\sigma} \frac{\partial x^0}{\partial x'^\nu} S'^{\nu\rho} v'^\sigma - \frac{\partial x^\alpha}{\partial x'^\mu} \Gamma'^\mu_{\rho\sigma} \frac{v^0}{v'^0} v'^\sigma S'^{0\rho}.$$

From Eq. (3.37), it is straightforward to show

$$\frac{\partial x^0}{\partial x'^\nu} \frac{\partial x^0}{\partial x'^\sigma} \frac{M'^{\sigma\mu\nu}}{v^0} = \frac{1}{2} \frac{\partial x^0}{\partial x'^\nu} \left(-S'^{\nu\mu} + \frac{v'^\nu}{v'^0} S'^{0\mu} + \frac{v'^\mu}{v'^0} S'^{0\nu} \right) = \frac{\partial x^0}{\partial x'^\nu} \frac{M'^{\nu\mu 0}}{v'^0}.$$

Putting all of them in Eq. (3.51), we finally find

$$\frac{1}{v^0} (M^{\alpha 0} + \Gamma^\alpha_{\rho\sigma} v^\sigma S^{\rho 0}) = \frac{\partial x^\alpha}{\partial x'^\mu} \frac{1}{v'^0} (M'^{\mu 0} + \Gamma'^\mu_{\rho\sigma} v'^\rho S'^{\sigma 0}). \quad (3.52)$$

This means that the left-hand side quantity is a vector.

Let us define an absolute derivative as

$$\frac{DS^{\alpha\beta}}{Ds} = \frac{dS^{\alpha\beta}}{ds} + \Gamma^\alpha_{\mu\nu} S^{\mu\beta} v^\nu + \Gamma^\beta_{\mu\nu} S^{\alpha\mu} v^\nu. \quad (3.53)$$

Equation (3.42) can be expressed as

$$\frac{DS^{\alpha\beta}}{Ds} + \frac{v^\alpha}{v^0} \frac{DS^{\beta 0}}{Ds} - \frac{v^\beta}{v^0} \frac{DS^{\alpha 0}}{Ds} = 0. \quad (3.54)$$

If we multiply Eq.(3.54) by v_β , we have

$$\frac{1}{v^0} \frac{DS^{\alpha 0}}{Ds} = v_\beta \frac{DS^{\alpha\beta}}{Ds} + \frac{v^\alpha}{v^0} v_\beta \frac{DS^{\beta 0}}{Ds}.$$

Putting this expression into Eq. (3.54), we arrive the final form

$$\frac{DS^{\alpha\beta}}{Ds} + v^\alpha v_\rho \frac{DS^{\beta\rho}}{Ds} - v^\beta v_\rho \frac{DS^{\alpha\rho}}{Ds} = 0. \quad (3.55)$$

This equation is the covariant form of the EOM of the spinning particle.

Next thing is to derive a covariant form of Eq. (3.43). With Eqs. (3.35) and (3.54), we can rewrite Eq (3.39);

$$M^{\alpha 0} + \Gamma_{\mu\nu}^\alpha S^{\mu 0} v^\nu = \frac{v^\alpha}{v^0} (M^{00} + \Gamma_{\mu\nu}^0 S^{\mu 0} v^\nu) + \frac{DS^{\alpha 0}}{Ds}.$$

If we multiply by v_α/v^0 , we obtain

$$\mu = \frac{1}{(v^0)^2} (M^{00} + \Gamma_{\mu\nu}^0 S^{\mu 0} v^\nu) + \frac{v_\rho}{v^0} \frac{DS^{\rho 0}}{Ds},$$

where

$$\mu \equiv \frac{1}{v^0} (M^{\alpha 0} + \Gamma_{\mu\nu}^\alpha S^{\mu 0} v^\nu) v_\alpha \quad (3.56)$$

and it is easy to prove μ is a scalar.

Therefore,

$$\frac{1}{v^0} M^{\alpha 0} = \mu v^\alpha - \Gamma_{\mu\nu}^\alpha S^{\mu 0} \frac{v^\nu}{v^0} + v_\beta \frac{DS^{\alpha\beta}}{Ds}.$$

Substituting this equation into Eq. (3.43), we get

$$\frac{d}{ds} \left(\mu v^\alpha + v_\beta \frac{DS^{\alpha\beta}}{Ds} \right) + \Gamma_{\mu\nu}^\alpha v^\nu \left(\mu v^\mu + v_\beta \frac{DS^{\mu\beta}}{Ds} \right) + S^{\mu\nu} v^\sigma (\Gamma_{\nu\sigma}^\alpha + \Gamma_{\mu\rho}^\alpha \Gamma_{\nu\sigma}^\rho) = 0. \quad (3.57)$$

If A^α is a vector, we define the absolute derivative of it by

$$\frac{dA^\alpha}{ds} + \Gamma_{\mu\nu}^\alpha v^\nu A^\mu \equiv \frac{DA^\alpha}{Ds}, \quad (3.58)$$

which is a vector as well. We have already proven that $(M^{\alpha 0} + \Gamma_{\rho\sigma}^\alpha v^\sigma S^{\rho 0})/v^0$ is the vector. So, $\mu v^\alpha + v_\beta DS^{\alpha\beta}/Ds$ is as well. The Riemann tensor is given as

$$R^\alpha_{\beta\mu\nu} = -\Gamma_{\beta\mu}^\alpha v^\nu + \Gamma_{\beta\nu}^\alpha v^\mu - \Gamma_{\sigma\nu}^\alpha \Gamma_{\beta\mu}^\sigma + \Gamma_{\sigma\mu}^\alpha \Gamma_{\beta\nu}^\sigma. \quad (3.59)$$

Putting these equations in Eq. (3.57), we finally arrive the covariant form of the equation :

$$\frac{D}{Ds} \left(\mu v^\alpha + v_\beta \frac{DS^{\alpha\beta}}{Ds} \right) + \frac{1}{2} S^{\mu\nu} v^\sigma R^\alpha_{\sigma\mu\nu} = 0. \quad (3.60)$$

In the absence of the spin, Eq. (3.60) can be reduced into Eq. (3.22); the geodesic equation. In this sense, Eq. (3.60) is a generalized equation of Eq. (3.22). Note that in the presence of the spin, the particle motion deviates from the geodesics motion.

Furthermore, we rewrite the Eqs. (3.55) and (3.60) to convenient forms. We define a total four-momentum of the particle p^μ as

$$p^\mu \equiv \mu v^\mu + v_\nu \frac{DS^{\mu\nu}}{Ds}. \quad (3.61)$$

Then, Eq. (3.60) is written as

$$\frac{Dp^\mu}{Ds} = -\frac{1}{2} R^\mu_{\nu\rho\sigma} v^\nu S^{\rho\sigma}, \quad (3.62)$$

and Eq. (3.55) is as

$$\frac{DS^{\mu\nu}}{Ds} = 2p^{[\mu} v^{\nu]}. \quad (3.63)$$

Equations (3.62) and (3.63) do not construct a closed system because v^μ is not in general parallel to p^μ . Therefore, we need a supplementary condition. Dixon [33] formulated such a condition as

$$p_\mu S^{\mu\nu} = 0. \quad (3.64)$$

This condition is called the center of the mass condition. A physical meaning of this condition is that the trajectory of the center of mass of the particle agrees with the world line.

Using Eq. (3.64), we derive the relation between v^μ and p^μ . By differentiating Eq. (3.64) with respect to the affine parameter s , we obtain

$$\frac{Dp_\nu}{Ds} S^{\nu\mu} + p_\nu \frac{DS^{\nu\mu}}{Ds} = 0. \quad (3.65)$$

Substituting Eqs. (3.62) and (3.63) into Eq. (3.65) we get

$$-\frac{1}{2} R_{\nu\lambda\rho\sigma} v^\lambda S^{\rho\sigma} S^{\nu\mu} + p_\nu (p^\nu v^\mu - p^\mu v^\nu) = 0. \quad (3.66)$$

Subsequently, we define μ , u^μ and N as

$$\mu^2 \equiv -p^\mu p_\mu, \quad u^\mu \equiv p^\mu / \mu, \quad N \equiv -u^\mu v_\mu \quad (N > 0).$$

We recognize u^μ as a unit vector parallel to p^μ . Using these quantities, Eq. (3.66) is

$$v^\mu = N \left(u^\mu - \frac{1}{2\mu^2 N} R_{\nu\lambda\alpha\beta} v^\lambda S^{\alpha\beta} S^{\nu\mu} \right). \quad (3.67)$$

From now on we rewrite the second term of this equation. The second term is rewritten as

$$\begin{aligned} S^{\mu\beta} S^{\rho\sigma} v^\alpha R_{\rho\sigma\alpha\beta} &= S^{\mu\beta} S^{\rho\sigma} R_{\rho\sigma\alpha\beta} \left(N u^\alpha - \frac{1}{2\mu^2} R_{\nu\lambda\chi\kappa} v^\lambda S^{\chi\kappa} S^{\nu\alpha} \right) \\ &= N u^\alpha S^{\mu\beta} S^{\rho\sigma} R_{\rho\sigma\alpha\beta} + \frac{1}{2\mu^2} S^{\rho\sigma} v^\lambda S^{\chi\kappa} R_{\nu\lambda\chi\kappa} S^{\mu\beta} S^{\alpha\nu} R_{\rho\sigma\alpha\beta}, \end{aligned} \quad (3.68)$$

where in the first equality we use Eq. (3.67). We can calculate the second term of the most right-hand side of Eq. (3.68) as

$$\begin{aligned} S^{\mu\beta}S^{\alpha\nu}R_{\rho\sigma\alpha\beta} &= \frac{1}{2}(S^{\mu\beta}S^{\alpha\nu}R_{\rho\sigma\alpha\beta} + S^{\mu\alpha}S^{\beta\nu}R_{\rho\sigma\beta\alpha}) \\ &= \frac{1}{2}(S^{\mu\beta}S^{\alpha\nu} - S^{\mu\alpha}S^{\beta\nu})R_{\rho\sigma\alpha\beta} \\ &= S^{\mu[\beta}S^{\alpha]\nu}R_{\rho\sigma\alpha\beta}. \end{aligned} \quad (3.69)$$

And using a relation

$$S^{\mu[\beta}S^{\alpha]\nu} = \frac{1}{2}S^{\alpha\beta}S^{\mu\nu}, \quad (3.70)$$

where this relation is obtained from the character of second-rank antisymmetric tensor, the left-hand side of Eq. (3.68) is finally rewritten as a following form:

$$S^{\mu\beta}S^{\rho\sigma}v^\alpha R_{\rho\sigma\alpha\beta} = Nu^\alpha S^{\mu\beta}S^{\rho\sigma}R_{\rho\sigma\alpha\beta} + \frac{1}{4\mu^2}S^{\rho\sigma}S^{\alpha\beta}R_{\rho\sigma\alpha\beta}S^{\mu\nu}S^{\chi\kappa}v^\lambda R_{\nu\lambda\chi\kappa}. \quad (3.71)$$

From this equation, we get

$$R_{\nu\lambda\chi\kappa}S^{\nu\mu}v^\lambda S^{\chi\kappa} = -\frac{N}{\Delta}R_{\nu\lambda\rho\sigma}S^{\mu\nu}u^\lambda S^{\rho\sigma}, \quad (3.72)$$

where

$$\Delta = 1 + \frac{1}{4\mu^2}R_{\alpha\beta\mu\nu}S^{\alpha\beta}S^{\mu\nu}. \quad (3.73)$$

Finally the relation between v^μ and p^μ is obtained as

$$v^\mu = N \left(u^\mu + \frac{1}{2\mu^2\Delta}R_{\nu\lambda\rho\sigma}S^{\mu\nu}u^\lambda S^{\rho\sigma} \right). \quad (3.74)$$

N is related to a choice of the affine parameter and if we choose v^μ as a four velocity of the particle N is determined by $v^\mu v_\mu = -1$. Therefore, we obtain the closed system for the particle with spin.

Spin vector

In Sec. 3.1.2, we review the basic equations of the spinning particle characterized by the spin tensor. The set of the equations can be transformed into a more convenient form if we introduce a spin vector S_μ [101]. The definition of this quantity is

$$S_\mu = -\frac{1}{2}\epsilon_{\mu\nu\rho\sigma}u^\nu S^{\rho\sigma}, \quad (3.75)$$

where $\epsilon_{\mu\nu\rho\sigma}$ is the Levi-Civita tensor in a curved space time. Using this quantity, the basic Eqs. (3.62) and (3.63) are rewritten in the form

$$\frac{dx^\mu}{ds} = v^\mu, \quad (3.76)$$

$$\frac{Dp^\mu}{Ds} = \frac{1}{\mu}R^{*\mu}_{\nu\rho\sigma}v^\nu S^\rho p^\sigma, \quad (3.77)$$

$$\frac{DS^\mu}{Ds} = \frac{1}{\mu^3}p^\mu R^*_{\nu\lambda\rho\sigma}S^\nu v^\lambda S^\rho p^\sigma, \quad (3.78)$$

where

$$R^*_{\mu\nu\rho\sigma} \equiv \frac{1}{2} R_{\mu\nu}^{\alpha\beta} \epsilon_{\alpha\beta\rho\sigma}. \quad (3.79)$$

The condition (3.64) is rewritten as

$$p_\mu S^\mu = 0 \quad (3.80)$$

and furthermore the relationship between v^μ and p^μ ((3.74)) is also rewritten as

$$v^\mu = \frac{N}{\Delta} \left[u^\mu + \frac{1}{\mu^2} {}^*R^*_{\nu\rho\sigma} S^\nu S^\rho u^\sigma \right], \quad (3.81)$$

where

$$\Delta = 1 + \frac{1}{\mu^2} {}^*R^*_{\alpha\beta\mu\nu} S^\alpha u^\beta S^\mu u^\nu, \quad (3.82)$$

$${}^*R^*_{\alpha\beta\mu\nu} \equiv \frac{1}{2} \epsilon_{\alpha\beta\rho\sigma} R^*{}^{\rho\sigma}_{\mu\nu}. \quad (3.83)$$

If we choose the affine parameter, N will be determined.

3.2 Constant Of Motion

Conserved quantities of test particle moving in the relativistic spacetime are classified into two classes. One is related to the symmetry that the background spacetime has and the other is related to the EOM of the particle. In the former, a Killing vector, which is satisfied a relation

$$\xi_{\mu;\nu} + \xi_{\nu;\mu} = 0, \quad (3.84)$$

plays an essential role. The Killing vector is also satisfied a following relation:

$$\xi_{\mu;\rho\sigma} = R_{\sigma\rho\mu}{}^\lambda \xi_\lambda. \quad (3.85)$$

If the Killing vector exists in a spacetime and we choose it as the basis of a coordinate, the coordinate does not explicitly appear in the metric of the background spacetime.

In the following section, we show that conserved quantities of the particle in the both case of single-pole particle and pole-dipole particle.

single-pole particle

We show that μ given by Eq. (3.23) is a conserved quantity. Differentiating Eq. (3.23) with respect to τ , we get

$$2\mu \frac{d\mu}{d\tau} = -2p_\mu \frac{Dp^\mu}{D\tau}. \quad (3.86)$$

Using Eq. (3.22), the right-hand side of the equation vanishes. Therefore, we obtain

$$\frac{d\mu}{d\tau} = 0. \quad (3.87)$$

μ is interpreted as a rest mass of the particle.

If a Killing vector ξ_μ exists in the background spacetime, the following quantity is a constant of motion:

$$C_\xi \equiv \xi^\mu p_\mu. \quad (3.88)$$

We will prove that this quantity is conserved. Differentiating Eq. (3.88) with respect to τ , we obtain

$$\frac{dC_\xi}{d\tau} = \xi^\mu_{;\nu} v^\nu p_\mu + \xi^\mu \frac{Dp_\mu}{D\tau}. \quad (3.89)$$

The second term of the right-hand side of Eq. (3.89) is vanished by using Eq. (3.22). Hence, we get

$$\begin{aligned} \frac{dC_\xi}{d\tau} &= \xi^\mu_{;\nu} v^\nu p_\mu \\ &= \mu \xi_{\mu;\nu} v^\mu v^\nu \\ &= \frac{1}{2} \mu (\xi_{\mu;\nu} + \xi_{\nu;\mu}) v^\mu v^\nu \end{aligned} \quad (3.90)$$

Using the Killing equation. (3.84), we finally obtain

$$\frac{dC_\xi}{d\tau} = 0.$$

Therefore, we have proven that the quantity C_ξ is a constant of motion.

pole-dipole particle

At first, we show that the magnitude of the four velocity $\mu^2 = -p^\mu p_\mu$ is conserved. Differentiating this equation with respect to τ ,

$$2\mu \frac{d\mu}{d\tau} = -2p^\mu \frac{Dp^\mu}{D\tau} \quad (3.91)$$

is obtained. Using the equation of motion, the right-hand side is

$$2\mu \frac{d\mu}{d\tau} = R_{\mu\nu\rho\sigma} p^\mu v^\nu S^{\rho\sigma}. \quad (3.92)$$

Differentiating Eq. (3.64), we obtain

$$\frac{Dp_\mu}{D\tau} S^{\mu\nu} + p_\mu \frac{DS^{\mu\nu}}{D\tau} = 0. \quad (3.93)$$

Multiplying Eq. (3.93) by $Dp_\nu/D\tau$, the first term is vanished by the antisymmetry of $S^{\mu\nu}$. Hence, using Eqs. (3.62) and (3.63) we get

$$-\frac{1}{2} p_\mu R_{\nu\lambda\rho\sigma} v^\lambda S^{\rho\sigma} (p^\mu v^\nu - p^\nu v^\mu) = 0. \quad (3.94)$$

The first term in the bracket is vanished by the antisymmetry of the Riemann tensor. Therefore,

$$p^\nu p_\mu v^\mu R_{\nu\lambda\rho\sigma} v^\lambda S^{\rho\sigma} = 0 \quad (3.95)$$

is obtained. Because both v^μ and p^μ are timelike vectors, we obtain $p_\mu v^\mu \neq 0$. Thus, we obtain

$$R_{\nu\lambda\rho\sigma} p^\nu v^\lambda S^{\rho\sigma} = 0 \quad (3.96)$$

and subsequently combining Eq. (3.92) we finally obtain

$$\frac{d\mu}{d\tau} = 0. \quad (3.97)$$

We can interpret that μ is an effective mass of the particle.

Secondly, we will prove that the spin magnitude S is also conserved. S is defined by a following equation:

$$S^2 \equiv \frac{1}{2} S^{\mu\nu} S_{\mu\nu} = S^\mu S_\mu. \quad (3.98)$$

Taking the derivative with respect to τ , we obtain

$$2S \frac{dS}{d\tau} = S_{\mu\nu} \frac{DS^{\mu\nu}}{D\tau}. \quad (3.99)$$

Using Eq. (3.63) in the right-hand side of the equation,

$$2S \frac{dS}{d\tau} = S_{\mu\nu} (p^\mu v^\nu - p^\nu v^\mu). \quad (3.100)$$

The right-hand side is vanished by Eq. (3.64). Finally, we obtain

$$\frac{dS}{d\tau} = 0. \quad (3.101)$$

We have proven that the spin magnitude is conserved.

Thirdly, we will prove that the following quantity defined by using the Killing vector of the background spacetime is also conserved:

$$C \equiv \xi^\mu p_\mu - \frac{1}{2} \xi_{\mu;\nu} S^{\mu\nu}. \quad (3.102)$$

We take the derivative with respect to τ and Dp^μ/Ds as well as $DS^{\mu\nu}/Ds$ in the right-hand side of Eq. (3.102). The equation can be eliminated by using Eqs. (3.62) and (3.63). As a result, we obtain

$$\frac{dC}{d\tau} = -\frac{1}{2} (\xi_{\mu;\nu\rho} + R^\sigma{}_{\rho\mu\nu} \xi_\sigma) v^\sigma S^{\mu\nu} + \frac{1}{2} (\xi_{\mu;\nu} + \xi_{\nu;\mu}) p^\mu v^\nu. \quad (3.103)$$

The first and second terms of this equation are vanished by the character of the Killing vector. Thus, the quantity C is a constant of motion.

3.3 Equation of motion in Tetrad frame

It is convenient to write the basic equations in a tetrad basis $e^\mu{}_i$. In the tetrad basis, the Ricci rotation coefficients, defined below, plays a substitute role of the Christoffel symbol. Covariant derivative of vector is given by

$$\begin{aligned} t^\mu{}_{;\nu} &= (e^\mu{}_i t^i)_{;\nu} \\ &= e^\mu{}_{i;\nu} t^i + e^\mu{}_i t^i{}_{,\nu} \\ &= \gamma_{ijk} e^j{}_\nu e^{k\mu} t^i + e^\mu{}_i t^i{}_{,\nu} \\ &= \gamma^k{}_{ij} e^j{}_\nu e^\mu{}_k t^i + e^\mu{}_i t^i{}_{,\nu}, \end{aligned} \quad (3.104)$$

where γ_{ijk} is the Ricci rotation coefficient. In the following tables, we show the basic equations of the particle in both coordinate frame and tetrad frame. For non-spinning particle, the first row in the table corresponds to the EOM and the second one does to conserved quantities. For spinning particle, the first, the second, and the third row correspond to the EOM, conserved variables, and supplementary conditions, respectively.

single-pole particle

coordinate basis	tetrad basis
$\frac{dx^\mu}{d\tau} = v^\mu$	$\frac{dx^\mu}{d\tau} = e^\mu{}_i v^i$
$\frac{Dp^\mu}{D\tau} = 0$	$\frac{dp^i}{d\tau} = -\gamma^i{}_{kj} v^j p^k$
$v^\mu = \frac{p^\mu}{\mu}$	$v^i = \frac{p^i}{\mu}$

pole-dipole particle (spin tensor)

coordinate basis	tetrad basis
$\frac{dx^\mu}{d\tau} = v^\mu$	$\frac{dx^\mu}{d\tau} = e^\mu{}_i v^i$
$\frac{Dp^\mu}{D\tau} = -\frac{1}{2} R^\mu{}_{\nu\rho\sigma} v^\nu S^{\rho\sigma}$	$\frac{dp^i}{d\tau} = -\gamma^i{}_{kj} v^j p^k - \frac{1}{2} R^i{}_{jk} v^j S^{kl}$
$\frac{DS^{\mu\nu}}{D\tau} = 2p^{[\mu} v^{\nu]}$	$\frac{dS^{ij}}{d\tau} = 2\gamma^{[i}{}_{lk} S^{j]l} v^k + 2p^{[i} v^{j]}$
$v^\mu = N \left[\frac{1}{\mu} p^\mu + \frac{1}{2\mu^3 \Delta} R_{\nu\lambda\rho\sigma} S^{\mu\nu} p^\lambda S^{\rho\sigma} \right]$	$v^i = N \left[\frac{1}{\mu} p^i + \frac{1}{2\mu^3 \Delta} R_{jklm} S^{ij} p^k S^{lm} \right]$
$\Delta = 1 + \frac{1}{4\mu^2} R_{\alpha\beta\mu\nu} S^{\alpha\beta} S^{\mu\nu}$	$\Delta = 1 + \frac{1}{4\mu^2} R_{ijkl} S^{ij} S^{kl}$
$\mu^2 = -p_\mu p^\mu$	$\mu^2 = -p_i p^i$
$S^2 = \frac{1}{2} S_{\mu\nu} S^{\mu\nu}$	$S^2 = \frac{1}{2} S_{ij} S^{ij}$
$C_\xi = \xi^\mu p_\mu - \frac{1}{2} \xi_{\mu;\nu} S^{\mu\nu}$	$C_\xi = \xi^i p_i - \frac{1}{2} (\gamma_{jik} \xi^i + \xi_{j,\mu} e^\mu{}_k) S^{jk}$
$p_\mu S^{\mu\nu} = 0$	$p_i S^{ij} = 0$

pole-dipole particle (spin vector)

coordinate basis	tetrad basis
$\frac{dx^\mu}{d\tau} = v^\mu$ $\frac{Dp^\mu}{D\tau} = \frac{1}{\mu} R^*{}^\mu_{\nu\rho\sigma} v^\nu S^\rho p^\sigma$ $\frac{DS^\mu}{D\tau} = \frac{1}{\mu^3} p^\mu R^*{}_{\nu\rho\sigma\lambda} S^\nu v^\rho S^\sigma p^\lambda$ $v^\mu = \frac{N}{\Delta} \left[\frac{1}{\mu} p^\mu + \frac{1}{\mu^3} {}^*R^*{}^\mu_{\nu\rho\sigma} S^\nu S^\rho \rho^\sigma \right]$ $\Delta = 1 + \frac{1}{\mu^4} {}^*R^*{}_{\alpha\beta\mu\nu} p^\alpha S^\beta p^\mu S^\nu$	$\frac{dx^\mu}{d\tau} = e^\mu{}_i v^i$ $\frac{dp^i}{d\tau} = -\gamma^i{}_{kj} v^j p^k + \frac{1}{\mu} {}^*R^*{}^{i*}_{jkl} v^j S^k p^l$ $\frac{dS^i}{d\tau} = -\gamma^i{}_{kj} v^j S^k + \frac{1}{\mu^3} p^i R^*{}_{jklm} S^j v^k S^l p^m$ $v^i = \frac{N}{\Delta} \left[\frac{1}{\mu} p^i + \frac{1}{\mu^3} {}^*R^*{}^{i*}_{jkl} S^j S^k p^l \right]$ $\Delta = 1 + \frac{1}{\mu^4} {}^*R^*{}_{ijkl} p^i S^j p^k S^l$
$\mu^2 = -p_\mu p^\mu$ $S^2 = S_\mu S^\mu$ $C_\xi = \xi^\mu p_\mu - \frac{1}{2\mu} \xi_{\mu;\nu} \epsilon^{\mu\nu\rho\sigma} p_\rho S_\sigma$	$\mu^2 = -p_i p^i$ $S^2 = S_i S^i$ $C_\xi = \xi^i p_i - \frac{1}{2} (\gamma_{jik} \xi^i + \xi_{j,\mu} e^\mu{}_k) \epsilon^{jklm} p_l S_m$
$p_\mu S^\mu = 0$ $v_\mu S^\mu = 0$	$p_i S^i = 0$ $v_i S^i = 0$

CHAPTER 4

CHAOS IN RELATIVISTIC TWO BODY PROBLEM

History of chaos in GR is short and researches on this field have started in 1990's. In Refs. [18, 19, 22], Contopoulos has analyzed a motion of test particle in the Majamudar-Papapetrou spacetime in which the gravitational force of the black holes exactly balances to the electrostatic force due to the black hole's charges. Test particle as well as photon moving in this spacetime show chaotic feature. His analysis was based on the Poincaré map. In Refs. [24, 30], Cornish et al. revisited this system and analyzed the chaotic feature with fractal analysis. Following a series of Contopoulos's works, many researchers investigated a chaotic motion of test particle in a wide variety of the spacetimes, such as a pp wave, an uniform magnetic field, a naked singularity and so on [13, 54, 67, 76, 82, 83, 96, 108, 111]. However, these systems are rather academic.

In 1997, Suzuki and Maeda have analyzed a motion of the spinning particle around the Schwarzschild black hole [97]. They have found a chaotic motion in the case of fast particle spin. This work has stimulated the research on a relativistic two spinning body problem. Main reason is that the compact binary systems, such as NS-NS, BH-NS, BH-BH binaries, are recognized as a relativistic two body problem and the gravitational waves from their coalescence is the main target of the ground based gravitational wave detectors as explained in Introduction. It is a crucial for the gravitational wave detection whether chaos occurs in merging binaries or not because of a following reason.

1. Matched filtering approach is one of the powerful method for gravitational wave data analysis and it requires waveform templates.
2. Chaos means unpredictability and a small deviation of initial condition grows exponentially. Thus, chaos in merging binaries implies that the number of theoretical templates increases enormously and the matched filtering method is no longer practical.

Considerable works on a closed binary system have been done in the framework of both test particle approximation and post-Newtonian approximation [24, 25, 26, 27, 28, 38, 40, 41, 42, 62, 68, 69, 70, 71, 92]. The main topic in these references is the emergence of the chaos in realistic closed binary systems.

In this section, we review the Suzuki and Maeda's work [97] and a mechanism of chaos in the Schwarzschild spacetime. Then, we give a short summary of the associated works.

4.1 Chaos in Schwarzschild Space Time

“Effective” Potential

In Sec. 3, we review the EOM and the constants of motion of for a spinning particle in general relativity. Therefore, we drop the explicit form of the EOM in this section.

First, a supplementary condition whose form is

$$p_\mu S^{\mu\nu} = 0, \quad (4.1)$$

is required (see Eq. (3.64)). The mass of the particle μ is defined by

$$\mu^2 = -p_\nu p^\nu. \quad (4.2)$$

In the previous section, we have shown that μ and S , the magnitude of the spin, are conserved quantities. This holds without any relation to the symmetry of the background spacetime. S is defined by

$$S^2 \equiv \frac{1}{2} S_{\mu\nu} S^{\mu\nu}. \quad (4.3)$$

The other constants of the motion are related to the Killing vectors of the background spacetime. The Schwarzschild spacetime has the two killing vectors $\xi_{(t)}^\mu$ and $\xi_{(\phi)}^\mu$. Therefore, the constants of motion (3.102) associated with these Killing vectors are

$$E \equiv -C_{(t)} = -p_t - \frac{M}{r^2} S^{tr}, \quad (4.4)$$

$$J_z \equiv C_{(\phi)} = p_\phi - r(S^{\phi r} - rS^{\theta\phi}\cot\theta)\sin^2\theta. \quad (4.5)$$

E is the energy and J_z is the angular momentum of test particle, respectively. Note that, without loss of generality, we choose the direction of the total angular momentum to be the z direction. In the spherical symmetric spacetime, the other components of the angular momentum, i.e., J_x and J_y , should be conserved as well;

$$\begin{aligned} J_x &= -p_\theta \sin\phi - p_\phi \cot\theta \cos\phi \\ &\quad + r^2 S^{\theta\phi} \sin^2\theta \sin\phi + rS^{\phi r} \sin\theta \cos\theta \sin\phi + rS^{r\theta} \cos\phi, \end{aligned} \quad (4.6)$$

$$\begin{aligned} J_y &= p_\theta \cos\phi - p_\phi \cot\theta \sin\phi \\ &\quad + r^2 S^{\theta\phi} \sin^2\theta \cos\phi + rS^{\phi r} \sin\theta \cos\theta \cos\phi - rS^{r\theta} \sin\phi. \end{aligned} \quad (4.7)$$

We set the each component as

$$(J_x, J_y, J_z) = (0, 0, J), \quad (4.8)$$

without loss of generality where $J > 0$. Three constraint equations (4.5)-(4.7) with Eq. (4.8) are reduced to

$$S^{\theta\phi} = \frac{J}{r^2} \cot\theta, \quad (4.9)$$

$$S^{r\theta} = -\frac{p_\theta}{r}, \quad (4.10)$$

$$S^{\phi r} = \frac{1}{r} \left(-J + \frac{p_\phi}{\sin^2\theta} \right). \quad (4.11)$$

S^{ti} ($i = r, \theta, \phi$) are fixed from equation (4.1) with Eqs. (4.9)-(4.11) as

$$S^{tr} = -\frac{1}{rp_t} \left(p_\theta^2 + \frac{p_\phi^2}{\sin^2\theta} - Jp_\phi \right), \quad (4.12)$$

$$S^{t\theta} = \frac{1}{rp_t} \left(p_r p_\theta + \frac{Jp_\phi}{r} \cot\theta \right), \quad (4.13)$$

$$S^{t\phi} = -\frac{1}{rp_t} \left(Jp_r - \frac{p_r p_\phi}{\sin^2\theta} + \frac{Jp_\theta}{r} \cot\theta \right). \quad (4.14)$$

The energy conservation equation (4.4) is now

$$E = -p_t + \frac{1}{p_t r^3} \left(p_\theta^2 + \frac{p_\phi^2}{\sin^2\theta} - Jp_\phi \right). \quad (4.15)$$

According to an analysis of a test particle without spin, we make use of an "effective" potential for a particle with spin [75]. For the test particle without spin, the effective potential is defined by

$$V^2(r; L) = \left(1 - \frac{2M}{r}\right) \left(\mu^2 + \frac{L^2}{r^2}\right), \quad (4.16)$$

where L is the angular momentum of test particle. Without loss of generality, the motion of the particle is confined in a plane, say $\theta = \pi/2$ plane. Given the particle energy E , a region $V^2(r) < E^2$ corresponds to a region in which the particle can move around. Furthermore, if $E < 0$, the motion of the particle is bounded. Otherwise, the particle will escape to infinity or fall into a black hole.

For the spinning test particle, there is no rigorous way for defining the effective potential. The spin-orbit coupling (3.63) does not ensure that the motion of the test particle is confined in a single plane. Instead, we seek a boundary of a region in which the particle can move around; $p^r = 0$ and $p^\theta = 0$. Putting them into Eq. (4.2), we obtain

$$\begin{aligned} p_t &= -\mu f^{1/2} \cosh X, \\ p_\phi &= \mu r \sin \theta \sinh X, \end{aligned} \quad (4.17)$$

where X is a function of r and θ . Substituting this equation into Eq. (4.3) with the help of Eqs. (4.9)-(4.11), the equation for X can be derived;

$$(\mu^2 r^2 - S^2 f) \sinh^2 X - 2\mu J r \sin \theta \sinh X + (J^2 - S^2) f + \frac{2M}{r} J^2 \sin^2 \theta = 0. \quad (4.18)$$

By solving this equation, Eq. (4.4) tells us the boundary of a region in which the spinning particle can move;

$$E = V_{(\pm)}(r, \theta; J, S), \quad (4.19)$$

where

$$V_{(\pm)}(r, \theta; J, S) = \mu \left[f^{\frac{1}{2}} \cosh X_{(\pm)} + \frac{M \sinh X_{(\pm)}}{f^{1/2} r \cosh X_{(\pm)}} \left(\frac{J \sin \theta}{\mu r} - \sinh X_{(\pm)} \right) \right], \quad (4.20)$$

and

$$\sinh X_{(\pm)} \equiv \frac{\mu J r \sin \theta}{\mu^2 r^2 - S^2 f} \pm \left[\frac{\mu^2 J^2 r^2 \sin^2 \theta}{(\mu^2 r^2 - S^2 f)^2} - \frac{(J^2 - S^2) f + \frac{2M}{r} J^2 \sin^2 \theta}{\mu^2 r^2 - S^2 f} \right]^{\frac{1}{2}}. \quad (4.21)$$

If the direction of the z component of the spin agrees with that of the total angular momentum, we choose the minus sign. Otherwise, we take the plus sign. Note that if $S = 0$ and $\theta = \pi/2$, $V_{(\pm)}$ can be reduced to the effective potential of the non-spinning particle (4.16). It is easy to show that a region of $V_{(\pm)}^2(r, \theta; J, S) < E^2$ corresponds to a region in which the particle with the energy E can move around. Then, $V(r, \theta; J, S)$ is the "effective" potential of a spinning particle in the Schwarzschild spacetime introduced by Suzuki and Maeda [97].

In Fig. 4.1, we plot a cross section of the "effective" potential (4.20). Obviously, given an energy E , the spinning particle in $V_{(-)}$ can move in a stronger gravitational field than that in $V_{(+)}$. The primarily reason of this is the spin-orbit coupling appeared in the EOM of the test particle. It is known that, if direction of the spin agrees with the angular momentum, the spin-orbit coupling produces a repulsive force. Otherwise, it produces an attractive force. Therefore, the particle in $V_{(-)}$ can get closer to a black hole horizon with the help of the repulsive force. Because we know that the motion of the non-spinning particle is non-chaotic, the strong spin-orbit coupling may be an essential to a chaotic motion. Hence, from now, we focus on $V_{(-)}$ case and omit the minus sign in the potential.

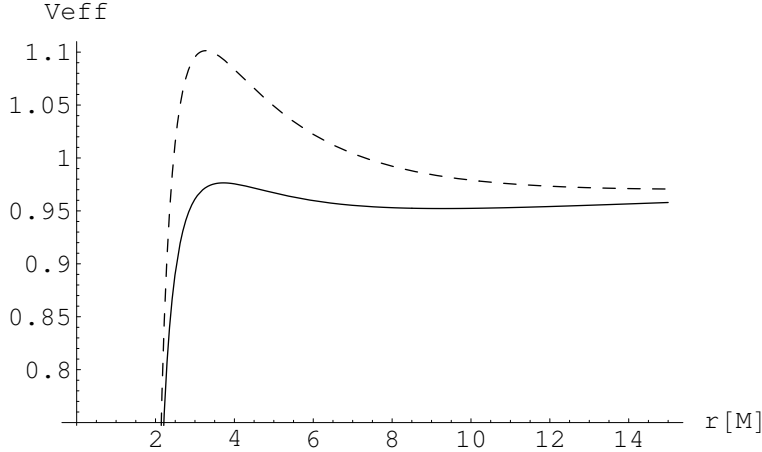


Figure 4.1: The “effective” potential $V_{(\pm)}$ on the $\theta = \pi/2$ plane. We set $J = 4\mu M$ and $S = 0.4\mu M$ in this plot. The solid (dashed) curve denotes $V_{(-)}(V_{(+)})$. Given an energy E , a spinning particle can get closer to the black hole horizon in $V_{(-)}$ than in $V_{(+)}$ [97].

Suzuki and Maeda classified the “effective” potential V into four types, which is characterized by J and S . In Fig. 4.2, we plot a representative potential contour in each cases. Qualitative features of the potentials are summarized as follows:

1. Type (B1): The top-left panel of Fig. 4.2. This shape appears in the case of small S and large J . On the equatorial plane, there is a saddle point around $\rho \approx 4M$ and a minimal point around $\rho \approx 10M$. In this case, an effect of the spin is small. Hence, the potential is essentially same as that for the non-spinning case and the motion of the particle can never exhibit a chaotic feature.

2. Type (B2): The top-right panel of Fig 4.2. If we increase S with a fixed value of J from the type (B1), we obtain this type of the potential. Two saddle points appear at $\rho \approx 4M$ and $z \approx \pm 1M$ and one minimal point do at $\rho \approx 6M$ on the equatorial plane. This shape is caused by the spin-orbit coupling and the saddle points implies that the motion of the test particle in this potential could be chaotic.

3. Type (U1): The bottom-left panel of Fig. 4.2. This potential appears in the case of relatively small J . Because of the absence of the centrifugal barrier, the particle will be inevitably swallowed by a black hole. Such a situation can be realized even for a spinless particle.

4. Type (U2): The bottom-right panel of Fig. 4.2. The potential has no bound region. Compared to the potential (U1), there is a saddle point on at $\rho \approx 3.6M$ and $z = 0M$. It is local minimum in r direction. It is local maximum in z direction. Due to the spin-orbit coupling, a black hole cannot capture the particle on the equatorial plane. Instead, it will move off the equatorial plane and be swallowed into a black hole in the end.

Because the potential type is categorized by the total angular momentum and the spin magnitude, we plot the classification in Fig. 4.3. The type (B2) and (U2) can be realized only in the spinning case. Suzuki and Maeda numerically found that the motion of the particle in the type (B2) potential becomes chaotic. They also specified a critical value of S , above which the particle can move chaotically, as $0.635\mu M$ with the Lyapunov exponent analysis.

Physical Maximum Value of S

Essential physical quantity that makes the system chaotic is a spin of the test particle. Therefore, the spin magnitude is important for the emergence of the chaos in this system. We give a short

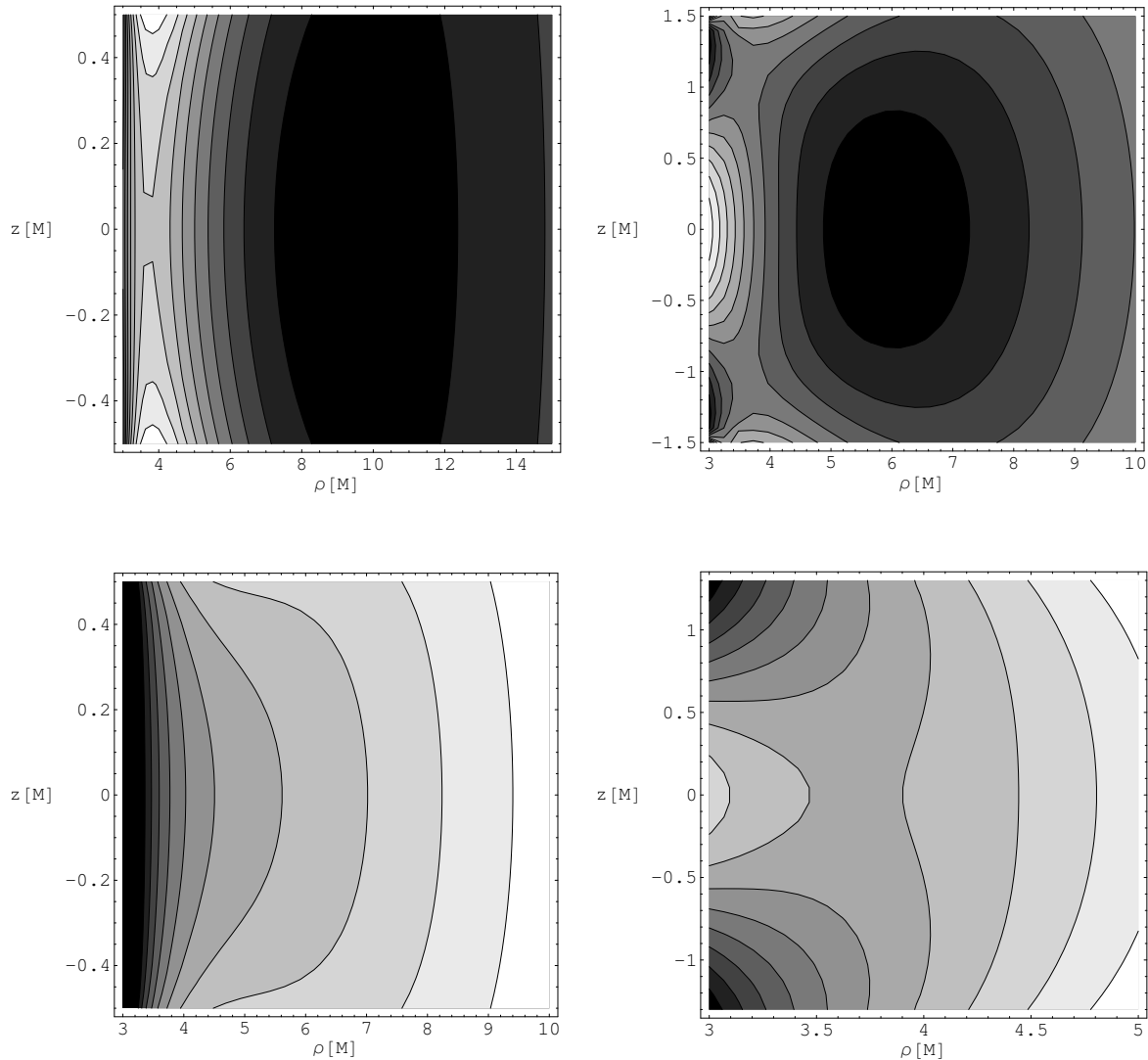


Figure 4.2: Contour plots of four types of “effective” potential (4.20) on a meridional plane. ρ is a radial coordinate. The dark region means that the potential has a negative value; bounded region. The white region indicates a positive value of the potential.

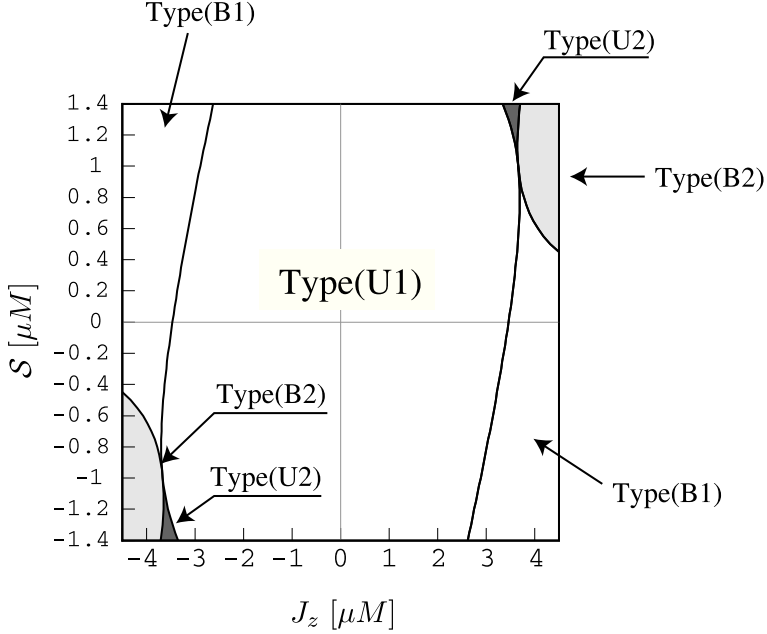


Figure 4.3: The classification of the “effective” potential in terms of the total angular momentum J and the spin magnitude S . This figure is cited from [98].

discussion about the spin magnitude. Realistic value of the spin holds a following relation,

$$S/\mu M = (S/\mu^2)\mu/M \leq O(\mu/M). \quad (4.22)$$

In the test particle approximation, that is $\mu \ll M$, the spin magnitude should be small. However, if we extrapolate this approximation to a relativistic binary composed of the comparable mass m_1 and m_2 , this limitation relaxes. μ should be replaced by the reduced mass as $\mu = m_1 m_2 / (m_1 + m_2)$. M should be the total mass as $M = m_1 + m_2$. The spin magnitude of the star 1 can be estimated by

$$S_1/\mu M = S_1/m_1 m_2 = (S_1/m_1^2)m_1/m_2. \quad (4.23)$$

Then, we have $S_1/\mu M = S_1/m_1^2 \leq O(1)$ for the case $m_1 = m_2$. Therefore, $S_1/\mu M$ can be large as unity. However, it should be again emphasized that the test particle approximation breaks down in this case and a question about the emergence of the chaos in a realistic binary system is still remained. The considerable works motivated by Suzuki and Maeda’s work [24, 25, 26, 27, 28, 38, 40, 41, 42, 62, 68, 69, 70, 71, 92] were devoted to this question and many of them used the post-Newtonian approximation, which allows us to analyze a binary with comparable mass in contrast to the test particle approximation.

4.2 Can relativistic binary really behave chaotically ?

4.2.1 Post-Newtonian Approximation

Before reviewing the related works, we summarize the post-Newton approximation. We will not explain this approach in details because it is beyond scope of this thesis (see a review [10] in details).

In the post-Newtonian approximation, an expansion parameter is determined from a condition,

$$\epsilon = \max \left[\left| \frac{T^{0i}}{T^{00}} \right|, \left| \frac{T^{ij}}{T^{00}} \right|^{1/2}, \left| \frac{U}{c^2} \right|^{1/2} \right], \quad (4.24)$$

where $T^{\mu\nu}$ is a stress energy tensor of the post-Newtonian source and U is Newtonian potential. This parameter represents essentially a slow motion estimate $\epsilon \sim v/c$, where v denotes a typical internal velocity. The parameter is required to be less than unity.

On the other hand, Einstein's equation is expanded in the form of

$$\square h^{\alpha\beta} = \frac{16\pi G}{c^4} \tau^{\alpha\beta}, \quad (4.25)$$

with

$$h^{\alpha\beta} = \sqrt{-g} g^{\mu\nu} - \eta^{\mu\nu}, \quad (4.26)$$

where $\square \equiv \eta^{\mu\nu} \partial_\mu \partial_\nu$. Note that we impose the harmonic condition; $\partial_\mu h^{\alpha\mu} = 0$. The source term is divided into two component, the matter contribution term $|g|T^{\alpha\beta}$ and a gravitational source term $\Lambda^{\alpha\beta}$, i.e.

$$\tau^{\alpha\beta} = |g|T^{\alpha\beta} + \frac{c^4}{16\pi G} \Lambda^{\alpha\beta}. \quad (4.27)$$

$\Lambda^{\alpha\beta}$ is expanded in terms of h to arrange the post-Newton order. Introducing a retarded scalar-, vector-, and tensor-type potentials, the post-Newtonian metric $g^{\alpha\beta}$ is expressed with these potentials. If we assume the stress-energy tensor, these potentials can be computed from the retarded integral. Hence, the post-Newtonian metric in requested order is given. Because, for the point particle case, it contains a delta function, a special technique, e.g., the Hadamard self-field regularization, is required (see [10]). Once the post-Newton metric is obtained, equations of motion can be calculated from a geodesic equation with the metric. So far, the 3PN(ϵ^6) equations of motion have been investigated [12]. If we assume an extend body as discussed in Chapter 3, a spin-orbit (SO) or a spin-spin (SS) coupling contribution can be introduced in the equations of motion [57]. Schematic form of the post-Newton EOM is

$$\ddot{\mathbf{r}} = \mathbf{a}_N + \mathbf{a}_{PN} + \mathbf{a}_{2PN} + \mathbf{a}_{SO} + \mathbf{a}_{RR} + \mathbf{a}_{3PN} + \mathbf{a}_{SS}, \quad (4.28)$$

where \mathbf{a} is acceleration and RR denoted a radiation reaction due to gravitational radiation. Benefit of the post-Newton approximation to the point particle approximation in a relativistic spacetime is to be able to calculate an accurate motion of two bodies with comparable masses. Moreover, the radiation reaction force can be taken account into. Therefore, this method is powerful to generate the theoretical templates of the gravitational waves from coalescing binary systems.

4.2.2 Chaos in binary merger

Discussion on a chaos in a realistic binary system has been started in 2000 [68]. First, Levin pointed that a relativistic spinning binary system with comparable masses can behave chaotically in Ref. [68]. She calculated a motion of binary systems with 2PN approximation including a SO and SS coupling terms. In the absence of the SO and SS coupling term, it is known that the EOM can be integrable, e.g. no chaos. Note that radiation reaction term was turned off because a theory of chaos in a diffusive system has not been established. She concluded with

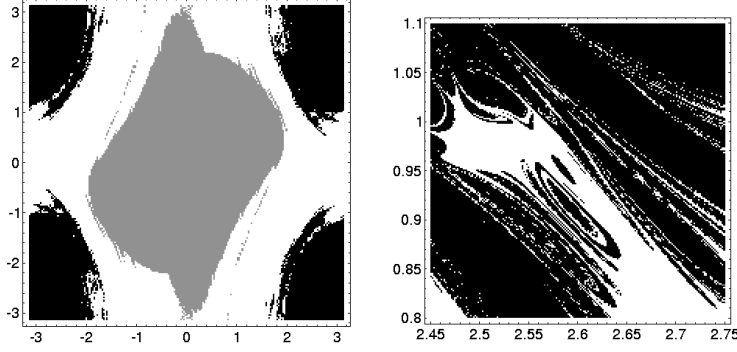


Figure 4.4: Left: The fractal basin boundaries. We set $m_2/m_1 = 1/3$, $S_1/m_1^2 = S_2/m_2^2 = 0.6$, $x_i/m = 5$, and $\dot{y}_i = 0.45$. The initial spin angles (θ_1, θ_2) in terms of the orbital angular momentum are randomly seeded and the axes are labelled in radians. 200×200 orbits are shown. The horizontal (vertical) axis is $\theta_1(\theta_2)$. The right panel is a magnification of the left panel. This figure is cited from [68].

the fractal basin boundary analysis that the SO and SS coupling can induce the chaos in the binary systems.

Figure 4.4 shows the fractal structure in phase space. Mass ratio, spin value of the each bodies and initial condition are chosen as $m_2/m_1 = 1/3$, $S_1/m_1^2 = S_2/m_2^2 = 0.6$ and $(x_i/m, \dot{y}_i) = (5, 0.45)$, respectively, where m_1 and m_2 denote mass of the each bodies. A center of mass coordinate is chosen. The initial angle of the spin is randomly chosen. This figure clearly shows the chaotic feature of this system.

Following this work, Schnittman and Rasio published the paper named “Ruling Out Chaos in Compact Binary System” [92]. They used the 2PN equation of motion with the spin interaction and the Lyapunov exponent to analyze chaos,

$$\gamma(t) = \frac{1}{t} \ln \left(\frac{dX(t)}{dX(0)} \right), \quad (4.29)$$

where dX is a difference between two points in the phase space. They calculated a trajectory of maximally spinning ($S_i = m_i^2$) two black holes with $10M_\odot$. Their set up is $(\theta_1, \theta_2) = (38, 70)$, which means misalignment of the spin and it could occur chaotic motion, and orbital separation $r/m = 50, 20, 10, 5$, which corresponds to the Newtonian gravitational wave frequencies of 10, 40, 100, 400 Hz, respectively.

Figure 4.5 shows the convergence of Lyapunov exponent for each orbits. They also estimated the inspiral time scale from the gravitational wave frequency and showed it in the figures as t_{inspiral} . This figure clearly shows that the inspiral time scale is shorter than the convergence time scale of the Lyapunov exponent. They concluded that the chaos does not occur in the coalescing binaries.

Cornish and Levin claimed an objection against Schnittman and Rasio’s result in 2002 [26]. They insisted that Schnittman and Rasio’s method of calculating the Lyapunov exponent (4.29) was improper. Their mistake was to make use of the Cartesian distance in phase space dX . With this, the Lyapunov exponent has only approximate meanings. They showed the appropriately calculated Lyapunov exponent and concluded the chaos does occurs. Figure 4.6 is their result. However, their discussion missed a point of the time scale. These works revealed the coalescing binary system has a potential to cause the chaos. But, if its time scale is longer than the inspiral time scale, it implies that *the chaos does not occur in reality*. This is an essential point of this

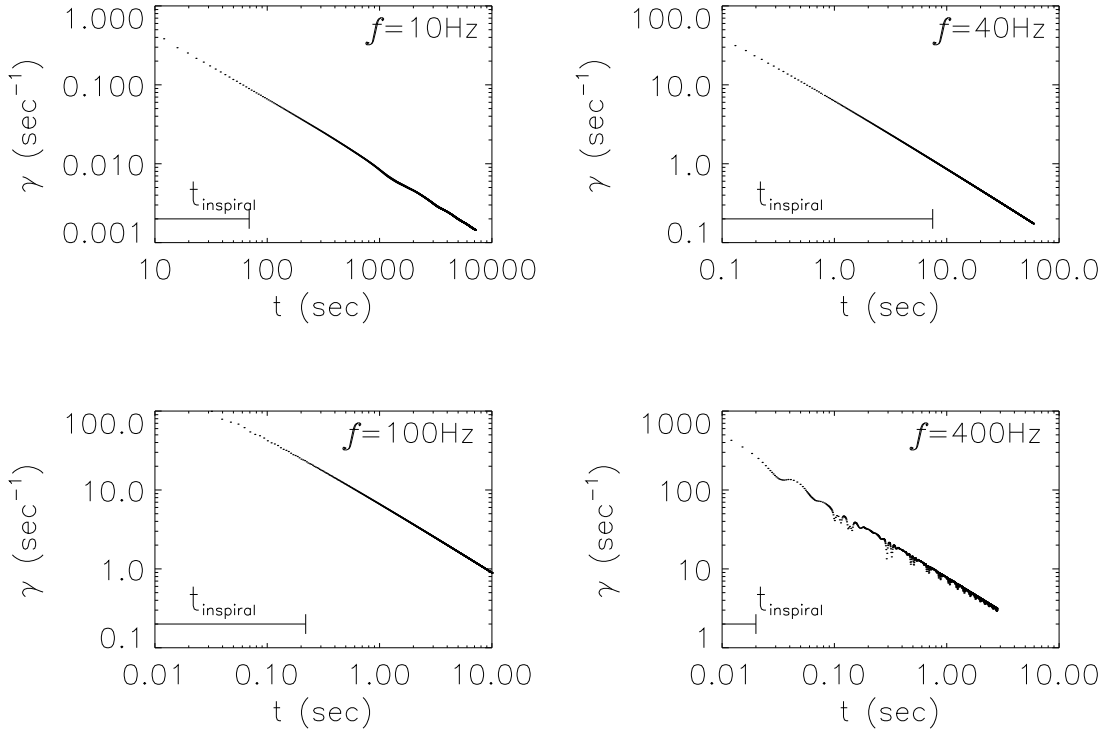


Figure 4.5: Lyapunov exponent $\gamma(t)$ as a function of the time for the maximally spinning black holes with $10M_\odot$. (Top-left) The initial orbital separation is $r/m = 47.25$, which corresponds to the Newtonian gravitational wave frequency $f_{\text{GW}} = 10\text{ Hz}$ and the inspiral time scale $t_{\text{insp}} = 69\text{ s}$. (Top-right) The initial orbital separation is $r/m = 18.75$, which corresponds to the Newtonian gravitational wave frequency $f_{\text{GW}} = 40\text{ Hz}$ and the inspiral time scale $t_{\text{insp}} = 7.5\text{ s}$. (Bottom-left) The initial orbital separation is $r/m = 9.2$, which corresponds to the Newtonian gravitational wave frequency $f_{\text{GW}} = 100\text{ Hz}$ and the inspiral time scale $t_{\text{insp}} = 0.2\text{ s}$. (Bottom-right) The initial orbital separation is $r/m = 4.0$, which corresponds to the Newtonian gravitational wave frequency $f_{\text{GW}} = 400\text{ Hz}$ and the inspiral time scale $t_{\text{insp}} = 0.01\text{ s}$. Because $t_L = 1/\gamma \gg t_{\text{insp}}$ in all cases, the chaos does not appear in this system. This figure is cited from [92].

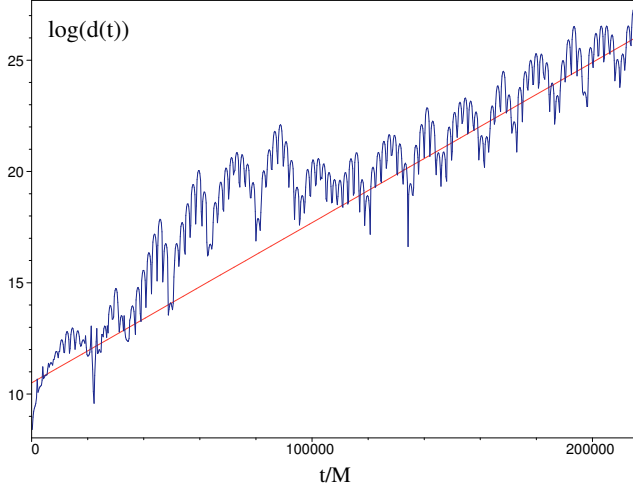


Figure 4.6: The recalculated Lyapunov exponent for an orbit taken from Fig. 4.5 as a function of time. This figure is cited from [26].

system.

In all the works, a specific parameter choice was taken. The mass ratio, spin magnitude, initial separation were chosen as special parameters. Levin investigated an effect of these parameters on the chaos [70]. Also, she estimated emitted gravitational waves. Her result was summarized as follows.

(1) Mass ratio : Small values result in an enhancement of precession.

(2) Spin magnitude : The large spin magnitude as well as the spin misalignment enhance a chance of chaos. Even in a single spinning case, the chaos can occur. In the case of a light companion, the spin magnitude should be greater than the maximal. Otherwise, the chaos can appear for a physically allowed value of the black hole spins. However, the rapid spin is still required.

(3) Eccentricity : If the spin misalignment is large, it results in a large eccentricity. Although the large eccentricity is a common feature of chaotic orbits, it is not a sufficient condition of the chaos. Even in a regular orbit, the spin misalignment causes a precession and consequently leads to a modulation of the gravitational wave forms.

The point is that she found some cases; in some eccentric orbits, the Lyapunov exponent exhibits a positive value and the characteristic time scale given by the inverse of the Lyapunov exponent is shorter than the inspiral time scale t_{inspire} . This work again sheds light on the chaos in the binary system.

Hartl and Buonanno [42] recently answered this question in some limited case. Their results are valid only in the BH-BH binary as explained below. New point in their work was taking account into a mass monopole/spin induced by the quadrupole interaction terms, which was not dealt in the previous works. However, these terms were known exactly only in the case of black holes at that time. This drawback was conquered very recently [11, 35].

In wide variety of the parameters, the initial conditions, and the PN terms, they sought a chaotic motion with the Lyapunov exponent analysis. Their analysis was based on the two type orbits; the quasi-circular orbit and the eccentric orbits. They parametrize the orbital separation

by “Newtonian gravitational-wave frequency”:

$$f_{\text{GW}}^{\text{Newt}} = \frac{1}{\pi} \left(\frac{GM}{r^3} \right)^{1/2}. \quad (4.30)$$

Note that high end of the LIGO/VIRGO frequency band is $f_{\text{GW}}^{\text{Newt}} = 240\text{Hz}$ and their upper limits of the orbital parametrization was set as this value. Figure 4.7 shows the result of their work. This reveals a relation between orbital parameters, e.g., the energy, angular momentum and spin magnitude and $f_{\text{GW}}^{\text{Newt}}$ in the case of quasi-circular orbit. The top-left, top-right and middle-left panels in this figure correspond to the relations between the angular momentum, the gravitational wave frequency, and the spin, and the Lyapunov exponents, respectively. The binary has equal masses $10M_{\odot}$ and 2PN terms are included. The middle-right and bottom-left panels show the Lyapunov exponent as functions of gravitational wave frequency and spin, respectively, in which the 3PN terms are added.

Figure 4.8 is the relations between Lyapunov exponent and pericenter/eccentricity. They investigated the chaos in a wider parameter region than that in Fig. 4.7. Their conclusion are summarized as follows: For the quasi eccentric orbits, the chaos only appears for high gravitational wave frequencies corresponding to small orbital radii. The high spin is a necessary condition. For the eccentric orbit, the chaos only appears in the parameter space which is likely to be rather academic or of a small pericenter. For the later, higher order PN terms are required to describe the EOM accurately, which is a beyond scope of the current status of the post-Newtonian theory.

4.3 Associated Topics

Final part of this chapter is devoted for introducing some related topics of the chaos in binary systems.

4.3.1 Radiation reaction effect

In all topics introduced above, a radiation reaction due to gravitational wave emission is turned off. In the phase space, the dissipation would play as an attractor. In that case, the system may not be formally chaotic. Although in this sense a chaotic binary motion with radiation reaction is not rigorous, Cornish and Levin have searched its effect qualitatively in Ref. [28]. They included the 2.5PN terms in the equations of motion and analyzed with the fractal basin boundary. Their result showed that, with the radiation reaction, the fractal structure in phase space vanishes. This implies that the chaos in merging binary would suppress and does not affect on the gravitational waves. However, we should note again that this work only showed a possibility of non-chaotic behavior in the binary mergers. Further analysis will be required.

4.3.2 Extreme mass ratio black hole binary

All topics introduced so far are the chaos in the binary systems. However, the model analyzed in Suzuki and Maeda [97] can describe the other system. This system is called an extreme-mass ratio binary and exists in the galactic nuclei [113]. It is composed of a supermassive black hole with $10^6 \sim 10^9 M_{\odot}$ and a compact object such as NS or BH orbiting around it. In this system, the mass ratio is quite smaller than unity. Hence, the test particle approximation works well.

As discussed in Sec. 4.1, Suzuki and Maeda have already shown that the spin magnitude to cause the chaos in the Schwarzschild spacetime should be unrealistically large in the extreme-mass ratio binary system. However, if the spacetime has less symmetry, this result would change

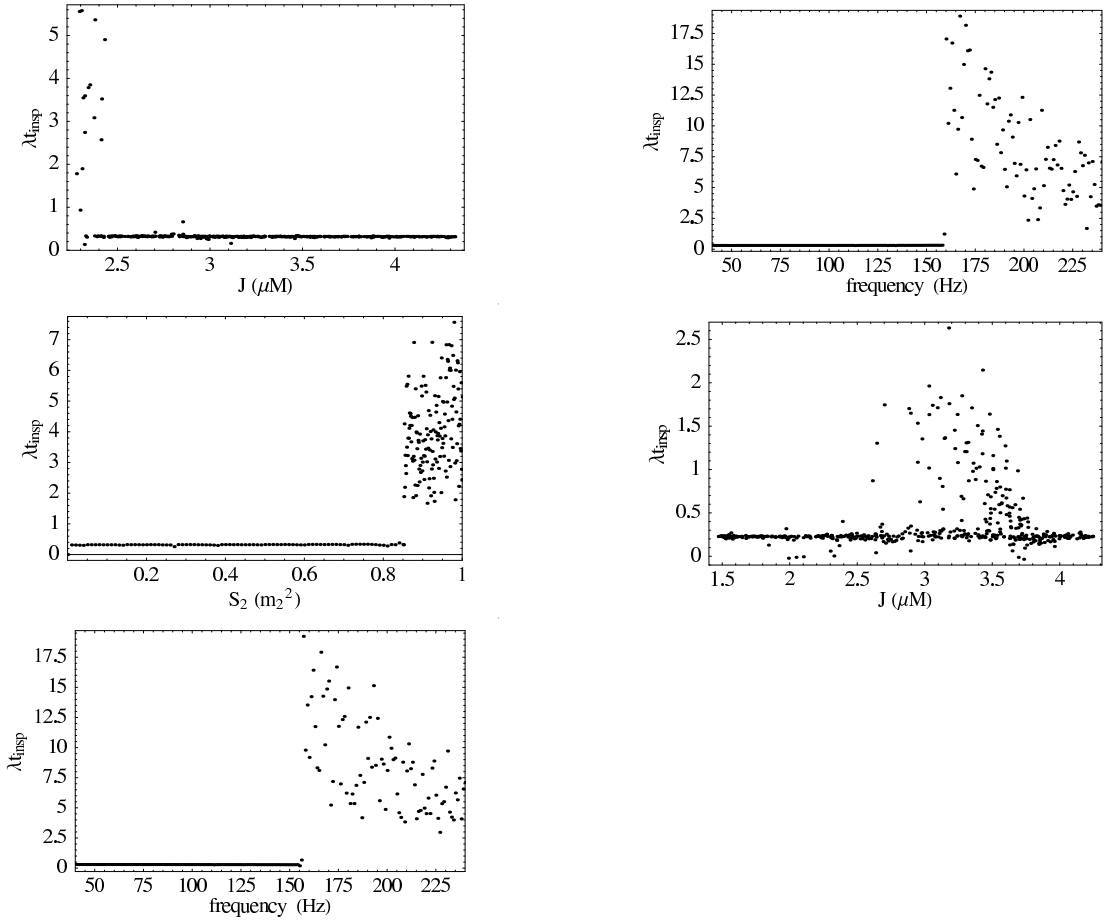


Figure 4.7: Dependence of Lyapunov exponent on the total angular momentum, the frequency of gravitational waves, and the spin, respectively, for a $(10 + 10)M_\odot$ BH-BH binary. Because the inverse of the Lyapunov exponent gives a characteristic timescale of the chaos, $\lambda t_{\text{insp}} > 1$ implies that the deviation of the two nearby trajectories grows exponentially within a inspiral timescale t_{insp} . For the details, see the text. These figures are cited from [42].

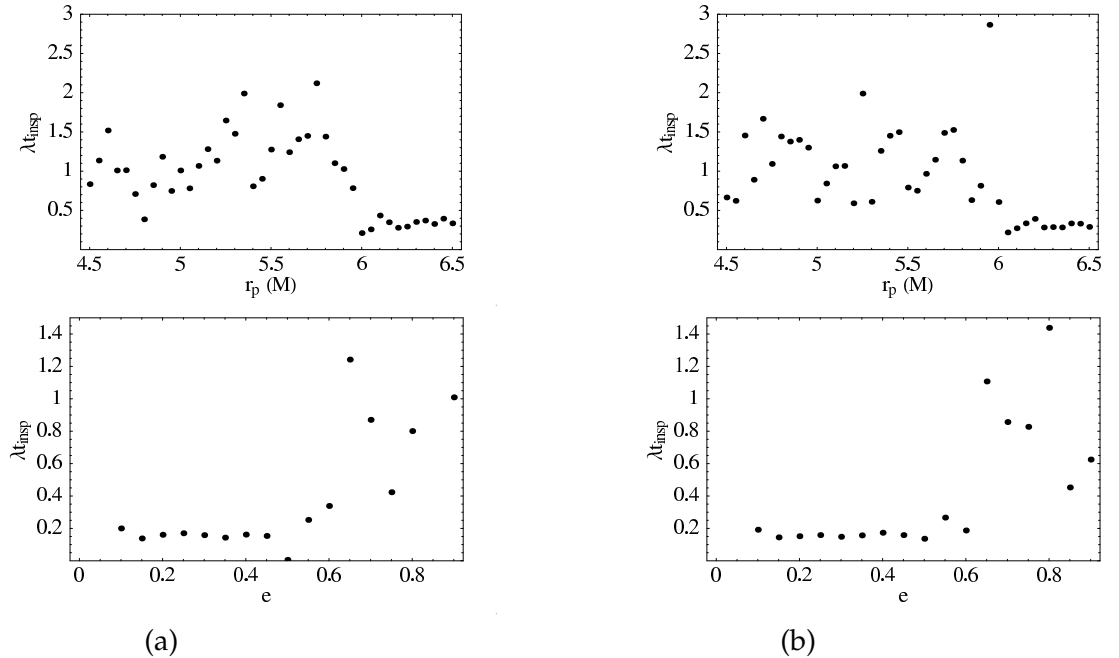


Figure 4.8: Dimensionless Lyapunov exponents λt_{insp} as functions of pericenter and eccentricity. (Left) All terms up to 2PN order are included. (Right) All terms up to 3PN order are included. This figure is cited from [42].

because less symmetry leads to a stronger chaotic motion. Hartl studied this issue [40, 41]. He assumed the background space time to be the Kerr space time and solved the Papapetrou equation. He also gave an orbital parametrization method based on the conventional one, which is well known as to parametrize the geodesics equations in the Kerr spacetime. From the analogy of the conventional method, he defined an eccentricity, pericenter and inclination angle in the spinning test particle system. Performing the wide range parameter survey, he concluded that the motion of the spinning particle with realistic parameters is not chaotic. The chaotic motion cannot be realized in realistic astrophysical systems.

In next chapter, we will show our work related to this topic. In our model, sometimes an unrealistic spin value is adopted. However, we should emphasize that our work has been done on the way of the long time controversy described above and some works were done after us. Moreover, concrete examples of the realistic chaotic systems are few.

CHAPTER 5

GRAVITATIONAL WAVE FROM PARTICLE ORBITING AROUND BLACK HOLE SPACETIME

As we review in the last chapter, it has been intensively discussed whether chaos really occurs or not in relativistic two body problem. The newest result [42] suggest that it is rare that chaos occurs in binary systems. However, a possibility of chaos is not completely excluded and topic to research still remains. In such the topics, we are interested in correlation between chaos and gravitational wave. How does chaos affect gravitational wave concretely ? Is it able to distinguish gravitational wave from non chaotic system to one from chaotic system ? Previous work with this view point is a few [99]. Although it may be impossible to detect gravitational wave from chaotic system with the current detectors with the matched filtering method in reality, this topic is academically interested or future detectors might observe gravitational wave from such a system.

Hence, we analyze gravitational wave from chaotic system. As a concrete example, we adopt spinning particle in the Kerr spacetime. The image of this system is depicted from Figure 5.1. To make a effect of chaos on gravitational wave, we also analyze a gravitational wave from spinless particle reported in [52]. Although orbit of spinless particle in the Kerr spacetime is proved to be integrable mathematically, we can arrange a complicated motion. On the other hand, the quadrupole formula means that gravitational wave is estimated by position, velocity, and acceleration of particle. Moreover, they appears in the formula with mixed form. Therefore, it is non trivial how gravitational wave can be emitted in such the complicated but non chaotic orbit.

Our aim in this chapter is to investigate how gravitational wave from chaotic or non chaotic system changes qualitatively.

5.1 Basic Equations for Test Particle

First we explain our basic assumption and review basic equations of both spinless and spinning particle.

5.1.1 Background Spacetime

We consider the Kerr metric as a background spacetime. In the Boyer-Lindquist coordinates, it is given by

$$ds^2 = - \left(1 - \frac{2Mr}{\Sigma}\right) dt^2 - \frac{4Mar \sin^2 \theta}{\Sigma} dt d\phi + \frac{\Sigma}{\Delta} dr^2 + \Sigma d\theta^2 + \sin^2 \theta \left(r^2 + a^2 + \frac{2Ma^2 r \sin^2 \theta}{\Sigma}\right) d\phi^2, \quad (5.1)$$

where

$$\Sigma = r^2 + a^2 \cos^2 \theta, \quad (5.2)$$

$$\Delta = r^2 - 2Mr + a^2. \quad (5.3)$$

M is a mass of black hole (BH) and a is the BH angular momentum, respectively.

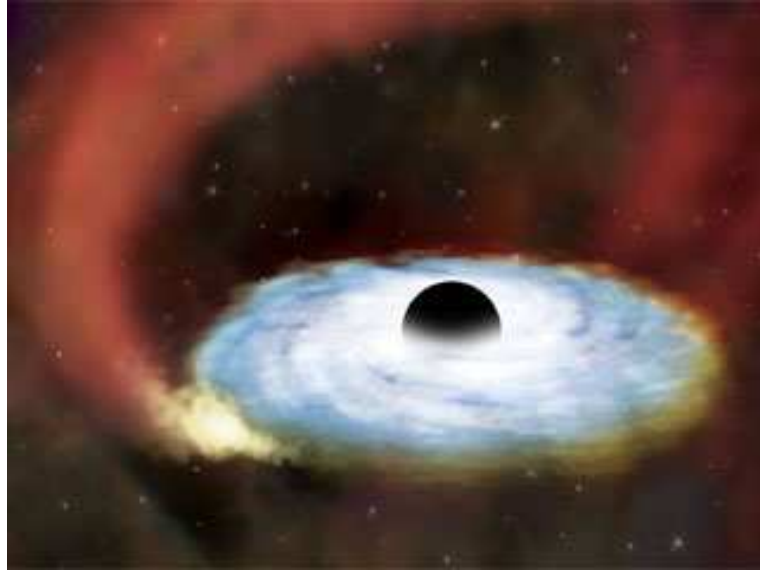


Figure 5.1: The image of a super massive black hole at galactic nuclei.
www.sorae.jp/031001/1220.html, image credit: NASA/CXC/SAO

5.1.2 Spinless Test Particle

In this subsection, we summarize the equations of motion for a spinless test particle. A spinless test particle moves along the geodesics;

$$\frac{d^2x^\mu}{d\tau^2} + \Gamma_{\nu\rho}^\mu \frac{dx^\nu}{d\tau} \frac{dx^\rho}{d\tau} = 0, \quad (5.4)$$

where τ is a proper time of the particle. In a stationary axisymmetric spacetime, a spinless particle has two constants of motion; the energy E and the z -component of the angular momentum L_z . The particle's rest mass μ is also constant. Carter discovered a fourth constant of motion and showed that the system is integrable [14, 75].

Carter Constant

The geodesic equation is derived from the Hamiltonian \mathcal{H} :

$$\frac{dx^\mu}{d\lambda} = \frac{\partial \mathcal{H}}{\partial p_\mu}, \quad (5.5)$$

$$\frac{dp_\mu}{d\lambda} = -\frac{\partial \mathcal{H}}{\partial x^\mu}, \quad (5.6)$$

where λ is an affine parameter and

$$\mathcal{H} \equiv \text{"super-Hamiltonian"} = \frac{1}{2}g^{\mu\nu}p_\mu p_\nu. \quad (5.7)$$

The four momentum is given by

$$\frac{d}{d\lambda} = \mathbf{p} = \text{4-momentum}, \quad (5.8)$$

The Hamiltonian formalism gives us two constants of motion. Because $g_{\mu\nu}$ is independent of t and ϕ , the superhamiltonian is independent as well. Therefore, the Hamilton's equation (5.6) leads to the consequence that p_t and p_ϕ are constants of motion.

Because the metric approaches to the Minkowski metric far from the black hole, the constants of motion are reduced to

$$\begin{aligned} p_t &= -p^t = \text{Energy}, \\ p_\phi &= (\text{projection of angular momentum along black hole's rotation axis}). \end{aligned} \quad (5.9)$$

Thus,

$$E \equiv (\text{"energy at infinity"}) \equiv -p_t, \quad (5.10)$$

$$L_z \equiv (\text{"angular momentum"}) \equiv p_\phi, \quad (5.11)$$

are the constants of motion.

The rest mass of the particle is a third constant of motion;

$$\mu = |\mathbf{p}| = (-g^{\mu\nu} p_\mu p_\nu)^{\frac{1}{2}}, \quad (5.12)$$

In general, if we have four constants of motion, we can specify the orbit of a particle moving in four dimensional spacetime uniquely. If the black hole possesses an additional symmetry such as spherical symmetry, rather than merely axially symmetry, we obtain a fourth constant of motion. However, in general, black holes rotate. Then, there are only three constants of motion of test particle moving around it. Carter showed that an additional constant exists in a rotating black hole spacetime [14].

The Hamilton-Jacobi equation can be utilized to derive the fourth constant of motion. With the superhamiltonian \mathcal{H} (5.7), the conjugate momentum p_t can be replaced by the gradient $\partial S/\partial x^\mu$ in the Hamilton-Jacobi equation;

$$-\frac{\partial S}{\partial \lambda} = \mathcal{H} = \frac{1}{2} g^{\alpha\beta} \frac{\partial S}{\partial x^\alpha} \frac{\partial S}{\partial x^\beta}. \quad (5.13)$$

Assuming the Kerr metric in the Boyer-Lindquist coordinate (5.1), the Hamilton-Jacobi equation is recast into

$$\begin{aligned} -\frac{\partial S}{\partial \lambda} &= -\frac{1}{2} \frac{1}{\Delta \Sigma} \left[(r^2 + a^2) \frac{\partial S}{\partial t} + a \frac{\partial S}{\partial \phi} \right]^2 + \frac{1}{2} \frac{1}{\Sigma \sin^2 \theta} \left[\frac{\partial S}{\partial \phi} + a \sin^2 \theta \frac{\partial S}{\partial t} \right]^2 \\ &\quad + \frac{1}{2} \frac{\Delta}{\Sigma} \left(\frac{\partial S}{\partial r} \right)^2 + \frac{1}{2} \frac{1}{\Sigma} \left(\frac{\partial S}{\partial \theta} \right). \end{aligned} \quad (5.14)$$

The equation is independent of λ , t , and ϕ . The solution should be

$$S = \frac{1}{2} \mu^2 \lambda - Et + L_z \phi + S_r(r) + S_\theta(\theta). \quad (5.15)$$

We can easily derive the Hamilton-Jacobi equation $\partial S/\partial \lambda = -\mathcal{H}$ and the constants of motion $\partial S/\partial t = p_t$ and $\partial S/\partial \phi = p_\phi$. Putting this equation into Eq. (5.14) and solving with respect to $S_r(r)$ and $S_\theta(\theta)$, we obtain

$$S_r = \int \Delta^{-1} \sqrt{R} dr, \quad (5.16)$$

$$S_\theta = \int \sqrt{\Theta} d\theta, \quad (5.17)$$

where

$$\Theta(\theta) = C - \cos^2 \theta \left\{ a^2(1 - E^2) + \frac{L_z^2}{\sin^2 \theta} \right\}, \quad (5.18)$$

$$R(r) = P^2 - \Delta \{r^2 + (L_z - aE)^2 + C\}. \quad (5.19)$$

Note that the constant C is a “separation-of-variables constant” and we call it the Carter constant.

As a result, Eq. (5.4) can be reduced to a set of the differential equations as

$$\Sigma \frac{d\theta}{d\tau} = \pm \sqrt{\Theta}, \quad (5.20)$$

$$\Sigma \frac{dr}{d\tau} = \pm \sqrt{R}, \quad (5.21)$$

$$\Sigma \frac{d\phi}{d\tau} = -\left(aE - \frac{L_z}{\sin^2 \theta}\right) + \frac{a}{\Delta} P, \quad (5.22)$$

$$\Sigma \frac{dt}{d\tau} = -a(aE \sin^2 \theta - L_z) + \frac{r^2 + a^2}{\Delta} P, \quad (5.23)$$

where

$$P(r) = E(r^2 + a^2) - aL_z. \quad (5.24)$$

Note that because of the presence of the Carter constant, the orbits of a particle will never be chaotic.

5.1.3 Spinning Test Particle

We use the Papapetrou equations (see Chapter 3). The set of equations with spin vector is given as

$$\frac{dx^\mu}{d\tau} = v^\mu, \quad (5.25)$$

$$\frac{Dp^\mu}{d\tau} = \frac{1}{\mu} R^{*\mu}_{\nu\rho\sigma} v^\nu S^\rho p^\sigma, \quad (5.26)$$

$$\frac{DS^\mu}{d\tau} = \frac{1}{\mu^3} p^\mu R^*_{\nu\rho\sigma\gamma} S^\nu v^\rho S^\sigma p^\gamma, \quad (5.27)$$

where

$$R^*_{\mu\nu\rho\sigma} \equiv \frac{1}{2} R_{\mu\nu}^{\alpha\beta} \epsilon_{\alpha\beta\rho\sigma}. \quad (5.28)$$

The center of mass condition is given by

$$p_\nu S^\nu = 0. \quad (5.29)$$

With this condition, the relation between p^μ and v^μ is determined as follow :

$$v^\mu = u^\mu + \frac{1}{\mu^2} R^*_{\nu\rho\sigma} S^\nu S^\rho u^\sigma, \quad (5.30)$$

where $u^\mu \equiv p^\mu/\mu$ and

$$R^*_{\mu\nu\rho\sigma} \equiv \frac{1}{2} \epsilon_{\mu\nu\alpha\beta} R^{*\alpha\beta}_{\rho\sigma}. \quad (5.31)$$

The affine parameter u is fixed by the normalization condition of $v^\mu u_\mu = -\delta$. This gives N as

$$N = 1 + \frac{1}{\mu^4} {}^*R_{\alpha\beta\mu\nu}^* S^\alpha p^\beta S^\mu p^\nu, \quad (5.32)$$

Constants of motion are

$$\mu^2 = -p_\mu p^\mu, \quad (5.33)$$

$$S^2 = S_\mu S^\mu, \quad (5.34)$$

$$C_\xi = \xi^\mu p_\mu - \frac{1}{2\mu} \xi_{\mu;\nu} \epsilon^{\mu\nu\rho\sigma} p_\rho S_\sigma. \quad (5.35)$$

5.2 Orbital parameters and initial condition

5.2.1 spinless particle

As we see in Sec. 5.1.2, the equations of the motion of a spinless particle are integrable because of the existence of the Carter constant. That is chaos does not occur. But Johnston found that the orbits of a spinless particle can be complicated as if chaos occurred [52]. To investigate a character of chaos of spinning particle, we adopt this trajectory. The parameters are set as

$$(a, E, L_z, C) = (1/\sqrt{2}, 0.968\mu, 2.0\mu M, 10\mu^2 M^2). \quad (5.36)$$

5.2.2 spinning particle

For a spinning particle, we have to search the orbital parameters region in which the motion could be chaotic. As like in the Schwarzschild case, it becomes possible if we were able to define the “effective” potential [97]. However, because the Kerr metric has less symmetry than the Schwarzschild, the assumption (4.8) is no longer valid. This implies one cannot define the “effective” potential in the Kerr case. Therefore, we make use the result of [98]. Before explaining this work, we review an effective potential for a particle with spin. The motion is limited on the equatorial plane [85].

effective potential of a particle with spin on equatorial plane

The background spacetime is the Kerr spacetime and the metric is given by Equation (5.1). To simplify the system we introduce the tetrad basis given as

$$e^0_\mu = \left(\sqrt{\frac{\Delta}{\Sigma}}, 0, 0, -a \sin^2 \theta \sqrt{\frac{\Delta}{\Sigma}} \right), \quad (5.37)$$

$$e^1_\mu = \left(0, \sqrt{\frac{\Delta}{\Sigma}}, 0, 0 \right), \quad (5.38)$$

$$e^2_\mu = (0, 0, \sqrt{\Sigma}, 0), \quad (5.39)$$

$$e^3_\mu = \left(-\frac{a}{\sqrt{\Sigma}} \sin \theta, 0, 0, \frac{r^2 + a^2}{\sqrt{\Sigma}} \sin \theta \right), \quad (5.40)$$

where $e^i_\mu = (e^i_t, e^i_r, e^i_\theta, e^i_\phi)$ ($i = 0 \sim 3$).

The Kerr spacetime has the timelike Killing vector $\xi_{(t)}^\mu$ and the spacelike Killing vector $\xi_{(\phi)}^\mu$. Therefore we can define the particle energy E and the particle angular momentum J_z as

$$E = -\sqrt{\frac{\Delta}{\Sigma}} p_0 + \frac{a}{\sqrt{\Sigma}} \sin \theta p_3 - \frac{M}{\Sigma^2} (r^2 - a^2 \cos^2 \theta) S^{01} + \frac{2Mar \cos \theta}{\Sigma^2} S^{23}, \quad (5.41)$$

$$\begin{aligned} J_z = & -a \sin^2 \theta \sqrt{\frac{\Delta}{\Sigma}} p_0 + \frac{r^2 + a^2}{\sqrt{\Sigma}} \sin \theta p_3 - \frac{a[(r - M)\Sigma + 2Mr^2]}{\Sigma^2} \sin^2 \theta S^{01} \\ & - \frac{a\sqrt{\Delta}}{\Sigma} \sin \theta \cos \theta S^{02} + \frac{[(r^2 + a^2)^2 - a^2 \Delta \sin^2 \theta]}{\Sigma^2} \cos \theta S^{23} - \frac{r\sqrt{\Delta}}{\Sigma} \sin \theta S^{31}. \end{aligned} \quad (5.42)$$

To restrict the motion of the test particle on the equatorial plane, the spin of the test particle have to be parallel to the rotating axis of the Kerr black hole. Hence, we impose

$$\theta = \frac{\pi}{2}, \quad S^0 = S^1 = S^3 = 0, \quad S^2 = -S, \quad p^2 = 0. \quad (5.43)$$

Substituting these values to Equations (5.41) and (5.42), we obtain

$$E = -\frac{\sqrt{\Delta}}{r} p_0 + \frac{1}{r} \left(a + \frac{MS}{\mu r} \right) p_3, \quad (5.44)$$

$$J_z = -\frac{\sqrt{\Delta}}{r} \left(a + \frac{S}{\mu} \right) p_0 + \frac{1}{r} \left[r^2 + a^2 + \frac{aS(r + M)}{\mu r} \right] p_3. \quad (5.45)$$

We solve these equations in terms of p_0 and p_3 and substitute the results and $p_2 = 0$ into $\mu^2 = -p_\mu p^\mu$. Then, we obtain

$$\alpha E^2 - 2\beta E + \gamma - \left(\frac{\sqrt{\Delta}}{r} \Sigma_s p_1 \right)^2 = 0, \quad (5.46)$$

where

$$\Sigma_s = r^2 \left(1 - \frac{MS^2}{\mu^2 r^3} \right), \quad (5.47)$$

$$\alpha = \left[(r^2 + a^2) + \frac{aS}{\mu r} (r + M) \right]^2 - \Delta \left(a + \frac{S}{\mu} \right)^2, \quad (5.48)$$

$$\beta = \left[\left(a + \frac{MS}{\mu r} \right) \left\{ (r^2 + a^2) + \frac{aS}{\mu r} (r + M) \right\} - \Delta \left(a + \frac{S}{\mu} \right) \right] J_z, \quad (5.49)$$

$$\gamma = \left(a + \frac{MS}{\mu r} \right)^2 J_z^2 - \Delta \left[r^2 \left(1 - \frac{MS^2}{\mu^2 r^3} \right)^2 + J_z^2 \right]. \quad (5.50)$$

The effective potential $V_{\text{eff}}^{(\pm)}$ is defined as

$$(p_1)^2 = \frac{\alpha r^2}{\Delta \Sigma_s^2} (E - V_{\text{eff}}^{(+)}) (E - V_{\text{eff}}^{(-)}). \quad (5.51)$$

The explicit form is

$$V_{\text{eff}}^{(\pm)} = \frac{\beta \pm \sqrt{\beta^2 - \alpha \gamma}}{\alpha}. \quad (5.52)$$

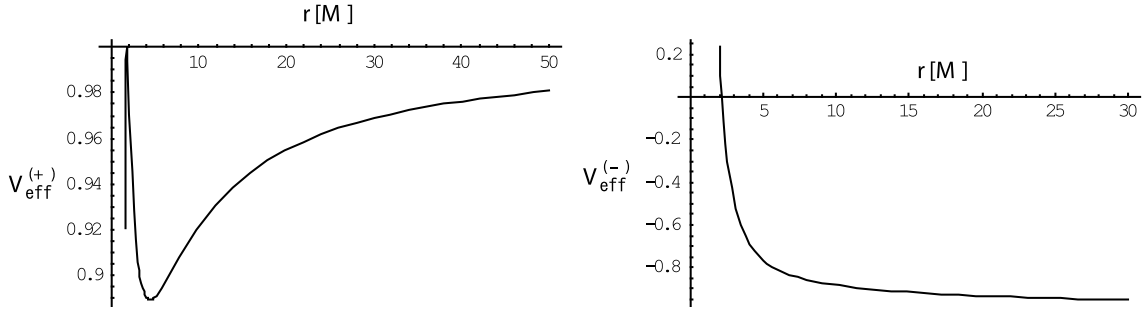


Figure 5.2: The effective potential for spinning particle on the equatorial plane.

	inner extremal point		outer extremal point	
	r direction	θ direction	r direction	θ direction
Type(B1)	Unstable	Stable	Stable	Stable
Type(B2)	Unstable	Unstable	Stable	Stable
Type(U1)	no extremal point			
Type(U2)	Unstable	Unstable	Stable	Unstable

Table 5.1: The stability of the motion of a particle with spin moving on the equatorial plane. This table is cited from [98].

S has the information about not only the spin magnitude but also the direction of the spin. $aS > 0$ implies that the particle spin direction agrees with the BH spin direction. On the other hand, $aS < 0$ implies that the particle spin direction is opposite with respect to the BH spin direction. $E \leq V_{\text{eff}}^{(+)}$ corresponds to the region in which the particle with the energy E can move around. We show the typical form of the effective potential in Figure (5.2). From this figure, we recognize that $V_{\text{eff}}^{(+)}$ has a physical meaning rather than $V_{\text{eff}}^{(-)}$.

circular orbit in equatorial plane

Figure 5.2 ($V_{\text{eff}}^{(+)}$) shows that the potential has two extrema. The local maximum corresponds to unstable circular orbit and local minimum does to stable orbit. Unstable(stable) means that the orbit is unstable(stable) to r -direction. This fact is well known in the case of particle without spin.

In [98], they analyzed a stability of these circular orbit for θ -direction in addition to r -direction. They solved linear perturbation equation of the equations of motion in circular orbit as eigenvalue problem. With this analysis, it was revealed that the radius of ISCO (inner stable circular orbit) depends on the parameters a, S, J_z . They also connected the stability of circular orbit to the potential types defined in [97] (see also Chapter 4). Figure 4.2 can be classified from the view point of the stability of circular orbit. Table 5.1 summarize their result.

With this analogy, they classified the $S - J_z$ parameter region into four types according the classification of the “effective” potentials 4.20. The result is depicted in Figure 5.3.

In Figure 5.3, the potential B2 is important because the trajectories of the spinning particle moving in this potential can be chaotic. We adopt the parameter region (a, S, J_z) from this figure. Subsequently, from Figure 5.2, we set the energy E such that orbits will be bounded. Initial conditions are chosen to be satisfied the constraints (5.29), (5.33)-(5.35).

Note that this procedure is not perfect to find a bound orbit because we do not have detailed

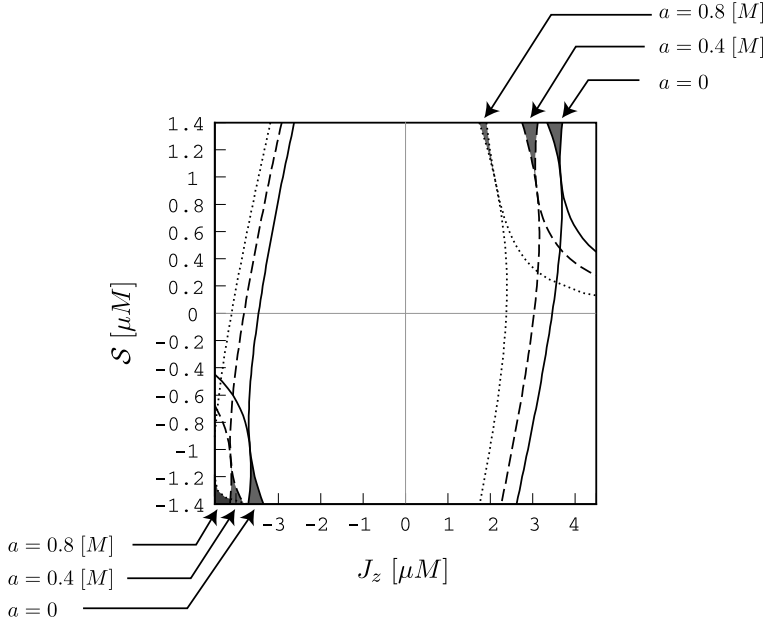


Figure 5.3: The potential category for a spinning particle in a Kerr space time. This figure is cited from [98].

information about the perfect effective potential of the particle with spin. This pathology results a capture of the particle by the BH. Hence, we search the parameters and initial conditions in the wide range and carefully monitor the particle's motion.

5.3 Numerical Analysis

In this section, we show our numerical results for the orbital motion of a test particle and the wave forms, the energy fluxes and the gravitational wave spectrum. To analyze chaotic behavior of a test particle, we use the Lyapunov exponent and the Poincaré map.

5.3.1 Particle Motion

At first, we analyze particle motions both without and with spin.

Spinless Particle

Integrating numerically the equations of motion (5.20)-(5.23), we show a typical complicated orbit in Figure 5.4. We adopt the parameters (E, J_z, C, a) Johnston have reported. This orbit is called the orbit (a) in this chapter. The behavior of the orbit (a) looks complicated. However, showing the Poincaré map in Figure 5.5, we find a closed curve, which confirms that the orbit (a) is not chaotic.

Spinning Particle

We utilized the Bulirsch-Stoer method [84] to integrate Eqs. (5.25)-(5.27). The constraint equations (5.29),(5.33), (5.34) and (5.35) is used to check the error of the numerical solution and we find the relative errors are smaller than 10^{-11} .

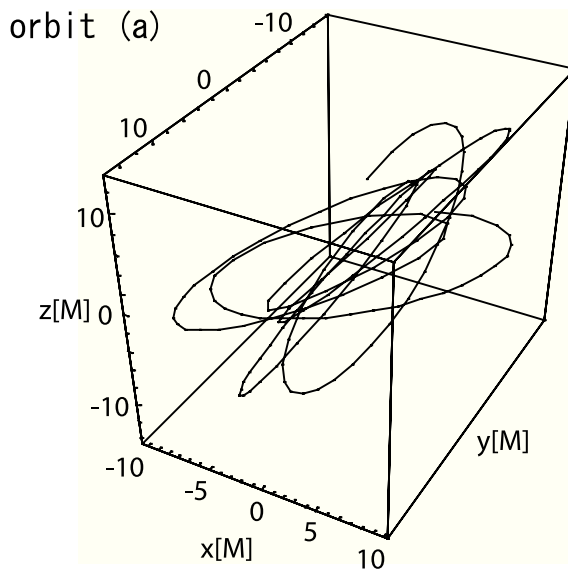


Figure 5.4: The orbit of a spinless particle with $E = 0.968\mu$, $J_z = 2.0\mu M$, $C = 10\mu^2 M^2$ and $a = 1/\sqrt{2}$. We choose the initial position and velocity as $(r, \theta, \phi) = (10M, \pi/2, 0)$ and $(v^r, v^\theta, v^\phi) = (0.14, 0.03, 0.02)$. This is called the orbit (a) in this chapter. This orbit looks very complicated as if chaos occurred.

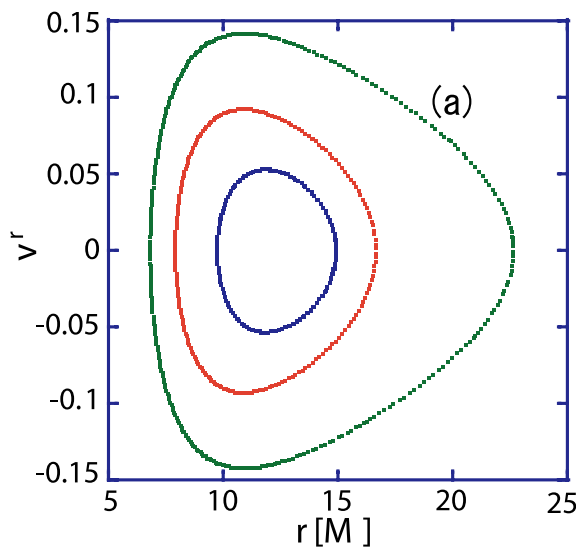


Figure 5.5: The Poincaré map of the orbit (a). The plot points consist of a closed curve in the $r-v^r$ plane. We also plot the Poincaré map of other two orbits with the same conserved quantities as those of the orbit (a). This confirms that the system is integrable.

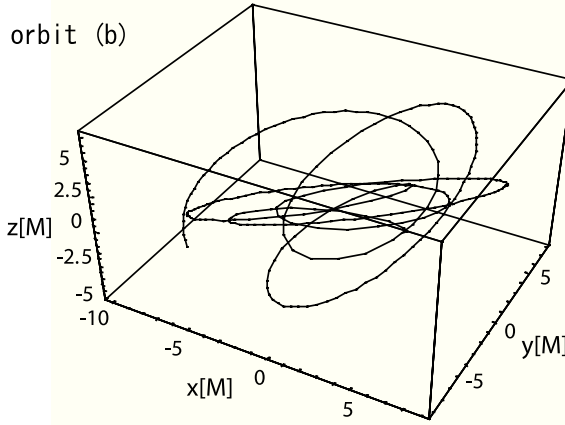


Figure 5.6: The orbit of a spinning particle with $E = 0.9328\mu M$, $J_z = 2.8\mu M$, and $S = 1.0\mu M$. We set $a = 0.8M$ and choose the initial position and velocity as $(r, \theta, \phi) = (6.0M, \pi/2, 0)$ and $(v^r, v^\theta, v^\phi) = (0.18, 0.05, 0.07)$. This is called the orbit (b), which is. complicated just as the orbit (a).

We show the typical orbit of the spinning test particle in Figure 5.6 and call it the orbit (b). Comparing Figure 5.4 with Figure 5.6, we cannot distinguish two orbits. However, the difference between chaotic orbit and nonchaotic one will be apparent when we draw the Poincaré maps. In Figure 5.7, we show the Poincaré map of the orbit (b). The plot points distribute randomly in Figure 5.7. We also calculate the Lyapunov exponent λ to evaluate the strength of chaos. The result is depicted in Figure 5.8. As shown in Figure 5.8, the Lyapunov exponent λ is positive, which means that the orbit (b) is chaotic. The typical time scale for chaos is given by $\lambda^{-1} \sim 18M$. To compare this time scale with the dynamical time scale, we determine the average of orbital period. The chaotic orbit we consider is not a closed orbit. Therefore it is difficult to determine the average of orbital period. The method we use is as follows:

- (i) At first, we take three intersections, the x-y plane, the y-z plane and the z-x plane.
- (ii) Secondly we calculate three kinds of the orbital periods when the particle crosses these plane.

We show the result in Figure 5.9. From Figure 5.9, we find the main orbital period is about $100M \sim 120M$ in the all cases. To calculate the average of orbital period we adopt Figure 5.9 (iii). As a result, we find the average of orbital period is $74.3M$, which is averaged after 10^2 rotations around the black hole. Comparing the time scale for chaos, we find that the orbit (b) becomes chaotic just after a few revolutions around a black hole.

5.3.2 Gravitational Wave

Based on the previous calculation of the orbits, we show the wave forms and its energy spectra and analyze an effect of chaos on the emitted gravitational waves. To estimate the gravitational waves, we use the multipole expansion of gravitational field [73, 103]. We briefly review this method in Sec. 2.4.

Giving the information of a particle orbit, we can evaluate h_{ij}^{TT} for each l . The gravitational waves from a chaotic orbit of a spinning particle may contain higher multipole moments ($l > 2$) than quadrupole ($l = 2$). This is the reason why we analyze the gravitational waves not only $l = 2$ but also $l = 3$. Note that because the orbit considered here is very relativistic, the multipole expansion may not be valid and then it will provide only a qualitative feature. In Figure 5.10

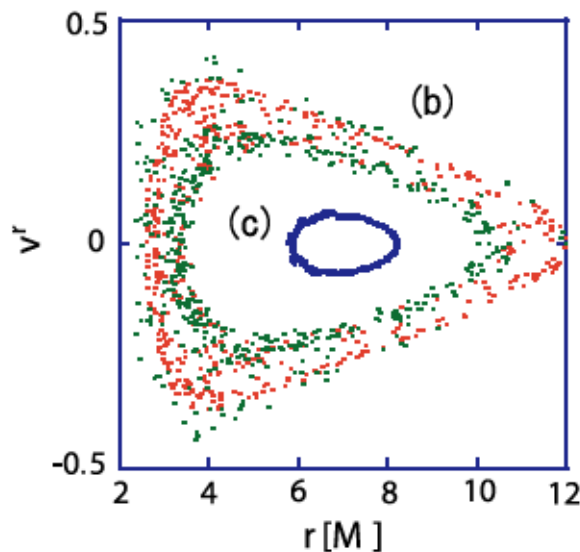


Figure 5.7: The Poincaré maps of the orbit (b) and (c). The plot points for the orbit (b) (green) distribute randomly, which confirms that it is a chaotic system. Different colors represent orbits with different initial conditions. For the orbit (c) (blue), we will discuss it later.

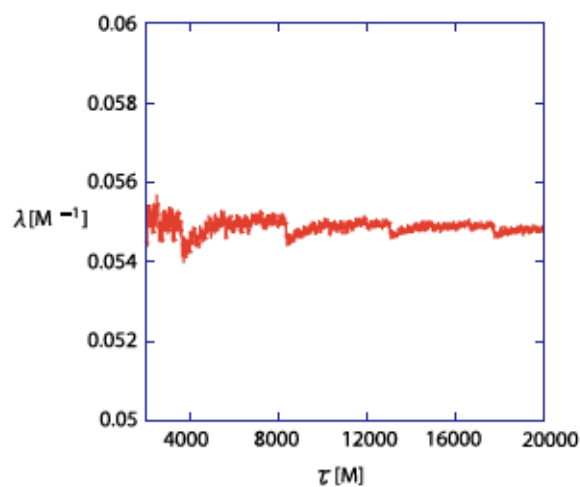


Figure 5.8: The maximal Lyapunov exponent λ for the orbit (b). The typical time scale for chaos is given by $\lambda^{-1} \sim 18M$, while the average of orbital period is $74.3M$.

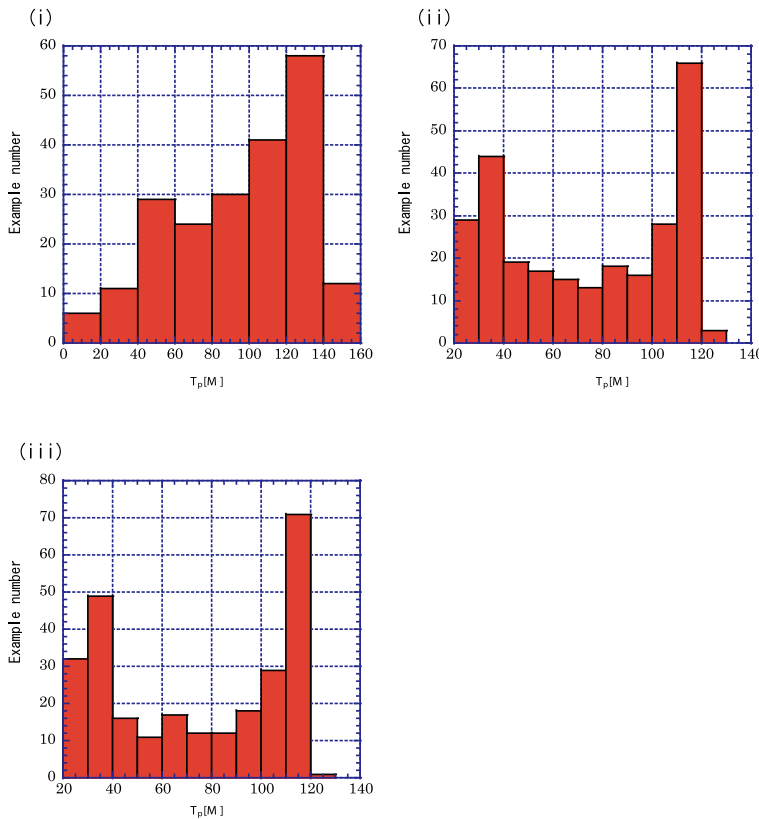


Figure 5.9: The distribution of the orbital period for the orbit (b). The vertical axis represents numbers of counts and the horizontal axis represents the orbital period T_p . Figures (i), (ii) and (iii) show the distribution of the orbital period for the x-y plane, the y-z plane and the z-x plane, respectively. The distributions are not so different from each other cases.

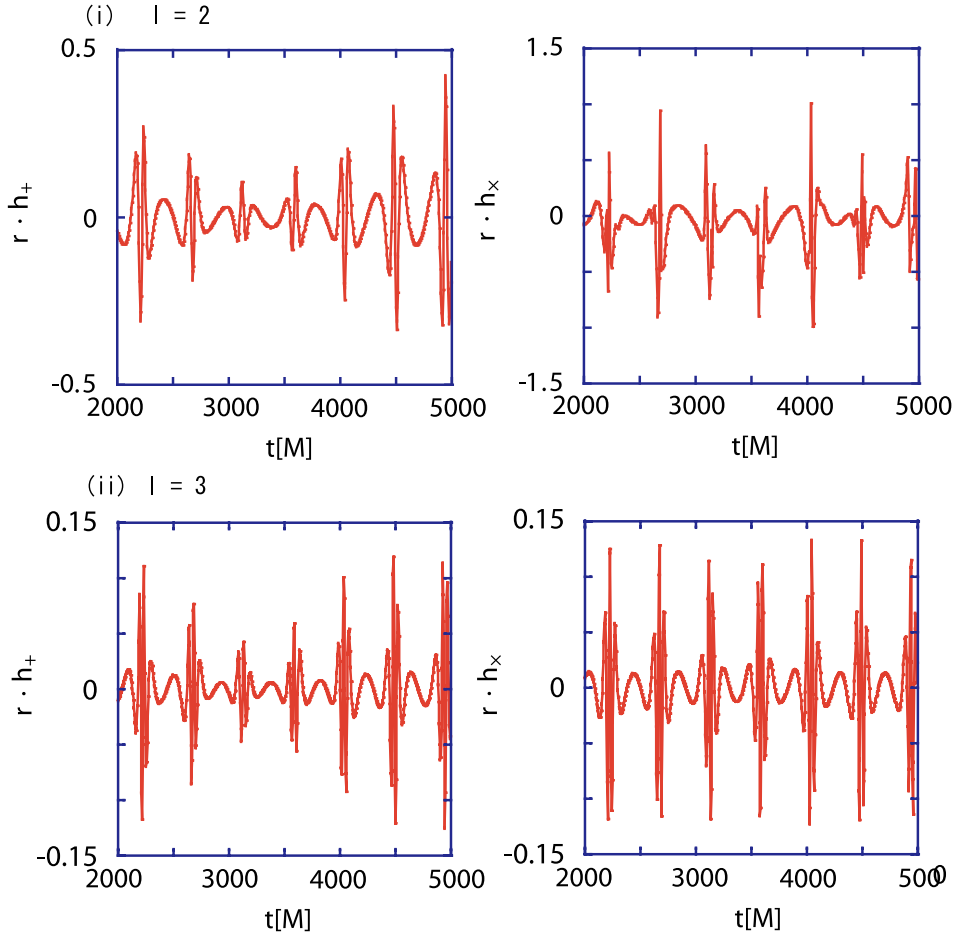


Figure 5.10: The two polarization mode $+$ and \times of gravitational waves for the orbit (a). Figures (i) and (ii) show the wave forms of $l = 2$ and 3 , respectively.

and Figure 5.11, we show the gravitational wave forms for the orbits (a) and (b), respectively.

These figures reveal two important points. One is that in the wave forms, there looks some difference between two orbits (a) and (b), but it may be difficult to distinguish which one is chaotic. Just as reference, we depict the wave form for a circular orbit in Figure 5.12, which is quite regular. The second points is that the amplitudes of the octupole wave ($l = 3$) are smaller than those of the quadrupole wave ($l = 2$). Comparing the peak values, we find that the ratio of the amplitude of $l = 3$ to that of $l = 2$ is about 30 percents.

In Figure 5.13, we show the quadrupole wave spectrum from the orbit (a). In Figure 5.14, we show the energy spectrum of the gravitational wave ($l = 2, 3$) from the spinning particle. From Figure 5.13 and Figure 5.14, we find that there is a clear difference in the energy spectra of the gravitational waves between the orbit (a) and (b). How about the orbit of a spinning particle which looks regular? In order to understand a role of chaotic behavior, we also analyze the orbit (c), which Poincaré map is nearly a closed circle (the e inner circle map in Figure 5.7). Although this map looks closed in Figure 5.7, we find that it is not really closed when we enlarge it (see Figure 5.15). We show the wave forms for the orbit (c) in Figure 5.16.

We also present the spectrum in Figure 5.17. From the figures, we may conclude that the spectrum of gravitational waves from nonchaotic orbits contains only discrete characteristic frequencies. On the other hand, the spectrum for the chaotic orbits contains the various frequencies. It seems to be a continuous spectrum with finite widths. The ratio of the octopole

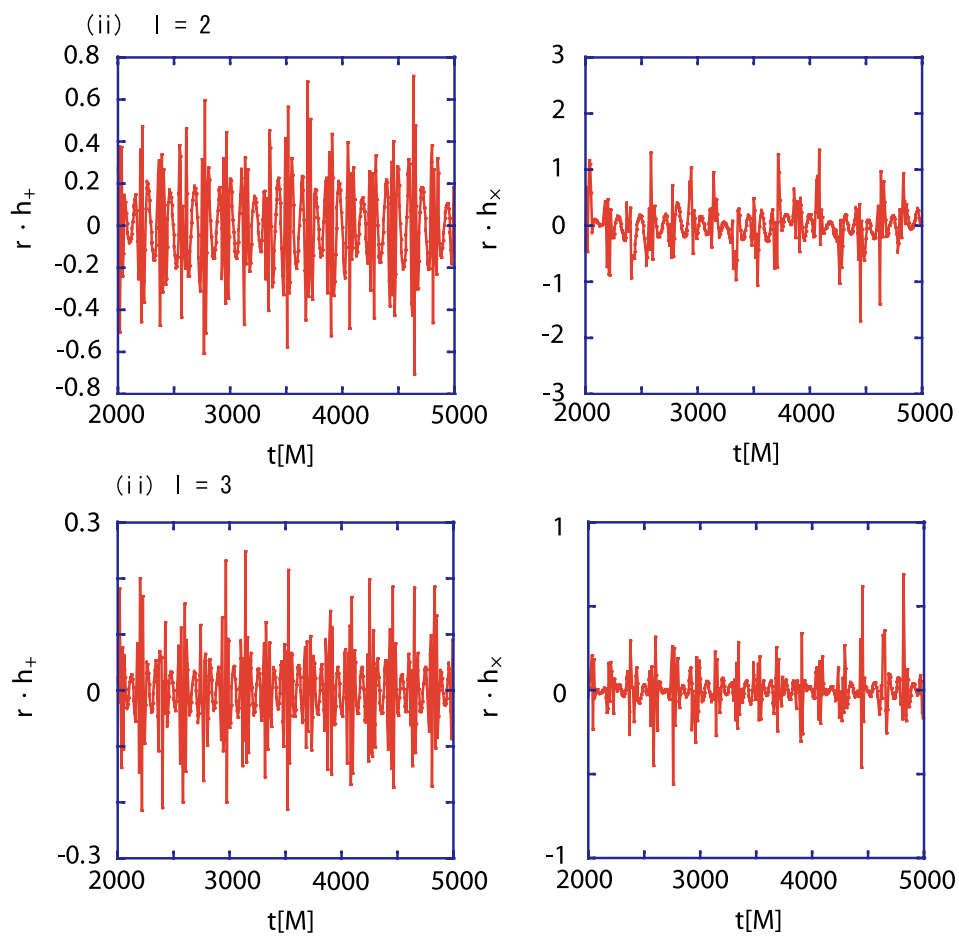
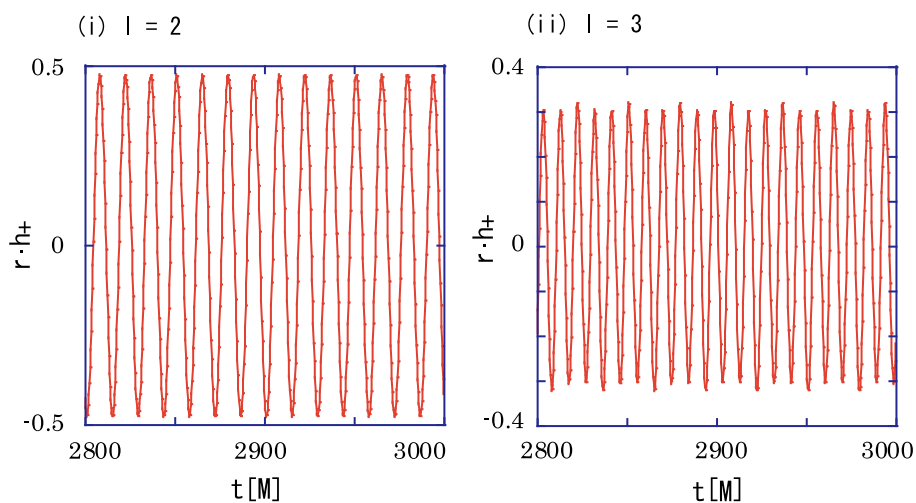


Figure 5.11: Same as Fig. 5.10, but for the orbit (b).

Figure 5.12: The wave forms for a circular orbit at $r = 2.45M$.

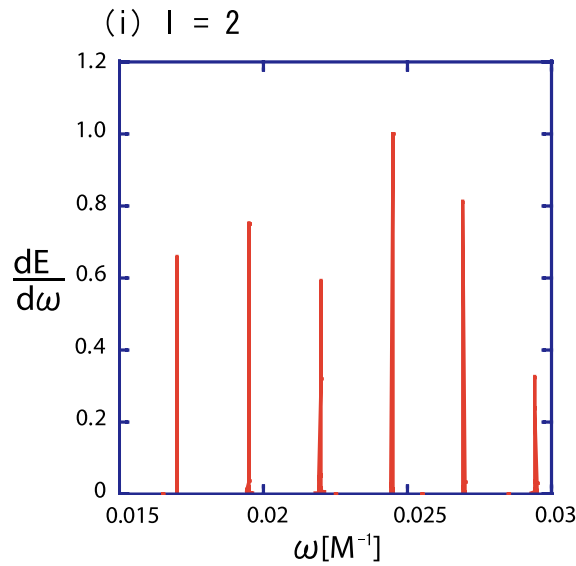


Figure 5.13: An energy spectrum of the gravitational wave from the orbit (a) normalized by its maximal.

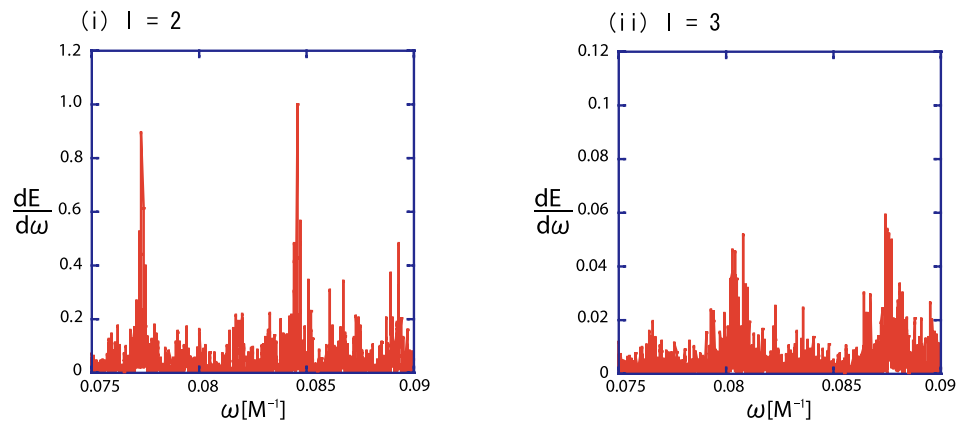


Figure 5.14: The quadrupole wave spectrum (left) and the octupole wave spectrum (right) for the orbit (b). The amplitude is normalize by the maximum value with $l = 2$ case.

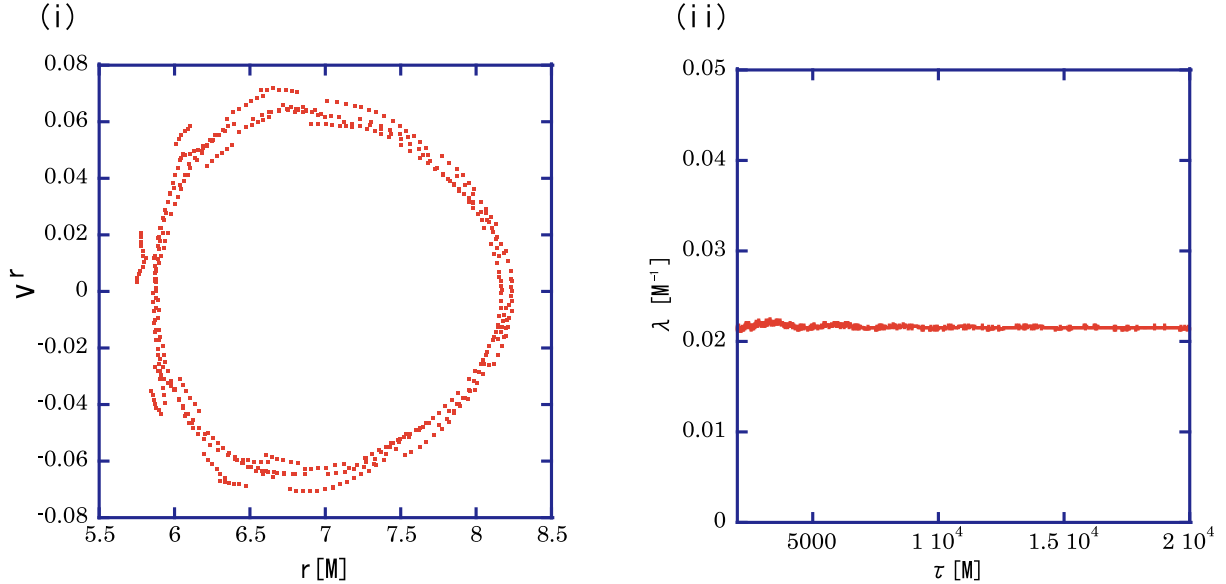


Figure 5.15: (i) The Poincaré map of the orbit (c). We also plot the Lyapunov exponent (ii), which value is smaller than that of the orbit (b) but is still positive ($\lambda \sim 0.02M$).

wave energy for the orbit (b) to that of the quadrupole wave is about 12.4 percents. Therefore the higher pole moment than the quadrupole moment does not contribute so much to the emitted gravitational waves, although the orbit is chaotic.

We plot the energy flux of the gravitational waves in Figure 5.18. Comparing Figure 5.18 (i) and (ii) we find that a form of the energy flux in the case of chaos is not clearly different from one in the case of nonchaos. Comparing Figure 5.18 (ii) and (iii) we also find that the stronger the chaos is, the large the magnitude of the energy flux is. That is if the behavior of the test particle is strongly chaotic, the gravitational wave can be emitted in large quantities.

5.4 Summary

In this chapter, we investigate the gravitational waves from a chaotic motion. As a concrete example, we analyze the particle motion in the Kerr space time. We confirm that the orbit of a spinning particle can be chaotic. Using the multipole expansion method of a gravitational field, we evaluate the gravitational waves from a chaotic and a non-chaotic orbit in order to analyze the effect of chaos on the emitted gravitational waves. As the results, there are not so much difference for the gravitational wave forms. However, the gravitational wave energy spectra show a clear difference. For a chaotic orbit, we find a continuous energy spectrum with several peaks. While, in the case of nonchaotic orbit, the spectrum contains the discrete characteristic frequencies. We also find that the higher pole moments than quadrupole moment of the system do not contribute so much to the emitted gravitational waves even for a chaotic orbit.

When the gravitational waves are detected and the energy spectrum is determined by observation, not only the astrophysical parameters, e.g., the mass, the angular momentum, and the spin are determined but also some fundamental physics such as relativistic nonlinear dynamics could be discussed.

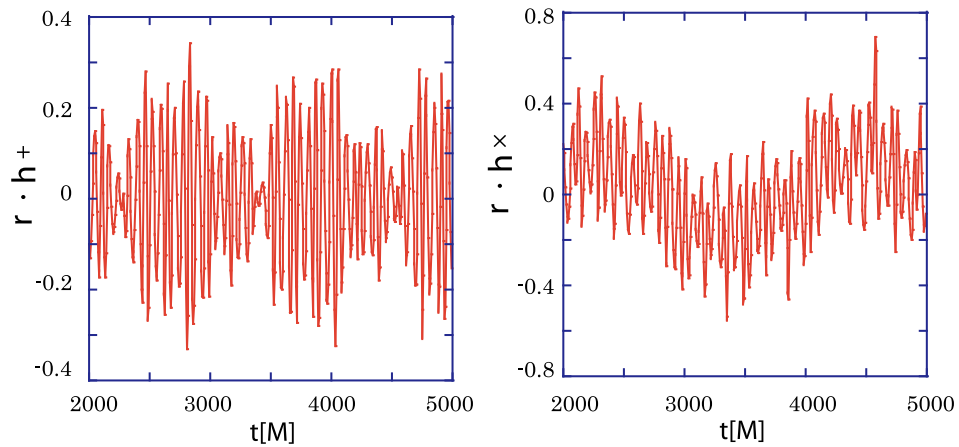
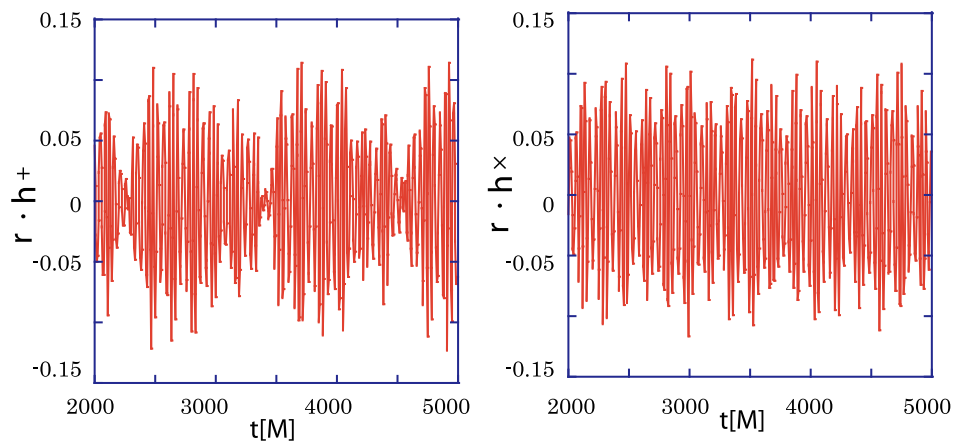
(i) $|l| = 2$ (ii) $|l| = 3$ 

Figure 5.16: Same as Fig. 5.10, but for the orbit (c).

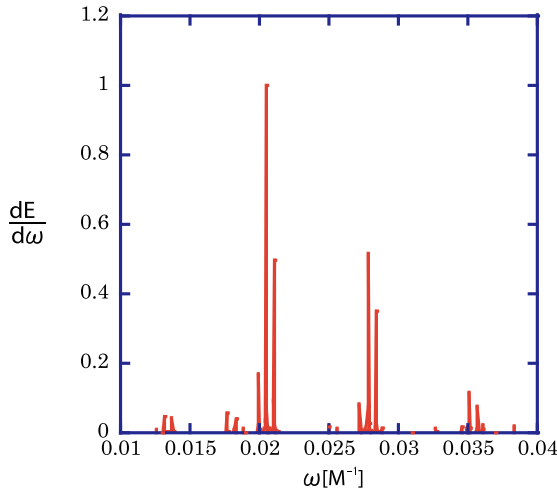
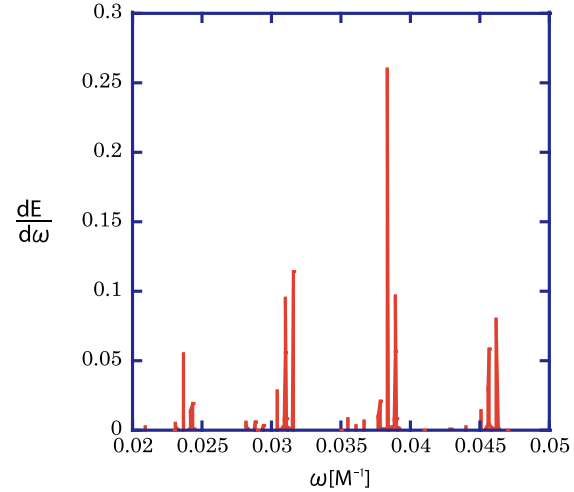
(i) $|l| = 2$ (ii) $|l| = 3$ 

Figure 5.17: Same as Fig. 5.13, but for the orbit (c).

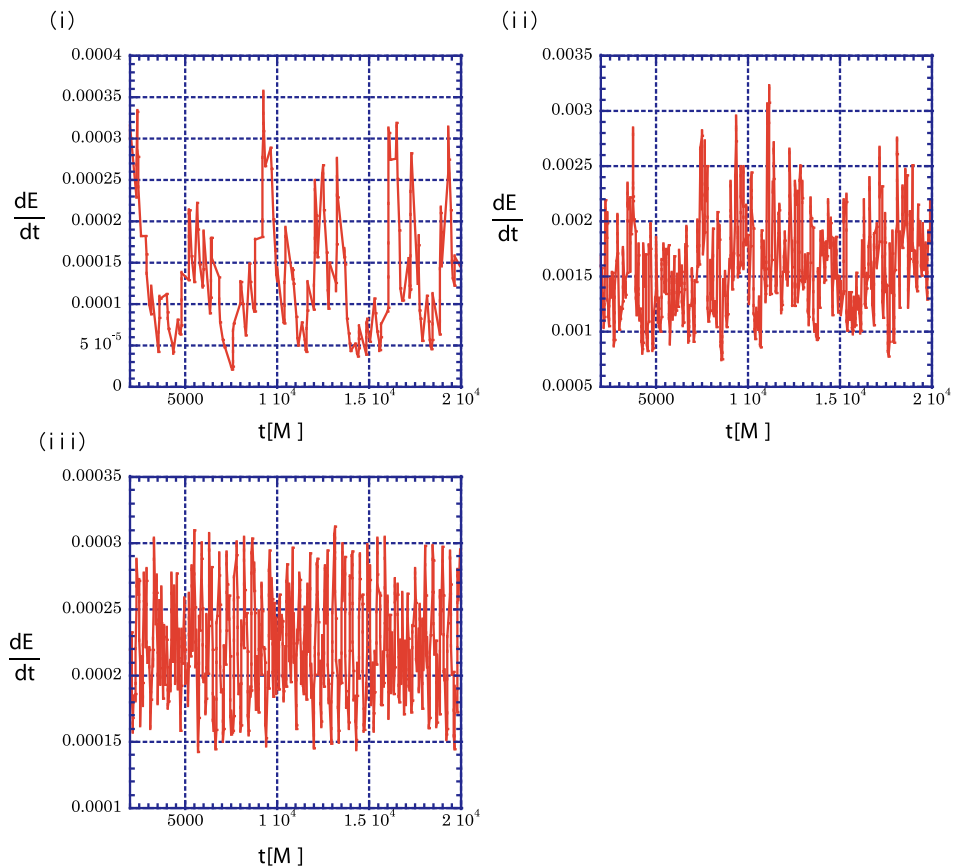


Figure 5.18: The energy flux of the gravitational waves. Figure (i), (ii) and (iii) present the energy flux of the orbit (a), (b) and (c), respectively.

CHAPTER 6

GRAVITATIONAL WAVE SIGNALS FROM CHAOTIC SYSTEM: A POINT MASS WITH DISK

As reviewed in Chapter 4, the chaos in relativistic binary or extreme-mass ratio binary has been intensively studied. As a result, it has revealed that chaos in binary system hardly occurs. However, this does not imply that chaos does not occur in universe because we can observe chaotic phenomena everywhere. Therefore, it is necessary to continue investigating chaos in various astrophysical systems. Furthermore, we have to try a different approach from the previous works to chaos in astrophysical systems. We will explain a motivation in this work [60].

So far many attempts to reveal the character of chaos have been done in dynamical systems. Following such works, considerable research in Newtonian gravity and general relativity have been done [6, 13, 20, 21, 22, 23, 24, 25, 26, 27, 28, 30, 46, 54, 55, 59, 64, 67, 68, 69, 70, 71, 76, 82, 83, 92, 96, 97, 98, 99, 108, 111]. But most of it, especially work on relativistic systems, has discussed only whether or not chaos occurs mainly by using the Poincaré map and the Lyapunov exponent (sometimes using fractal basin boundary analysis). However, we know there appear various types of chaotic behaviours depending on the strength of chaos and its analysis will play a very important role to understand the essence of nonlinear dynamics [20, 21, 55]. A cogent view of how one can extract and use information from a chaotic system may be also missing. So one can address two new important issues in the research of chaos in Newtonian gravity and general relativity. One is, of course, to make clear the character of chaos for each system, and the other is to find some methods to extract useful information from chaotic systems. As for the first point, we have recently shown the possibility to classify the character of chaos in a system of a particle with spin in a Schwarzschild space time [64]. The method used in [64] is a power spectrum analysis of the particle orbit. The spectra are mainly classified into a power-law type and a white-noise type. As a result, we find that there is a close relation between the so-called “stagnant motion” (or “stickiness” [20, 21, 55]) and a “power-law” spectrum.

As for the second point, an indirect method to extract information from chaotic systems is required for the following reason: In chaotic systems in astrophysics, it is sometimes too difficult to observe chaotic motions directly. Because these systems are often far from the earth and the ambient surroundings of these systems may not be clean. Therefore, in [60] we propose the use of gravitational waves as a new method to analyze chaos. The reason we choose gravitational waves is as mentioned in Introduction.

In [59], we analyzed the gravitational waves from a particle with spin in a Kerr space time. We find that there is a difference between the spectra of the gravitational waves from a chaotic orbit and from a regular one. There appear many small spikes in the spectrum of the chaotic orbit. However, as we mentioned, there are various types of chaotic motions, and it is important in the analysis of such a dynamical system to know which type of chaos appears as well as to show the difference between a regular motion and a chaotic one. Hence, in order to study whether one can make a distinction between various types of chaos by use of gravitational waves, we should reanalyze them in a chaotic system.

As a concrete model of a chaotic system, here we consider a point mass with a thick disk in Newtonian gravity [87, 88]. This model mimics a system of a black hole with a massive accretion disk [113]. Saa analyzed this system and showed that a particle motion is chaotic [87]. This model can describe almost regular to highly chaotic motion by changing the ratio of a disk

mass to a black hole mass. In [87], however, only the Poincaré map has been analyzed to judge whether chaos occurs or not, and the characteristics of chaos have not been studied much.

So our strategy in this work is the following: First, we analyze the particle motion and make clear the characteristics of chaos appearing in this system. Secondly, we evaluate the quadrupole gravitational waves. Finally, to study some observational feature of chaos appearing in the gravitational waves, we investigate correlation between types of chaotic motions and gravitational waves, and then point out a possibility to extract information from this chaotic system via the gravitational waves.

This chapter is organized as follows. In Sec. 6.1, we shall briefly summarize the basic equations. Numerical analysis results will be presented in Sec. 6.2. The summary and discussion follow in Sec. 6.3.

6.1 Basic equations

We start by considering the Newtonian limit of a black hole disk system [88]. The equations of motion for a test particle in this background are very simple. We use the cylindrical coordinates (ω, φ, z) .

A point mass with a mass M is located at the origin, while a disk exists on the equatorial plane ($z = 0$). A smooth distribution of disk matter is assumed. If the radial gradient of the density is much smaller than vertical one, we can approximate the density as $\rho = \rho(z)$. A minimal but realistic model for a rotating thick disk may be described by Emden's equation [91]. As in [87], ignoring the radial gradient, we find that Emden's equation for disk matter density $\rho(z)$ is given by

$$\kappa\gamma\rho^{\gamma-2}\frac{d^2\rho}{dz^2} + \kappa\gamma(\gamma-2)\rho^{\gamma-3}\left(\frac{d\rho}{dz}\right)^2 = -4\pi\rho, \quad (6.1)$$

where κ and $\gamma = 1 + 1/n$ are the polytropic constant and the polytropic index, respectively. The matter density ρ should obey the Poisson equation $\nabla^2 V_D = 4\pi\rho$, where V_D is the potential of the disk. For the isothermal case ($\gamma = 1$), equation (6.1) has the analytic solution,

$$\rho(z) = \frac{\alpha}{4\pi z_0} \operatorname{sech}^2\left(\frac{z}{z_0}\right), \quad (6.2)$$

which corresponds to the disk potential

$$V_D(z) = \alpha z_0 \ln \cosh\left(\frac{z}{z_0}\right), \quad (6.3)$$

where z_0 and α describe the “thickness” of a disk and the surface mass density, respectively. These two parameters determine the polytropic constant by the relation $2\kappa = \alpha z_0$. In the limit of $z_0 \rightarrow 0$, we recover the potential of an infinitesimally thin disk ($V_D \sim \alpha|z|$). The corresponding matter distribution is given by the δ function from equation (6.2).

Thus, the dynamics of a test particle with a mass μ moving around a system of a point mass with a smooth thick isothermal disk will be governed by the following (effective) Hamiltonian

$$H = \mu \left[\frac{\dot{\omega}^2}{2} + \frac{\dot{z}^2}{2} + \frac{L^2}{2\mu^2\omega^2} - \frac{M}{\sqrt{\omega^2 + z^2}} + \alpha z_0 \ln \cosh\left(\frac{z}{z_0}\right) \right], \quad (6.4)$$

where L is the angular momentum of a particle and the dot denotes the time derivatives.

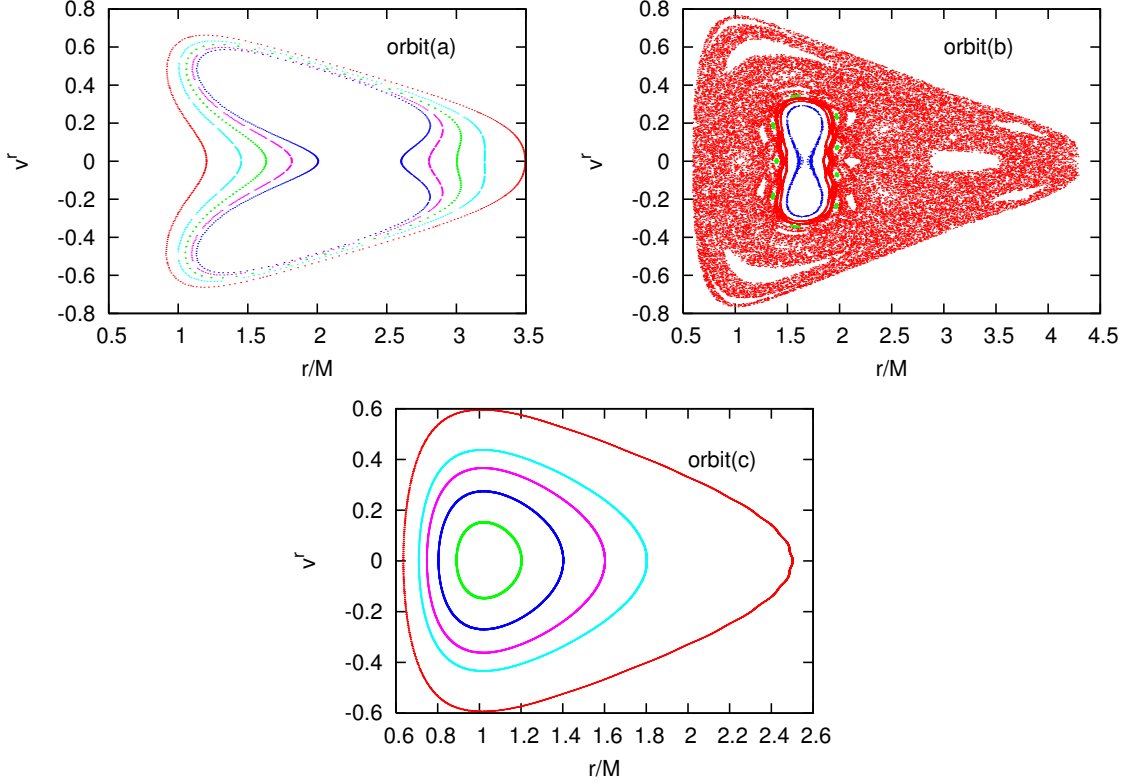


Figure 6.1: Poincaré maps of orbits of a particle with $H = -0.2$ and $L = 1$ across the plane $z = 0$ in a system of a point mass with a disk. We set the thickness of the disk $z_0 = 0.5$, and its surface density (a) $\alpha = 0.01$, (b) $\alpha = 0.1$, or (c) $\alpha = 10.0$. All figures are superpositions of trajectories starting from different initial conditions. In Figures (a) and (c), all trajectories form regular tori. In Figure (b), some trajectories from certain initial conditions still seem to form tori, but others do not. In fact, one initial condition, $(\omega, v^\omega, z, v^z) = (1.2, 0, 0, 0.76)$ gives an almost two dimensional map on which the orbital points are widely scattered, which means that the particle motion is chaotic (We call it Orbit (b)). The outermost trajectories in Figure (a) and (c) are called Orbit (a) and (c), whose initial conditions are $(\omega, v^\omega, z, v^z) = (1.2, 0, 0, 0.76)$ and $(2.5, 0, 0, 0.49)$, respectively.

6.2 Numerical Analysis

6.2.1 Two phases of chaos in particle motion

At first, we analyze particle motion. We numerically integrate the equations of motion of a test particle. The symplectic scheme is used because we have the analytic form of the Hamiltonian in this system. The integrated time is enough long such that a particle moves thousands times around the central mass. The numerical accuracy is monitored by the conservation of the Hamiltonian, which is typically $10^{-8} \sim 10^{-9}$. It guarantees that our numerical calculation is reliable. We set $M = 1$ to fix our units. There are two parameters of a disk which we can change, i.e., the surface density α and the width z_0 . Which parameter dependence we should analyze? When we change α , there are two extreme limits, i.e., $\alpha \rightarrow 0$ and $\alpha \rightarrow \infty$, in which the system becomes integrable (see equation (6.4)). The gravity by the central mass becomes dominant when $\alpha \rightarrow 0$, while the force driven by the disk is dominant as $\alpha \rightarrow \infty$. On the other hand, if we consider two extreme limits of z_0 , i.e., the limits of $z_0 \rightarrow 0$ and of $z_0 \rightarrow \infty$, we

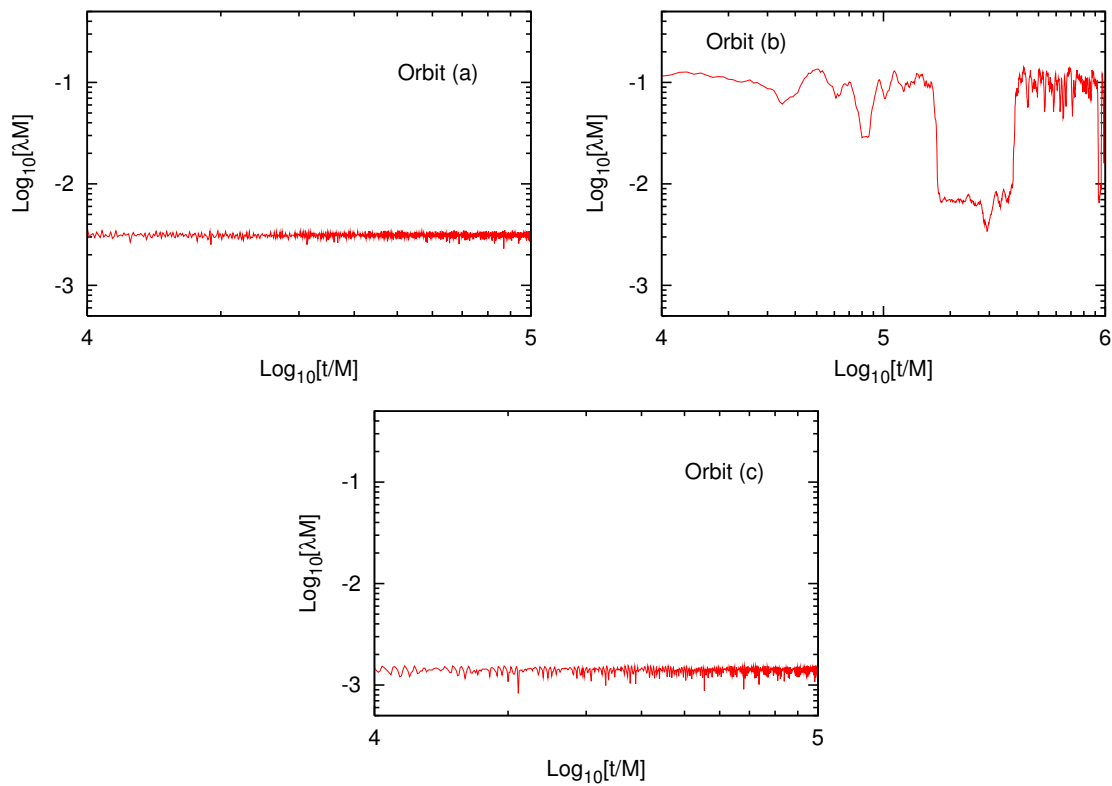


Figure 6.2: The time evolutions of “local” Lyapunov exponents for Orbits (a), (b), and (c) in Figure 6.1. The Lyapunov exponents for Orbits (a) and (c) settle down to very small values, but that for Orbit (b) is large and changing in time. It decreases to a very small value in the time interval of $t/M = (1.6 \sim 3.8) \times 10^5$.

find that the system is still nonintegrable even in such limits [88]. Our main aim is to make a distinction between various types of chaotic behaviours. For our purpose, the comparison of the cases with different values of z_0 may not be appropriate. Hence we analyze the cases with different values of α , which may provide us continuous change from a regular orbit to a very strongly chaotic one.

The parameters of particle orbits such as the energy and angular momentum are appropriately chosen such that the motion is bounded. We choose the orbital parameters as $H = -0.2$ and $L = 1$, and the disk width as $z_0 = 0.5$. Figure 6.1 shows a set of Poincaré maps for different values of the surface density ((a) $\alpha = 0.01$, (b) $\alpha = 0.1$, and (c) $\alpha = 10.0$). The equatorial plane ($z = 0$) is chosen for a Poincaré section. We plot the points on the (ω, v^ω) plane when the particle crosses the Poincaré section with $v^z > 0$. In these figures, trajectories starting from various initial conditions are shown. From Figures 6.1 (a) and (c), we confirm these system are almost integrable. The outermost trajectories are called Orbit (a) and Orbit (c). On the other hand, a widespread chaotic sea is found in Figure 6.1 (b). This is because the forces by the point mass and by the disk are comparable and those are competing each other. In Figure 6.1 (b), we see the “outermost” trajectory with the initial condition of $(\omega, v^\omega, z, v^z) = (1.2, 0, 0, 0.76)$ (called Orbit (b)) is not a simple torus but forms an almost two dimensional distribution in which the orbital points are widely scattered. It means that the particle motion is chaotic.

Figure 6.2 shows the time evolution of the Lyapunov exponents for Orbits (a), (b), and (c) in Figure 6.1. Here we show a “local” Lyapunov exponent defined in Appendix B. We only refer to the integration time interval t_Δ to define it (see Appendix in more details). t_Δ is chosen to be $t_\Delta = 10^4$, which satisfies the condition of $t_D \ll t_\Delta \ll t_T$ with $t_D (\approx 10 \sim 10^2)$ and $t_T (\approx 10^6)$ being the dynamical time and the total integration period of our calculation, respectively. We also calculate it with other time intervals, $t_\Delta = 2$ or 4×10^4 . We find that the result is not sensitive to this choice. We numerically calculate the exponents with the algorithm shown in [95] and show the maximum component of it.

The value for Orbit (a) is very small and almost constant [114]. For Orbit (c), the system is not exactly integrable. The system in the limit of $\alpha \rightarrow \infty$ is of course integrable, but there is no bound orbit in such a limit. Since we are analyzing a bound orbit, even if α is very large, we cannot ignore the gravitational effect of a point mass. It makes the system nonintegrable. Nevertheless, the motion looks very regular (see the Poincaré map in Figure 6.1). In fact we find a very small Lyapunov exponent, which is smaller than that of Orbit (a) as shown in Figure 6.2. This value is also almost constant, which means that the strength of the chaos does not change much in time. Hence we may regard this orbit as a regular one.

On the other hand Orbit (b) gives large positive Lyapunov exponent. It also shows time variation. We should note that the value quickly goes down to a very small one in the time interval of $t/M = (1.6 \sim 3.8) \times 10^5$. We pick up the data around this interval and show the time evolution of the r -position of the particle and the Poincaré map in Figure 6.3. From this, we find that although the particle motion in Orbit (b) is chaotic, it stays around $r \sim 1.2 - 2.2M$ in the time interval of $t/M = (1.6 \sim 3.8) \times 10^5$. The motion in this period seems to be nearly regular. In fact, the “local” Lyapunov exponent decreases to $5 \sim 6 \times 10^{-3}$, which is almost the same as those of Orbits (a) and (c). We call this phase of motion Orbit (b-2). The phase before this interval, in which a particle motion looks very chaotic, is called Orbit (b-1). We have also performed numerical integration for longer time period and confirm such phases as Orbit (b-2) often appears in a chaotic orbit (see Figure 6.4). The important point is that two different phases of motion appear and both a nearly integrable and a more strongly chaotic motion coexist in the same trajectory.

The Poincaré map of Orbit (b-2) in Figure 6.3 shows that many small tori exist. It is well known that such a structure appears if an orbit is nearly integrable and produces the so-called $1/f$ fluctuation [20, 21, 55, 64]. Then we also analyze the power spectrum of the r -component

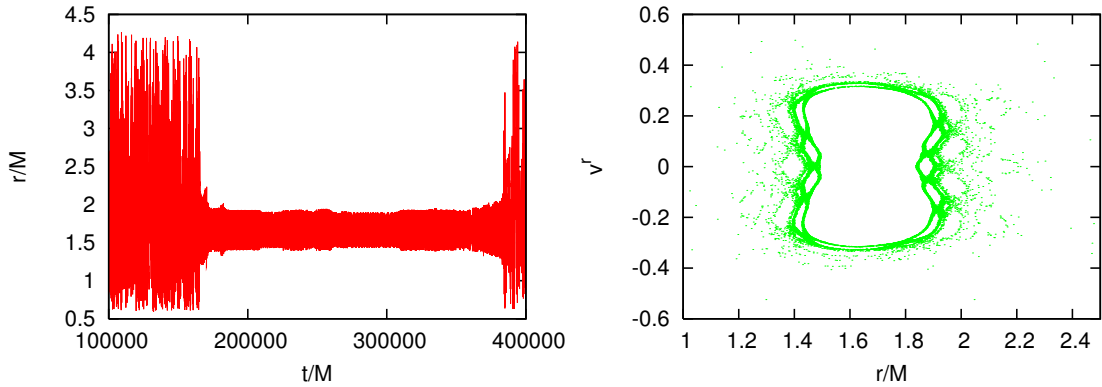


Figure 6.3: The particle motion in the r -direction in terms of time and its Poincaré map for the time interval between $t/M = 10^5$ and $t = 4 \times 10^5$ for Orbit (b). The Poincaré map shows there exist many small tori around the origin.

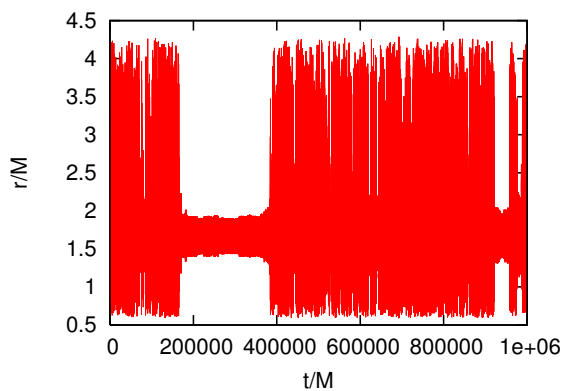


Figure 6.4: The particle motion of Orbit (b) in the r -direction for a longer time interval than that in Figure 6.3. There exists new stagnant motion as the same one in Figure 6.3.

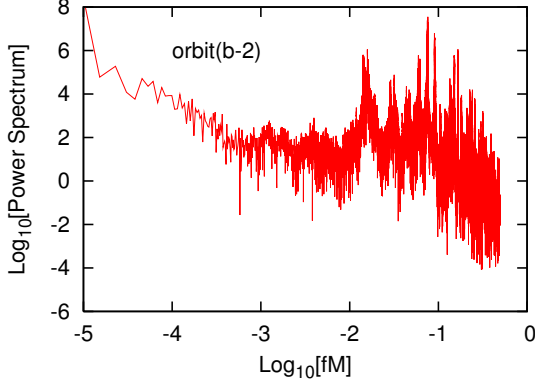


Figure 6.5: The power spectrum of the motion in the r -direction of Orbit (b-2), which is part of nearly regular motion in Orbit (b) ($t/M = (1.6 \sim 3.8) \times 10^5$). We find a power-law spectrum, e.g., a $1/f$ fluctuation. This reflects the existence of small tori in the phase space, and the particle moves almost regularly there [64].

of Orbit (b-2), which clearly shows a $1/f$ fluctuation for $f \leq 10^{-2}M^{-1}$ (see Figure 6.5). This confirms our previous result [64] in the present model.

6.2.2 Indication of chaos in gravitational waves

Next we study how to extract information from such a chaotic system and distinguish the orbits, i.e., a nearly integrable and more strongly chaotic motions.

In [64], the authors focused on the power spectrum of particle motion moving in Schwarzschild spacetime and found that it shows a power-law behaviour. In this work, we use a similar analysis for the gravitational waves emitted from our system. It could be a new and robust way to observe chaotic behaviors in astrophysical objects, as mentioned in our Introduction. The quadrupole gravitational waves [65] are given by

$$h_+ = [(h_{xx}^Q - h_{yy}^Q) \cos 2\varphi + 2h_{xy}^Q \sin 2\varphi] \frac{(\cos^2 \theta + 1)}{4} - (h_{xx}^Q + h_{yy}^Q - 2h_{zz}^Q) \frac{\sin^2 \theta}{4} - (h_{xz}^Q \cos \varphi + h_{yz}^Q \sin \varphi) \sin \theta \cos \theta, \quad (6.5)$$

$$h_\times = [2h_{xy}^Q \cos 2\varphi - (h_{xx}^Q - h_{yy}^Q) \sin 2\varphi] \frac{\cos \theta}{2} + (h_{xz}^Q \sin \varphi - h_{yz}^Q \cos \varphi) \sin \theta, \quad (6.6)$$

where

$$h_{ij}^Q \equiv \frac{2}{r} \frac{d^2 Q_{ij}}{dt^2} \quad \text{with} \quad Q_{ij} \equiv \mu \left(Z^i Z^j - \frac{1}{3} \delta_{ij} Z^2 \right) \quad (\text{the reduced quadrupole moment of a point mass}). \quad (6.7)$$

(r, θ, φ) [or (x, y, z)] is the position of a distant observer in spherical coordinates [or Cartesian coordinates], and $Z(t)$ is a trajectory of a particle. We assume that the observer is on the equatorial plane, i.e. $(\theta, \varphi) = (\pi/2, 0)$. Figure 6.6 shows the waveforms from Orbits (a), (b), and (c). The left panels show the "+" polarization modes of those waves, while the right ones are the "×" polarization. The top, middle, and bottom panels correspond to the waves from Orbits (a), (b), and (c), respectively. The waves from Orbits (a) and (c) show a periodic feature, which is expected from the Poincaré maps in Figure 6.1. On the other hand, the waves from Orbit (b) show a completely different behaviour. We find much random spiky noise in the waveform before $t/M = 1.6 \times 10^5$ and after $t/M = 3.8 \times 10^5$. This is a typical feature of the gravitational

waves from highly chaotic motion [59, 99]. We also find that the amplitude decreases for the time interval of $t/M = (1.6 \sim 3.8) \times 10^5$. As shown in Figure 6.3, in this time interval, the particle moves near the small tori in the phase space. This adjectice feature of this particle motion appears clearly in the gravitational amplitudes. That is, in the phase of a nearly regular motion, the particle position and its velocity do not change much compared with those in the more strongly chaotic phase (b-1) (see Figure 6.1(b) and Figure 6.3(b)). The time variation of the quadrupole moment of the system is small and hence the wave amplitude decreases as well.

We also calculate the energy spectra of the gravitational waves, which will be one of the most important observable quantities in the near future. In Figure 6.7, we show the energy spectra for each orbit. Figures 6.7(a) and (c) show many sharp peaks at certain characteristic frequencies. If a motion is regular, we expect several typical frequencies with those harmonics. So such a result reflects that the particle moves regularly. Figure 6.7 (b) gives the spectrum of Orbit (b). It is clearly different from the previous two almost regular cases. It looks just like white noise, below a typical frequency $fM \sim 10^{-2}$, i.e., the shape of the spectrum is flat and it contains many noisy components. However, the spectrum of Orbit (b-2) (Figure 6.7(b-2)), which is analyzed by the orbit only in the time interval of $t/M = (1.6 \sim 3.8) \times 10^5$, does not do so. Rather it looks similar to the spectrum of a regular orbit. Contrary to Figure 6.7(b), it does not contain much noise at the low frequency region ($fM \leq 10^{-2}$).

To see more detail, dividing the time interval of Orbit (b) into two, we show the magnifications of the spectra of Orbits (a), (b-1), (b-2), and (c) in Figure 6.8. Compared to the spectra (a) and (c), the spectra (b-1) and (b-2) contain many noisy spikes. Such noisy spikes are usually found in the gravitational waves from a chaotic orbit [59]. However, the spectra (b-1) and (b-2) are completely different. The spectrum (b-1) is just white noise. No structure is found. On the other hand, the spectrum (b-2) looks similar to those for regular orbits. The “sharp” peaks appear at some frequencies, but the widths of those peaks are broadened by many noisy spikes. Therefore, we conclude that Orbit (b-2) looks nearly regular but still holds its chaotic character, and such a feature imprints in the spectrum of the waves. The important point is that two phases in the particle orbit (b), i.e., the nearly regular phase and the more strongly chaotic one, are also distinguishable in the gravitational wave forms and the energy spectra. With this analysis, we could constrain orbital parameters.

6.3 Summary and Discussion

In this paper we have investigated chaos characteristic for a test particle motion in a system of a point mass with a massive disk in Newtonian gravity. To distinguish such characteristics, we propose the gravitational waves emitted from this system. At first, we analyzed the motion of the particle by use of the Poincaré map and the “local” Lyapunov exponent. We found that the phase in which particle motion becomes nearly regular always appears even though the global motion is chaotic. We emphasize that both phases of nearly regular and more strongly chaotic motions are found in the same orbit.

The gravitational wave forms and their energy spectra have been evaluated by use of the quadrupole formula in each case. In two almost regular cases, the waves show the periodic behaviour and certain sharp peaks appear in those energy spectra. In the chaotic case, we have found that the waves show two phases, the nearly regular phase and a more strongly chaotic one. In the nearly regular phase, wave amplitude gets smaller in the more strongly chaotic phase. The energy spectra are also clearly different. The spectrum in the more strongly chaotic phase looks like white noise, but in the nearly regular one, it becomes similar to those in the regular ones. However it is accompanied by many small noisy spikes, which is a characteristic feature of a chaotic system. These spikes make the widths of the spectrum peaks broader than

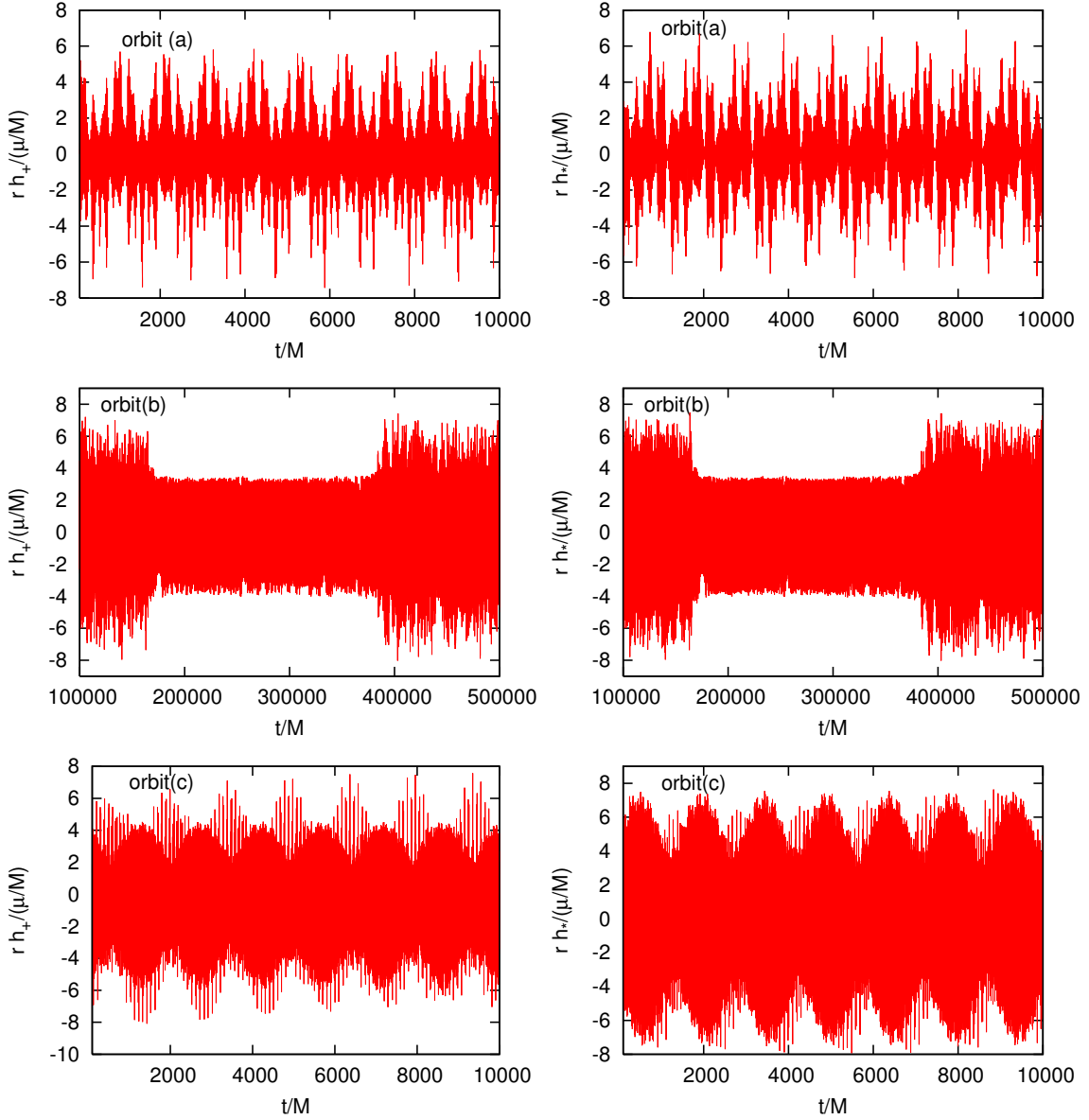


Figure 6.6: The gravitational waveforms evaluated by the quadrupole formula. Top, middle, and bottom figures correspond to those for Orbits (a), (b), and (c), respectively. The left and right rows give the “+” and “ \times ” polarization modes, respectively.

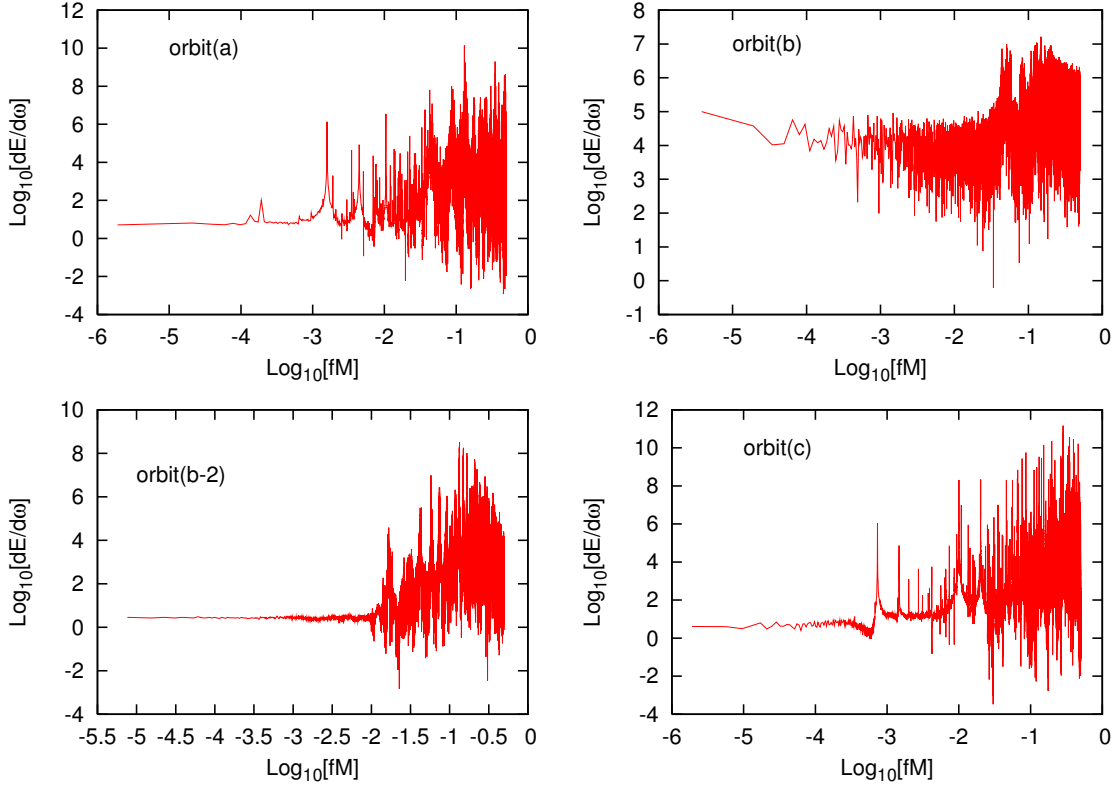


Figure 6.7: The energy spectra of the gravitational waves shown in Figure 6.6. Orbit (b-2) gives the spectrum of the waves for the “stagnant motion”, i.e., when the particle motion of Orbit (b) becomes near regular for $t/M = (1.6 \sim 3.8) \times 10^5$. Figures (a) and (c) show many sharp peaks at certain characteristic frequencies. This is because of the regular motion. The spectrum in Figure (b), which looks like white noise for $fM \leq 10^{-2}$, is clearly different from those in Figures (a) and (c), but the spectrum in Figure (b-2) does not look like white noise. It looks similar to the cases (a) and (c). However, the peaks are not sharp but rather broadened by appearing so many other spikes. Note that the typical frequency of the orbits is in the range of $fM = 10^{-2} \sim 10^{-1}$ (see Figure 6.5).

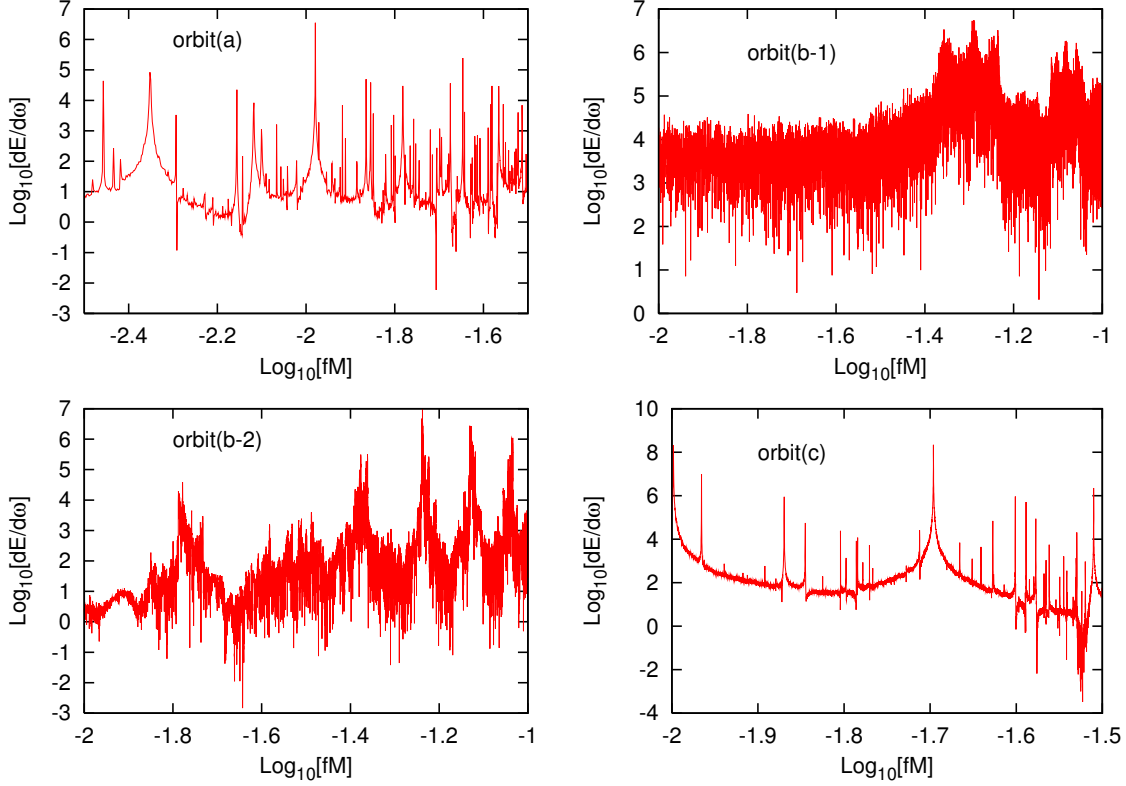


Figure 6.8: Magnification of energy spectra of Orbits (a), (b-1), (b-2), and (c).

those in the regular cases. Comparing information from the waves with the particle motion, we conclude that we can extract chaotic characteristics of a particle motion of the gravitational waves of the system. In the present analysis, in the spectrum (b-2) of the gravitational waves, we do not find a power-law structure, which appears in the spectrum of the particle motion. This may be because the waveform is given by the change of the quadrupole moment, which contains higher time derivatives of a particle trajectory such as acceleration. It may be much more interesting if one can find the $1/f$ behaviour in some information of the gravitational waves because such an indication may specify the type of chaos more clearly. This is under investigation.

Finally, we mention a possibility to constrain parameters in a dynamical system. If the gravitational waves are observed for a sufficiently long time, we can monitor the time variation of the wave amplitudes, their forms and polarizations. We can then calculate the energy spectra for some durations. If the spectra show one of the typical characteristics found in this paper, the parameters of a particle motion could be constrained. Of course, a realistic system can be more complicated, and the present model may be too simple. But we believe the characteristic behaviour of the gravitational waves found in this paper will help us to understand a chaotic system. Therefore our next task is to analyze the gravitational waves from various chaotic systems, especially relativistic chaotic systems [13, 54, 59, 64, 66, 67, 76, 82, 83, 96, 97, 98, 99, 108, 111]. Then, we should investigate whether or not the correlation between the gravitational waves and chaos in dynamical systems found in this work is generic.

CHAPTER 7

CONCLUSION

The subject of this thesis is studying the correlation between chaos and gravitational wave. We analyzed this subject in the two concrete chaotic systems. The both models imitate the system of supermassive black hole with compact object. The factor to cause chaos is different in the two models. We actually perform the two step analysis. The first step is devoted to investigate a particle motion and character of chaos. The second step is to estimate a gravitational wave and search a correlation with chaos. Finally, we discuss some observation features of chaos.

7.1 Spinning particles in the Kerr spacetime

Using the Papapetrou-Dixon equations, we construct the model of spinning test body in relativistic spacetime. The spin of test body couples to the curvature of background spacetime. Due to the coupling, motion of test body can become chaotic. The spinning particle no longer moves along the geodesics. Therefore, the factor of causing chaos is a connection of inner motion of test body itself with general relativistic effect. We used the Poincaré map and the Lyapunov exponent as the tools for analyzing chaos. As a result, we confirmed the motion of particle certainly shows a chaotic character. That is the Poincaré map consists of randomly distributed points and the Lyapunov exponent has a positive value.

We also analyzed the motion of test body without spin, which is equivalent to the geodesic. However, a fine tuning of orbital parameters, e.g., E , J_z , C , and so on, makes it possible for the orbits to be complicated and multi periodic motion. The orbits are indistinguishable from the chaotic orbits from the direct appearance. However, we confirmed the integrability of the orbits with the Poincaré map, which consists of a closed curve.

In the two systems, we investigated gravitational waves emitted by the test particles with quadrupole and octapole formula. Waveforms, energy spectrum, and energy emission rate were investigated. The waveforms did not show a certain feature with which we are able to distinguish the chaotic from the non chaotic systems. We also found that the quadrupole wave is a dominant mode even if the chaotic case. The energy spectrum has a notable feature. The spectrum of the wave from the non chaotic system has sharp peaks at the characteristic frequency of the orbital motion. It should be emphasized that it is non trivial whether the gravitational wave has this feature or not because the wave contains the position, velocity, and acceleration of the complicated and multi periodic particle's motion.

On the other hand, the spectrum from the chaotic system continuously distributes. The peaks of the spectrum are broaden and the noisy component is mixed in the spectrum. This means that the gravitational wave extract the feature of chaos, i.e., trajectory randomly moves in phase space.

Hence, we conclude that gravitational wave can distinguish from the chaotic and the non chaotic system. The important point of this research is that this distinguish is possible even if the non chaotic motion is complicated and multi periodic. Using this characteristics, we might restrict the physical quantity which induces chaos.

7.2 Test particle in point mass and disk system

Using the Newtonian point mass and disk system, we studies characteristics of chaos in this system. We also analyzed the correlation between chaos and gravitational wave. We confirmed the chaos is induced by the inhomogeneity of interactive forces, e.g., gravity by central point mass and force driven by disk density distribution. If the two forces is comparable, the particle's motion can be chaotic. We also confirmed in the two limiting cases, e.g., gravity dominate case and disk-driven force dominate case, the system reduces to be almost integrable.

With Poincaré map, Lyapunov exponent, and power spectrum analysis, we found that chaotic phase can be classified into the two phases, fully chaotic phase and weakly chaotic phase. In the fully chaotic phase, we obtained the randomly distributed Poincaré map, the large Lyapunov exponent, and the white-noise power spectrum of particle's motion. On the other hand, in the weakly chaotic phase, we obtained the Poincaré map with the fine structure, the small Lyapunov exponent, power-law power spectrum. The Poincaré map consists of the main torus and small tori surrounding it. In general, trajectory in phase space with such a structure shows a stagnant motion. As a result, it produces power-law spectrum, or $1/f$ fluctuation. Hence, our Poincaré map and power-spectrum analysis are consistent. We also found that the fully and the weakly chaotic phase appears one after the other in long time evolution. The important point is the two phases appears in the same trajectory.

The gravitational waves from this system is evaluated by the quadrupole formula. The waveform in the weakly chaotic phase has smaller amplitude than that in the fully chaotic phase. This feature is a reflect of the phase space structure because in the weakly chaotic phase the trajectory is confined in the narrower region than that in the fully chaotic phase. The energy spectrum also reflects the characteristic of chaos. The energy spectrum in the fully chaotic phase is white noise. On the other hand, that in the weakly chaotic phase has sharp peaks with noisy components. We also found that if the system is completely integrable, the spectrum has only sharp peaks at the characteristic frequencies. Therefore, we conclude that gravitational wave can extract the characteristics of the chaos.

If it were possible to detect gravitational wave for sufficiently long time, we might catch a state that motion comes and goes to weakly and fully chaotic phase. Moreover, it may be much more interesting if one can find the $1/f$ behaviour in some information of the gravitational waves because such an indication may specify the type of chaos more clearly.

Throughout the results of the two researches, we conclude gravitational wave can be useful tool for extracting information of chaotic system.

7.3 Future works

The systems investigated in this thesis are relatively simplified model. We simplify both gravitational and matter field. However, the nature could have more complicated structure. Therefore, as a future work, we will approach a fully nonlinear system with numerical relativity. In such a system, non linearity both in gravitational field and matter field plays an important role. With numeral relativity, we can deal with interesting object for both relativist and astronomist. We plane to investigate black hole formation via gravitational collapse of massive star.

Acknowledgments

I would like to thanks my thesis adviser, Professor Kei-ichi Maeda for invaluable suggestions and continuous encouragement. Thanks are as well due to Dr. Hiroko Koyama, who is a collaborator of part of the present work, for stimulating discussion. I am grateful to Professor Shoichi Yamada, Dr Shijun Yoshida, Professor Kei Kotake and Professor Tetsuro Konishi for helpful discussions and comments. Also thanks to my office-mate and members in Yamada laboratory, whose combined help and friendship have made the office such an enjoyable place to be.

Finally I deeply grateful to my wife Haluna and my parents.

This work was supported by JSPS (17-00473) and Grants-in-Aid for the 21st Century COE Program at Waseda University.

APPENDIX A

RICCI ROTATION, RIEMANN TENSOR, CHRISTOFFEL SYMBOL

We represent the explicit forms of the Ricci rotation γ_{ijk} and the Riemann tensor R_{ijkl} and the Christoffel symbol $\Gamma_{\beta\mu}^\alpha$.

The Ricci rotation is defined as

$$\gamma_{kij} \equiv e_k^\mu e_{i\mu;\nu} e_j^\nu. \quad (\text{A.1})$$

The Riemann tensor and the Christoffel symbol are defined as

$$R^\mu_{\nu\rho\sigma} \equiv -\Gamma_{\nu\rho,\sigma}^\mu + \Gamma_{\nu\sigma,\rho}^\mu - \Gamma_{\lambda\sigma}^\mu \Gamma_{\nu\rho}^\lambda + \Gamma_{\lambda\rho}^\mu \Gamma_{\nu\sigma}^\lambda. \quad (\text{A.2})$$

$$\Gamma_{\mu\nu}^\alpha \equiv \frac{1}{2} g^{\alpha\beta} (g_{\beta\mu,\nu} + g_{\beta\nu,\mu} - g_{\mu\nu,\beta}). \quad (\text{A.3})$$

For the metric (5.1), the tetrad components of the Ricci rotation and the Riemann tensor are given as

$$\begin{aligned} \gamma_{010} &= -\frac{1}{\Delta^{\frac{1}{2}} \Sigma^{\frac{3}{2}}} [M(r^2 - a^2 \cos^2 \theta) - a^2 r \sin^2 \theta], \\ \gamma_{301} = \gamma_{103} = -\gamma_{310} &= -\frac{ar \sin \theta}{\Sigma^{\frac{3}{2}}}, \\ \gamma_{200} = -\gamma_{211} &= -\frac{a^2 \sin \theta \cos \theta}{\Sigma^{\frac{3}{2}}}, \\ \gamma_{302} = -\gamma_{203} = \gamma_{320} &= \frac{a \Delta^{\frac{1}{2}} \cos \theta}{\Sigma^{\frac{3}{2}}}, \\ \gamma_{212} = \gamma_{313} &= \frac{r \Delta^{\frac{1}{2}}}{\Sigma^{\frac{3}{2}}}, \\ \gamma_{323} &= \frac{(r^2 + a^2) \cos \theta}{\Sigma^{\frac{3}{2}} \sin \theta}, \end{aligned}$$

$$\begin{aligned} \frac{1}{2} R_{0101} = -R_{0202} = -R_{0303} &= -\frac{1}{2} R_{2323} = R_{3131} = R_{1212} = \frac{Mr(3a^2 \cos^2 \theta - r^2)}{\Sigma^3}, \\ \frac{1}{2} R_{0123} = -R_{0231} = -R_{0312} &= \frac{aM(3r^2 - a^2 \cos^2 \theta) \cos \theta}{\Sigma^3}. \end{aligned}$$

The Christoffel symbol is give as

$$\begin{aligned}
\Gamma_{tr}^t &= \frac{M(r^2 + a^2)(r^2 - a^2 \cos^2 \theta)}{\Delta\Sigma^2}, & \Gamma_{t\theta}^t &= -\frac{2Ma^2 r \sin \theta \cos \theta}{\Sigma^2}, \\
\Gamma_{r\phi}^t &= -\frac{Ma \sin^2 \theta \{3r^4 + a^2 r^2(1 + \cos^2 \theta) - a^4 \cos^2 \theta\}}{\Delta\Sigma^2}, \\
\Gamma_{\theta\phi}^t &= \frac{2Ma^3 r \sin^3 \theta \cos \theta}{\Sigma^2}, & \Gamma_{tt}^r &= \frac{M\Delta(r^2 - a^2 \cos^2 \theta)}{\Sigma^3}, \\
\Gamma_{t\phi}^r &= -\frac{M\Delta a(r^2 - a^2 \cos^2 \theta) \sin^2 \theta}{\Sigma^3}, & \Gamma_{rr}^r &= \frac{-Mr^2 + a^2 r \sin^2 \theta + Ma^2 \cos^2 \theta}{\Delta\Sigma}, \\
\Gamma_{r\theta}^r &= -\frac{a^2 \sin \theta \cos \theta}{\Sigma}, & \Gamma_{\theta\theta}^r &= -\frac{\Delta r}{\Sigma}, & \Gamma_{\phi\phi}^r &= -\frac{\Delta[r\Sigma^2 - Ma^2(2r^2 - \Sigma) \sin^2 \theta]}{\Sigma^3} \sin^2 \theta, \\
\Gamma_{tt}^\theta &= -\frac{2Ma^2 r \sin \theta \cos \theta}{\Sigma^3}, & \Gamma_{t\phi}^\theta &= \frac{2Mar(r^2 + a^2) \sin \theta \cos \theta}{\Sigma^3}, & \Gamma_{rr}^\theta &= \frac{a^2 \sin \theta \cos \theta}{\Delta\Sigma}, \\
\Gamma_{r\theta}^\theta &= \frac{r}{\Sigma}, & \Gamma_{\theta\theta}^\theta &= -\frac{a^2 \sin \theta \cos \theta}{\Sigma}, & \Gamma_{\phi\phi}^\theta &= -\frac{[\Delta\Sigma^2 + 2Mr(r^2 + a^2)^2]}{2\Sigma^3} \sin 2\theta, \\
\Gamma_{tr}^\phi &= \frac{Ma(r^2 - a^2 \cos^2 \theta)}{\Delta\Sigma^2}, & \Gamma_{t\theta}^\phi &= -\frac{2Mar \cos \theta}{\Sigma^2 \sin \theta}, & \Gamma_{r\phi}^\phi &= \frac{r\Sigma(\Sigma - 2Mr) - Ma^2(2r^2 - \Sigma) \sin^2 \theta}{\Delta\Sigma^2}, \\
\Gamma_{\theta\phi}^\phi &= \frac{[(\Delta - a^2 \sin^2 \theta)\{(r^2 + a^2)^3 - a^2 \Delta \sin^2 \theta(2\Sigma + a^2 \sin^2 \theta)\} + 4M^2 a^2 r^2(r^2 + a^2) \sin^2 \theta]}{\Delta\Sigma^3} \cot \theta.
\end{aligned}$$

APPENDIX B

LOCAL LYAPUNOV EXPONENT

In this appendix, we give the definition of “local” Lyapunov exponent. Our definition of “local” Lyapunov exponent is somewhat different from the conventional one [39, 53], but those are essentially the same.

At first, we consider a set of ordinary differential equations in N -dimensional space,

$$\dot{\mathbf{x}} = \mathbf{F}(\mathbf{x}), \quad (\text{B.1})$$

where $\mathbf{x}(t)$ is a N -dimensional vector.

The time evolution of the orbital deviation $\delta\mathbf{x}$, which is the difference between two nearby orbits, can be expressed as

$$\delta\dot{\mathbf{x}} = \frac{\partial \mathbf{F}}{\partial \mathbf{x}}(\mathbf{x}(t))\delta\mathbf{x}. \quad (\text{B.2})$$

The solution of Eq. (B.2) can be written formally as

$$\delta\mathbf{x}(t) = U_{t_0}^t \delta\mathbf{x}_0, \quad (\text{B.3})$$

where $\delta\mathbf{x}_0$ is an “initial” deviation at some time t_0 and $U_{t_0}^t$ is an evolution matrix, which is given by the following integration;

$$U_{t_0}^t = \exp \left[\int_{t_0}^t \frac{\partial \mathbf{F}}{\partial \mathbf{x}}(\mathbf{x}(t')) dt' \right]. \quad (\text{B.4})$$

We define the “local” Lyapunov exponent in time interval $[t_0, t]$ by

$$\lambda(e^k, t) = \frac{1}{t - t_0} \log \frac{\|U_{t_0}^t \mathbf{e}_1 \wedge U_{t_0}^t \mathbf{e}_2 \wedge \cdots \wedge U_{t_0}^t \mathbf{e}_k\|}{\|\mathbf{e}_1 \wedge \mathbf{e}_2 \wedge \cdots \wedge \mathbf{e}_k\|} \quad (\text{B.5})$$

for $k = 1, 2, \dots, N$, where e^k is a k -dimensional subspace in the tangent space at the initial point \mathbf{x}_0 , which is spanned by k independent vectors \mathbf{e}_i ($i = 1, 2, \dots, k$). \wedge is an exterior product. $\|\cdot\|$ is a norm in terms of some appropriate Riemannian metric. If we take a limit of $t \rightarrow \infty$, $\lambda(e^k, \infty)$ correspond to the conventional Lyapunov exponents.

If the integration time interval $t_\Delta \equiv t - t_0$ is much longer than a characteristic timescale of the system such as the dynamical timescale, we may find convergent values for each $\lambda(e^k, t)$, which are almost independent of t_Δ (or t_0). We may call them “local” Lyapunov exponents at t . The maximum value of “local” Lyapunov exponents, i.e. $\lambda(t) = \max\{\lambda(e^k, t) | k = 1, 2, \dots, N\}$ is the most important one for our discussion. So we also call it the “local” Lyapunov exponent at t .

Bibliography

- [1] Abramovici, A. *et al.*, "LIGO: The Laser interferometer gravitational wave observatory," *Science* **256**, 325 (1992).
- [2] Armstrong, J. W., Estabrook, F. B., and Tinto M., *Class. Quant. Grav.*, 18:4059, (2001).
- [3] Aizawa, Y., Koguro, N., and Antoniou, L., *Prog. Theor. Phys.* **98**, 1225 (1997).
- [4] Arnowitt, R. Deser, S. and Misner, C. W., The dynamics of general relativity, in *Gravitation : An Introduction to Current Research*, edited by Held A., (Plenum, New York, 1962).
- [5] Bardeen, J. M., and Press, W. H., *J. Math. Phys* **14**, 7 (1973).
- [6] Barrow, J. D., *Phys. Rep.* **85**, 1 (1982).
- [7] Baumgarte, T. W., and Shapiro, S. L., *Phys. Rev. D* **59**, 024007 (1999)
- [8] Baumgarte, T. W., and Shapiro, S. L., *Phys. Rept.* **376**, 41 (2003)
- [9] Belinski, V. A., Khalatnikov, L. M., and Lifshitz, E. M., *Adv. Phys.* **19**, 525 (1970).
- [10] Blanchet, L., *Living Rev. Relativity*, **9**, 4 (2006).
- [11] Blanchet, L., Buonanno, A., and Faye, G., *Phys. Rev. D* **74**, 104034 (2006). [Erratum-*ibid. D* **75**, 049903 (2007)]
- [12] Blanchet, L., and Faye, G., *Phys. Rev. D* **63**, 062005 (2001).
- [13] Bombelli, L., and Calzetta, E., *Class. Quant. Grav.* **9**, 2573 (1992).
- [14] Carter, B., *Phys. Rev* **174**, 1559 (1968).
- [15] Chandrasekhar, S., *Proc. R. Soc. London A***343**, 289 (1975).
- [16] Chandrasekhar, S., *The Mathematical Theory of Black Hole* (Clarendon Press, Oxford, 1985).
- [17] Chandrasekhar, S., and Detweiler, S., *Proc. R. Soc. London A***345**, 145 (1975).
- [18] Contopoulos, G., *Proc. R. Soc. London A***431**, 183 (1990).
- [19] Contopoulos, G., *Proc. R. Soc. London A***435**, 551 (1991).
- [20] Contopoulos, G., *Order and Chaos in Dynamical Astronomy*, (Springer, 2002).
- [21] Contopoulos, G., Harsoula, M., and Voglis, N., *Celest. Mech. Dyn. Astron.* **78**, 197(2000).
- [22] Contopoulos, G., and Papadaki, H., *Celest. Mech.* **55**, 47 (1993).
- [23] Cornish, N. J., and Levin, J. J., *Phys. Rev. D* **55**, 7489 (1997).

- [24] Cornish, N. J., and Frankel, N. E., Phys. Rev. D **56**, 1903 (1997).
- [25] Cornish, N. J., Phys. Rev. Lett. **85**, 3980 (2000).
- [26] Cornish, N. J., and Levin, J. J., Phys. Rev. Lett. **89**, 179001 (2002).
- [27] Cornish, N. J., and Levin, J. J., Class. Quant. Grav. **20**, 1649 (2003).
- [28] Cornish, N. J., and Levin, J. J., Phys. Rev. D **68**, 024004 (2003).
- [29] Cutler, C., and Thorne, K. S., in Proceedings of GR16, Durban, South Africa (World Scientific, Singapore, 2001), gr-qc/0204090 (2002).
- [30] Dettmann, C. P., Frankel, N. E., and Cornish, N. J., Phys. Rev. D **50**, 618 (1994).
- [31] Detweiler, S. L., and Szedenits, J. E., Astrophys. J. **231**, 211 (1979).
- [32] DeWitt, S., and Brehme, R. W., Ann. Phys. **9**, 220 (1960).
- [33] Dixon, W. G., Proc. R. Soc. London **A314**, 499 (1970).; **A319**, 509 (1970).
- [34] Epstein, R., and Wagoner, R. V., Astrophys. J. **197**, 717 (1975).
- [35] Faye, G., Blanchet, L., and Buonanno, A., Phys. Rev. D **74**, 104033 (2006).
- [36] Geroch, R., Held, A., and Penrose, R., J. of Math. Phys. **14**, 874 (1973).
- [37] Giazotto, A., Nucl. instrum. Meth. **A 289**, 518 (1990).
- [38] Gopakumar, A., and Konigsdorffer, C., Phys. Rev. D **72**, 121501 (2005).
- [39] Grassberger, P., Badii, R., and Politi, A., J. Stat. Phys. **51**, 135 (1988).
- [40] Hartl, M. D., Phys. Rev. D **67**, 024005 (2003).
- [41] Hartl, M. D., Phys. Rev. D **67**, 104023 (2003).
- [42] Hartl, M. D., and Buonanno, A., Phys. Rev. D **71**, 024027 (2005).
- [43] *General Relativity* (An Einstein Centenary Survey), edited by S. W. Hawking and W. Israel.
- [44] Hénon, M., and Heiles, C., Astron. J. **69**, 73 (1964)
- [45] Hough, J. *et al.*, *Prepared for TAMA Workshop on Gravitational Wave Detection, Saitama, Japan, 12-14 Nov 1996*
- [46] *Deterministic Chaos in General Relativity*, edited by D. Hobill, A. Burd, and A. Coley, (Plenum, New York, 1994), and references therein.
- [47] Hough, J. *et al.*, Seventh Marcel Grossman Meeting on recent developments in theoretical and experimental general relativity, gravitation and relativistic fields theories, New Jersey, edited by R. T. Jantzen, G. M. Keiser, R. Ruffini, and Edge, R. (World Scientific, 1996), p1352.
- [48] Hulse, R. A., and Taylor, J. H., Astrophys. J. **195**, L51 (1975).
- [49] Isaacson, R. A., Phys. Rev. **166**, 1263 (1968).
- [50] Isaacson, R. A., Phys. Rev. **166**, 1272 (1968).

- [51] Janis, A. I., and Newman, E. T., J. of Math. Phys. **6**, 902 (1973).
- [52] Johnston, M., and Ruffini, R., Phys. Rev. D **10**, 2324 (1974).
- [53] Kandrup, H. E., Eckstein, B. L., and Bradley, B. O., Astron. Asrophys. **320**, 65 (1997).
- [54] Karas, V., and Vokrouhlicky, D., Gen. Rela. Grav. **24**, 729 (1992).
- [55] Karney, C. F. F., Physica D **8**, 360(1983).
- [56] Khanna, G., Phys. Rev. D **69**, 024016 (2004)
- [57] Kidder, L. E., Phys. Rev. D **52**, 821 (1995).
- [58] Kinnersley, W., J. of Math. Phys. **10**, 1195 (1969).
- [59] Kiuchi, K., and Maeda, K., Phys. Rev. D **70**, 064036(2004).
- [60] Kiuchi, K., Koyama, H., and Maeda, K. i., arXiv:0704.0719 [gr-qc].
- [61] Kojima, Y., in Proceeding of the Workshop on General Relativity and Gravitation, 1 (1991).
- [62] Konigsdorffer, C., and Gopakumar, A., Phys. Rev. D **71**, 024039 (2005).
- [63] Koyama, H., and Konishi, T., Phys. Lett. A **295**, 109 (2002)
- [64] Koyama, H., Kiuchi, K., and Konishi, T., arXiv:gr-qc/0702072.
- [65] Landau, L. D., and Lifshitz, E. M., *The Classical Theory of Fields*(Pergamon, Oxford, 1951).
- [66] Lemos, J. P. S., and Letelier, P. S., Phys. Rev. D **49**, 5135(1994).
- [67] Letelier, P. S., and Vieira, W. M., Phys. Rev. D **56**, 8095 (1997).
- [68] Levin, J. J., Phys. Rev. Lett. **84**, 3515 (2000).
- [69] Levin, J. J., O'Reilly, R. and Copeland, E. J., Phys. Rev. D **62**, 024023 (2000).
- [70] Levin, J. J., Phys. Rev. D **67**, 044013 (2003).
- [71] Levin, J., Phys. Rev. D **74**, 124027 (2006).
- [72] Martel, K., Phys. Rev. D **69**, 044025 (2004)
- [73] Mathews, J., J. Soc. Ind. Appl. Math. **10**, 768 (1962).
- [74] Misner, C. W., Phys. Rev. Lett. **22**, 1071 (1696).
- [75] Misner, C. W., Thorne, K. S., and Wheeler, J. A., *Gravitation* (W. H. Freeman and Company, New York, 1973).
- [76] Moeckel, R., Commun. Math. Phys. **150**, 415 (1992).
- [77] Nakamura, T., Oohara, K., and Kojima, Y., Progress of Theoretical Physics supplement **90** (1987).
- [78] Newman, E. T., and Penrose, R., J. of Math. Phys. **3**, 566 (1962).
- [79] Newman, E. T., and Penrose, R., J. of Math. Phys. **4**, 998 (1963).

- [80] Papapetrou, A., Proc. R. Soc. London **A209**, 248 (1951).
- [81] Poincaré, H., *New Methods of Celestial Mechanics*, edited by D. L. Groff (American Institute of Physics).
- [82] Podolsky, J., and Vesely, K., Phys. Rev. D **58**, 081501 (1998).
- [83] Podolsky, J., and Vesely, K., Class. Quant. Grav. **15**, 3505 (1998).
- [84] Press, W., Flannery, B. P., Teukolosky, S., and Vetterling, W. T., *Numerical Recipies in C* (Cambridge University Press, Cambridge, England, 1986).
- [85] Rasband, S. N., Phys. Rev. Lett. **30**, 111 (1973).
- [86] Regge, T., and Wheeler, J. A., Phys. Rev. **108**, 1063 (1957).
- [87] Saa, A., Phys. Lett. A **269**, 204(2000).
- [88] Saa, A. and Venegeroles, R., Phys. Lett. A **259**, 201(1999).
- [89] Sasaki, M., and Nakamura, T., Phys. Lett. A **87**, 85 (1981).
- [90] Sasaki, M., and Nakamura, T., Phys. Lett. A **89**, 68 (1982).
- [91] Saslaw, W. C., *Gravitational physics of stellar and galactic systems*, Cambridge University Press, 1985.
- [92] Schnittman, J. D., and Rasio, F. A., Phys. Rev. Lett. **87**, 121101 (2001).
- [93] Semerák, O., Mon. Not. R. Astron. Soc **308**, 863 (1999).
- [94] Shibata, M., and Nakamura, T., Phys. Rev. D **52**, 5428 (1995).
- [95] Shimada, I., and Nagashima, T., PTP **61**, 1605 (1979).
- [96] Sota, Y., Suzuki, S., and Maeda, K. i., Class. Quant. Grav. **13**, 1241 (1996).
- [97] Suzuki, S., and Maeda, K. i., Phys. Rev. D **55**, 4848 (1997).
- [98] Suzuki, S., and Maeda, K. i., Phys. Rev. D **58**, 023005 (1998).
- [99] Suzuki, S., and Maeda, K. i., Phys. Rev. D **61**, 024005 (2000).
- [100] Szydlowski, M., and Lapeta, A., Phys. Lett. A **148**, 239 (1990).
- [101] Tanaka, T., Mino, Y., Sasaki, M., and Shibata, M., Phys. Rev. D **54**, 3762 (1996).
- [102] Teukolsky, S. A., Astrophys. J. **185**, 635 (1973).
- [103] Thorne, K. S., Rev. Mod. Phys **52**, 299 (1980).
- [104] Thorne, K. S., arXiv:gr-qc/9506086.
- [105] Thorne, K. S., in Proceedings of Snowmass 95 Summer Study on Particle and Nuclear Astrophysics and Cosmology, edited by Kolb, E. W. and Peccei, R. (World Scientific, Singapore. 1995), p398.
- [106] Tsubono, K., *Prepared for Edoardo Amaldi Meeting on Gravitational Wave Experiments, Rome, Italy, 14-17 Jun 1994*

- [107] Tsubono, K., in proceedings of First Edoardo Amaldi Conference on Gravitational Wave Experiments, Villa Tuscolana, Frascati, Rome, edited by E. Coccia, G. Pizzella, and F. Ronga (World Scientific, Singapore. 1995), p112.
- [108] Varvoglis, H., and Papadopoulos, D. B., Astron. Astrophys. **261**, 664 (1992).
- [109] Will, C. M., and Zagular, H. W., Astrophys. J. **346**, 366 (1989).
- [110] York, J. W., Kinematics and Dynamics of General Relativity, in *Sources of gravitational radiation*, edited by Smarr, L. (Cambridge University Press, Cambridge, 1979).
- [111] Yurtsever, U., Phys. Rev. D **52**, 3176 (1995).
- [112] Zerilli, F. J., Phys. Rev. D **2**, 2141 (1970).
- [113] The recent observation suggests there exist huge black holes at the centers of many galaxies. See, for example,
Kormendy, J., and Richstone, D., Astrophys. J. **393**, 559(1992).
- [114] The reason why we find non-zero positive Lyapunov exponent for an integrable system is that we solve the equation of motion by a finite difference method and the finite difference approximation does not provide an exact integrable system. In fact, if we reduce the time step for integration, the value decreases.